Synthesis and Characterization of Novel Bay-Substituted Perylene Dyes for Dye- Sensitized Solar Cells

Maryam Pakseresht

Submitted to the
Institute of Graduate Studies and Research
in partial fulfillment of the requirements for the degree of

Doctor of Philosophy
in
Chemistry

Eastern Mediterranean University
July 2018
Gazimağusa, North Cyprus

Approval of the Institute of Graduate Studies and Research

Assoc. Prof. Dr. Ali Hakan Ulusoy
Acting Director

I certify that this thesis satisfies the requirements as a thesis for the degree of Doctor of Philosophy in Chemistry.

Prof. Dr. Izzet Sakalli
Chair, Department of Chemistry

We certify that we have read this thesis and that in our opinion it is fully adequate in scope and quality as a thesis for the degree of Doctor of Philosophy in Chemistry.

Prof. Dr. Huriye İcil
Supervisor

Examining Committee

1. Prof. Dr. Ramazan Altundaş
2. Prof. Dr. Metin Balci
3. Prof. Dr. Huriye İcil
4. Assoc. Prof. Dr. Nur P. Aydınlık
5. Asst. Prof. Dr. Süleyman Aşır

ABSTRACT

Nowadays the development and fabrication of Perylene dyes with suitable absorption and improved mechanical and electrical properties are widely investigated. The purpose of the present studies were focused to synthesize the high soluble perylene diimides, easy processable and good photonic properties. Substitution of perylene diimides in bay position causes a remarkable increase in optical, electronic properties, solubility, the more red shifted absorption band, good molar absorptivity and thermal stability. In the first section nano silica, nanosilica sulfunic acid (NSSA), were synthesized, also different parameters which is thought to have influence on the size of synthesized nanosilica particles were studied. In the next section of this research, first step was Bay-substitution Bromination of Perylene dianhydide, then some sorts of bay substituted perylene-diimides consist of N,N′-Di(phenoxy)-1,7-diphenoxyperylene-3,4,9,10-perylenetetracarboxy-diimide (BP-PPI), N,N′-Di(dodecyl)-1,7-di-3-amino-9-ethylcarbazol-perylene-3,4,9,10-perylenetetracarboxy-diimide (BC-PDD), 1, 7-(diphenoxyperylene perylene-3, 4:9, 10-tetracarboxylic acid dicarboximide)-3,4:9,10-tetracarboxylic anhydride (BPDA-PDA), N,N′-Didehyoebiethyl-1,7-di(N`-dehyoebiethyl,N-phenoxy) perylene-3,4,9,10-tetracarboxylic acid diimide) perylene-3,4,9,10-tetracarboxylic acid diimide (BPDI-PDI), N,N′-bis(3-triethoxysilylpropyl)-1,7-di-phenoxyperylene-3,4:9,10-tetra-caboxdiimide (BP-PDISi) also its nano-bay substituted alkoxysilane-functionalized perylenediimide (PDI) by using 3-amino-propyl triethoxysilane (APTES) were synthesized. Finally Poly-N,N′-bis(3-triethoxysilylpropyl)-1,7-di-phenoxyperylene-3,4:9,10-tetra-caboxdiimide (BP-PPDISi) and Nanosilica-N, N-bis((S)-(−)-1-

phenylethyl)-3,4,9,10-perylene (NSPDI), with fluorescence emission in the near infrared (NIR) were synthesized by sol-gel method, also the effects of different parameters on particle size has been studied. The compounds were characterized by FT-IR, Elemental analysis, CNMR, HNMR, UV-visible, Fluorescence, TGA thermogram, DSC, SEM, TEM and AFM techniques.

Keywords: perylene, bay substitution, macromolecule, nanoperylene.

ÖZ

Günümüzde, uygun absorpsiyon, geliştirilmiş elektriksel ve mekanik özelliklere sahip perilen boyalarının geliştirilmesi ve imalatı yaygın bir şekilde araştırılmaktadır. Bu araştırmanın amacı, kolay işlenebilir, iyi fotonik özelliklere ve yüksek çözünürlüğe sahip perilen diimidleri sentezlemektir. Perilen diimidlerin körfez bölgesinden sübstitüe edilmesi optik ve elektronik özelliklerde, çözünürlükte, absorpsiyon bandının kırmızıya kaymasında, molar absorpsiyon ve termal kararlılıkta dikkat çekici bir artışa neden olmaktadır. İlk olarak, nanosilika ve nanosilika sülfürik asit sentezlenerek, sentezlenen nanosilika parçacıklarının boyutu üzerinde etkisi olduğu düşünülen parametreler araştırılmıştır. Bu araştırmanın bir sonraki bölümünde, ilk adım olarak perilen dianhidrit bromlaştırılarak, körfez-sübstitüe perilen diimidler N,N'-Di(fenoksi)-1,7-difenoksiperilen-3,4,9,10-perilendikarboksidiimid (BP-PPI), N,N'-Di(dodesil)-1,7-di-3-amino-9-etilkarbazolperilen-3,4,9,10-perilendikarboksi-diimid (BC-PDD), 1,7-(difenoksiperilen perilen-3,4:9,10-tetrakarboksilik asit dikarboksimid)-3,4:9,10-tetrakarboksilik anhidrid (BPDA-PDA), N,N'-Di(dehidroabietil)-1,7-di((N'-dehidroabietil,N-fenoksi)perilen-3,4,9,10-terakarboksi-lik asit diimid) perilen-3,4,9,10-tetrakarboksilik asit diimid (BPDI-PDI), N,N'-bis(3-trietoksisililpropil)-1,7-difenoksiperilen-3,4:9,10-tetrakarboksidiimid (BP-PDISi) ve aynı zamanda 3-aminopropil trietoksisilan (APTES) kullanarak nano - körfez pozisyonunda fenoksi-sübstitüe edilmiş alkoksisilan perilendiimid sentezlenmiştir. Son olarak, poli- N,N'-bis (3-trietoksisililpropil)-1,7-difenoksiperilen-3,4:9,10-tetrakarboksidiimid (BP-PPDISi) ve yakın ifrared bölgesinde floresans emisyonu veren nanosilika-N,N'-bis ((S)-(─)-1-feniletil)-3,4:9,10-perilentetrakarboksidiimid

(NSPDI) sol-jel yöntemi ile sentezlenerek farklı parametrelerin parçacık boyutu üzerinedeki etkileri saptanmıştır. Elde edilen ürünler FTIR, elementel analiz, C-NMR, H-NMR UV-Görünür bölge absorpsiyon spektroskopisi, floresans emisyon spektroskopisi, TGA, DSC, SEM, TEM ve AFM ölçümleri ile karakterize edilmiştir.

Anahtar Kelimeler: perilen, körfez pozisyonu, makromolekül, nanoperilen

To My Lovely Family

ACKNOWLEDGMENT

First, I would like to say my thanks to my supervisor **Prof. Dr. Huriye İcil** for all of her support during my PhD thesis and her supervision motivated me during of my research over the past years. I extremely grateful to have opportunity to be under her supervisions during this work and to have her guidance in my life.

I would like to thank Dr. Duygu Uzun, for her supports and useful comments in my research.

I am immensely thanks to Dr. Jagadeesh Babu Bodapati, for his creative guides and his assistance in analysis facilities.

I would like to give my grateful thanks to our organic group for friendship and moral supports and encouragements.

I gratefully acknowledge the scientific research council of Turkey (TUBITAK Organization) for all of their cooperation in my research.

TABLE OF CONTENTS

LIST OF TABLES

LIST OF FIGURES

LIST OF SYMBOLS/ABBREVIATIONS

Å	Armstrong
A	Absorption
AU	Arbitrary unit
C	Concentration
Calcd	Calculated
ε	Molar Absorption Coefficient
ε_{max}	Maximum Extinction Coefficient / Molar Absorptivity
$E_{1/2}$	Half- Wave Potential
F	Oscillator Strength
h	Hour
k_d	Rate constant of Radiationless Deactivation
k_f	Fluorescent
l	Path Length
max	Maximum
min	Minimum
mmol	Millimole
mol	Mole
Φ_f	Fluorescence Quantum Yield
Std	Standard
τ_0	Theoretical Radiative Lifetime
t	Time
$\bar{\vartheta}$	Wavenumber

$\Delta\upsilon_{1/2}$	Half-Width (of the selected absorption)
$\bar{\upsilon}_{max}$	Maximum Wavenumber
λ	Wavelength
λ_{exc}	Excitation Wavelength
λ_{em}	Emission Wavelength
λ_{max}	Maximum Wavelength
DMAc	Dimethylacetamid
DMF	Dimethylformamide
DMSO	Dimethyl Sulfoxide
DSSC	Dye Sensitized Solar Cells
FT – IR	Fourier Transform Infrared Spectroscopy
HOMO	Highest Occupied Molecular Orbital
IR	Infrared Spectrum/Spectroscopy
LUMO	Lowest Unoccupied Molecular Orbital
NMP	*N*-Methylpyrrolidinone
PDA	Perylene 3, 4, 9, 10-Tetracarboxylic Dianhydride
PDI	Perylene 3, 4, 9, 10-Tetracarboxylic Diimide
TCE	1,1,2,2-Tetrachloroethane
TFAc	Tri-fluoro Acetic Acid
TGA	Thermogravimetric Analysis
THF	Tetrahydrofuran
UV	Ultraviolet
UV-vis	Ultraviolet Visible Light Absorption

Chapter 1

INTRODUCTION

The derivatives of perylene-3, 4, 9, 10-tetracarboxylic-dianhydride (PDA) Figure 1.1, have been widely applied as industrial dyes, Figure 1.2, Perylene-3, 4, 9, 10-tetracarboxylic-acid-diimide (PDI) as a basic class of this compounds was founded in 1910. The various types of N,N′-perylene diimide substituents with different chemical and physical properties have been synthesized by suitable modification of the PDI's in 1, 6, 7, or/and 12 positions which usually settled down by the halogenated derivatives, principally bromine and chlorine. Depending on type and position of these substituents, pigments display various chemical, fluorescence quantum yields, thermal, photochemical and weather stability properties. High optical and electronic properties of Perylene causes an intensive subject for using as a functional dyes in industry and huge variety of applications such as sensors, organics field-effect transistor (OFETs), lasers, fluorescent light collectors, in photovoltaic cells, light-emitting diode (OLEDs), electrophotography and etc[1-3].

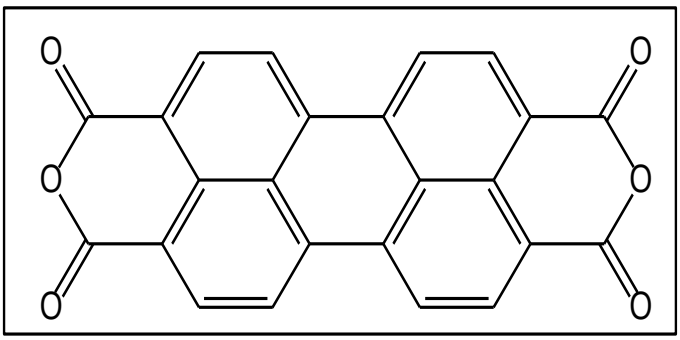

Figure 1.1: Structure of PDA

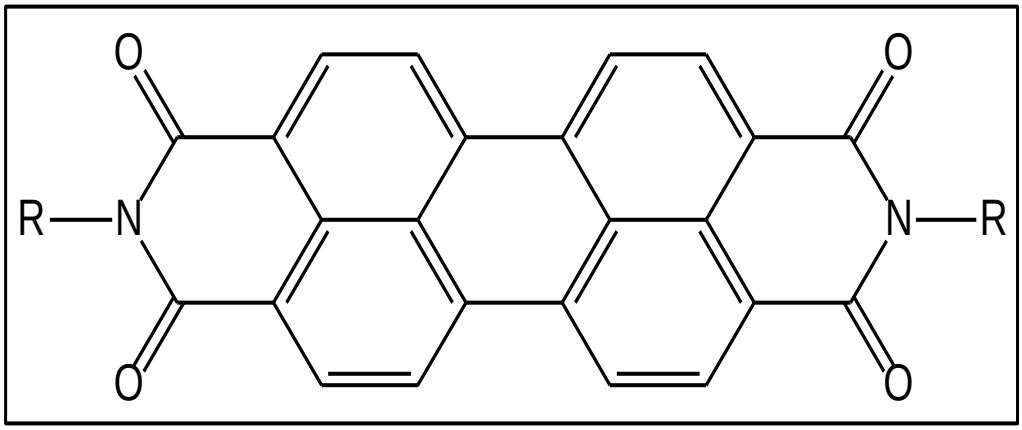

Figure 1.2: A Common Structure of PDI

Nowadays sun is used as a basic sources of renewable energy in the world. Photovoltaic technology, solar cells can convert the energy of sun to electricity. Dye-sensitized solar cells (DSSCs) because of low cost and simple technic are significant among the photovoltaic technologies. The specific kind of dye sensitized solar cells are Organic dye sensitized solar cells which has intensive attraction because of unique properties such as good photochemically stability, more molar absorptivity and higher red shifted absorption bands. Perylene imide derivatives are one of the most important practical dyes in which significantly have been applied in DSSCs as well as its optical and electronic properties is adjustable by chemical modification at imide position or functionalization at cores usually by halogens, in particular, boromine[2-5].

Nanotechnology is rapidly extend through various field of technology and science, for example, Biology, chemistry, physics and all of engineering fields which all are focused to investigation of substances at the nanoscale. Nanotechnology gives opportunity to produce new sort of upgraded materials in nanoscale which, display diverse biological, chemical and physical properties.

Nanotechnology to control the size of substance have been investigated different techniques, such as, co-precipitation, microwave radiation, impregnation, flame hydrolysis and chemical vapor deposition. Among these, sol gel method has been need extensively to control the surface and size properties of the produced oxides also is used widely to produced pure nano silica particles with controllable size distribution and morphology.

The nano silica have been extensively used due to their wide range of properties such as high specific surface area, low thermal conductivity, low dielectric constant, high optical transmission in the visible region, high porosity, low refractive index and low sound velocity. Therefor it has been extensively applied in industrial applications and engineering composite. In this research the coupling of perylene-nanosilica is used to increase their performance and extend their application range.

First part of this research is focused on the synthesis of different types of bay substituted PDIs, then in second part, surface modification and effects on nanosilica particles by sol-gel method have been studied. Finally bay substituted Perylene-nanosilica compound have been produced.

In this research new type of bay substituted Perylene derivatives and nano composites of them were synthesized, also their properties and characterization studied. FT-ir, Uv-vis, HNMR, CNMR and elemental analysis were emphasized the structure of this compounds, also their electrochemical properties have been studied by cyclic voltammetry and UV–vis and fluorescence spectroscopy.

In the secend part of this study tetraethylorthosilicate (TEOS) was used to produce nanosilica particles with sol gel method by the hydrolysis of TEOS, for this purpose function of different parameters such as compositions of TEOS/NH_3 and H_2O/NH_3 and also temperature and time of reactions in sonication on particle size have been studied (Table 1.1). Distribution, shape and size of particles were determined by Scanning-Electron Microscopy (SEM), Transmission-Electron Microscopy (TEM) and also Atomic-Force Microscopy (AFM). The function of effective parameters and appropriate properties on particle size are summarized in Table 1.1[5].

Table 1.1: Parameters that Effect on Nanosilica Preparations

	Parameters that effect of synthesis nanosilica	**Size (nm)**	**Sonication , Time (min) Temp ºC,**
1	[TEOS/H_2O=100], [($H_2O.NH_3$)=2/3]	400	_
2	oven (500 ℃, 12h), [TEOS/H_2O=70], [($H_2O.NH_3$)=2/3]	250	_
3	oven (180℃, 2h), [TEOS/H_2O=50], [($H_2O.NH_3$)=2/3]	70-150	50ºC, 30 min
4	oven (180℃, 2h), [TEOS/H_2O=40], [($H_2O.NH_3$)=2/3]	60-120	50ºC, 30 min
5	oven (500 ℃, 12h), [TEOS/H_2O=70], [($H_2O.NH_3$)=2/3]	200-300	50ºC, 45 min
6	oven (500 ℃, 12h), [TEOS/H_2O=60], [($H_2O.NH_3$)=2/3]	150-250	50ºC, 45 min
7	oven (180℃, 2h), [TEOS/H_2O=50], [($H_2O.NH_3$)=2/3	125-166	60ºC, 45 min
8	oven (180℃, 2h), [TEOS/H_2O=25], [($H_2O.NH_3$)=1/3]	54	70ºC, 30 min
9	oven (180℃, 2h), [TEOS/H_2O=25], [($H_2O.NH_3$)=1/3]	59	60ºC, 30 min
10	oven (180℃, 2h), [TEOS/H_2O=25], [($H_2O.NH_3$)=1/2]	60	30ºC, 20 min
11	oven (500 ℃, 12h), [TEOS/H_2O=25], [($H_2O.NH_3$)=2/3]	10	70ºC, 30 min
12	oven (180℃, 2h), [TEOS/H_2O=40], [($H_2O.NH_3$)=2/3]	125.2	60ºC, 30 min
13	oven (500 ℃, 8h), [TEOS/H_2O=25], [($H_2O.NH_3$)=2/3]	45.3	70ºC, 30 min
14	oven (500 ℃, 6h), [TEOS/H_2O=25], [($H_2O.NH_3$)=1/3]	54.9	60ºC, 30 min
15	oven (500 ℃, 6h), [TEOS/H_2O=25], [($H_2O.NH_3$)=2/3]	59.9	60ºC, 30 min
16	oven (700 ℃, 12h), [TEOS/H_2O=25], [($H_2O.NH_3$)×1/2]	35.4	60ºC, 30 min

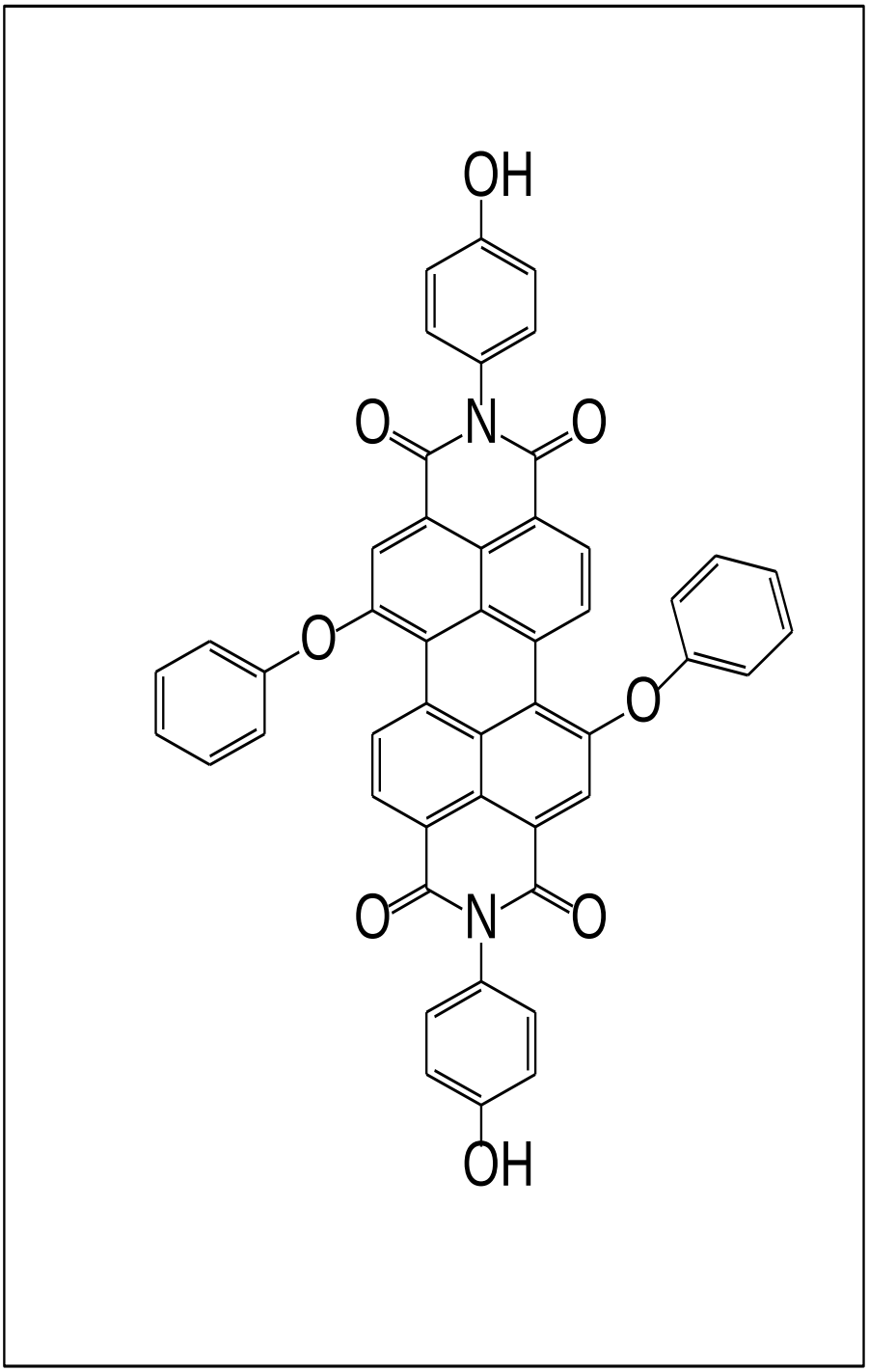

Figure 1.3: N,N´-Di(phenoxy)-1,7-Diphenoxyperylene-3,4,9,10-Perylenetetracarboxy-Diimide (BP-PPI)

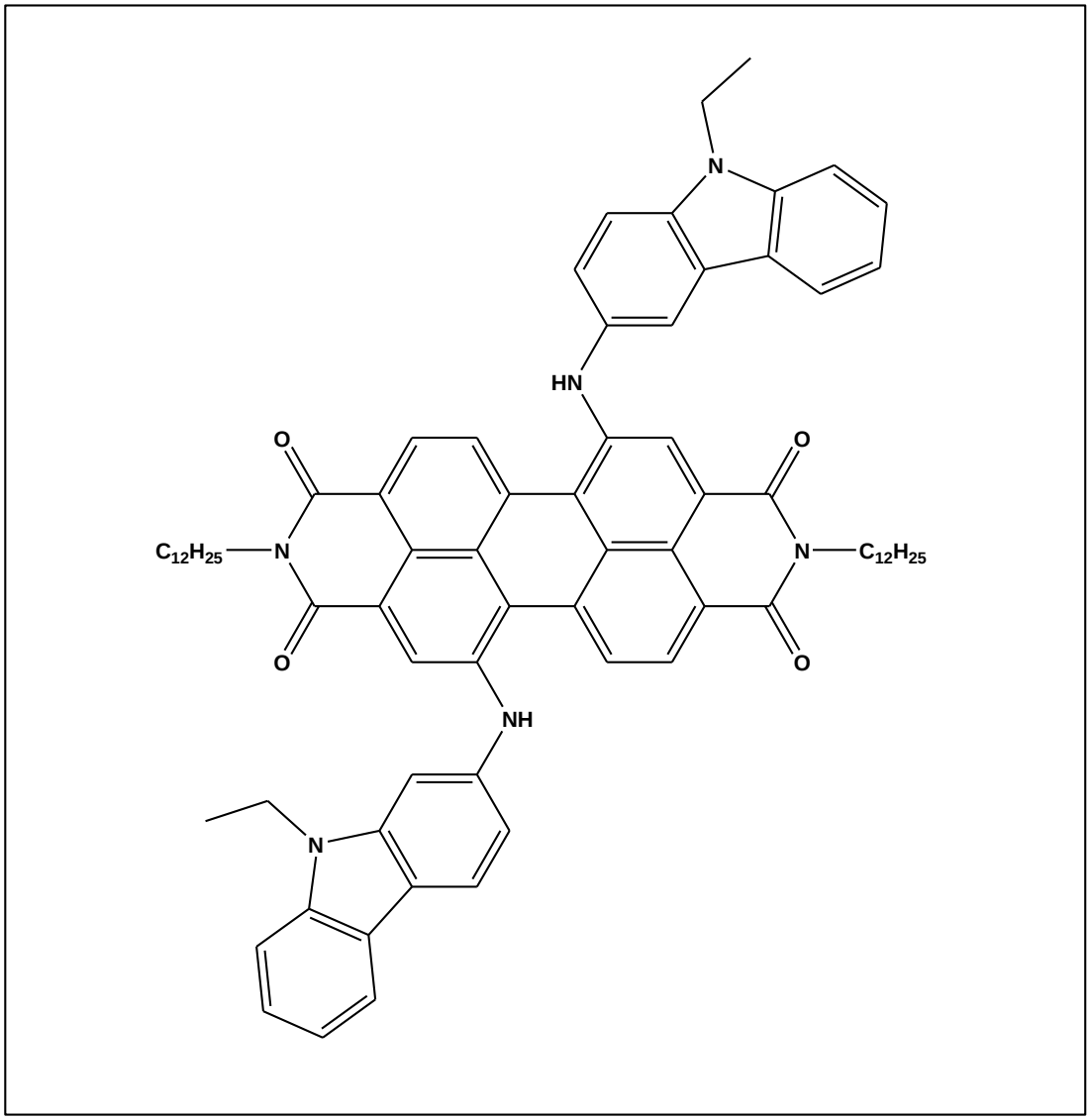

Figure 1.4: N,N´-Di(dodecyl)-1,7-di-3-amino-9-ethylcarbazol Perylene-3,4,9,10-Perylenetetracarboxy Diimide (BC-PDD)

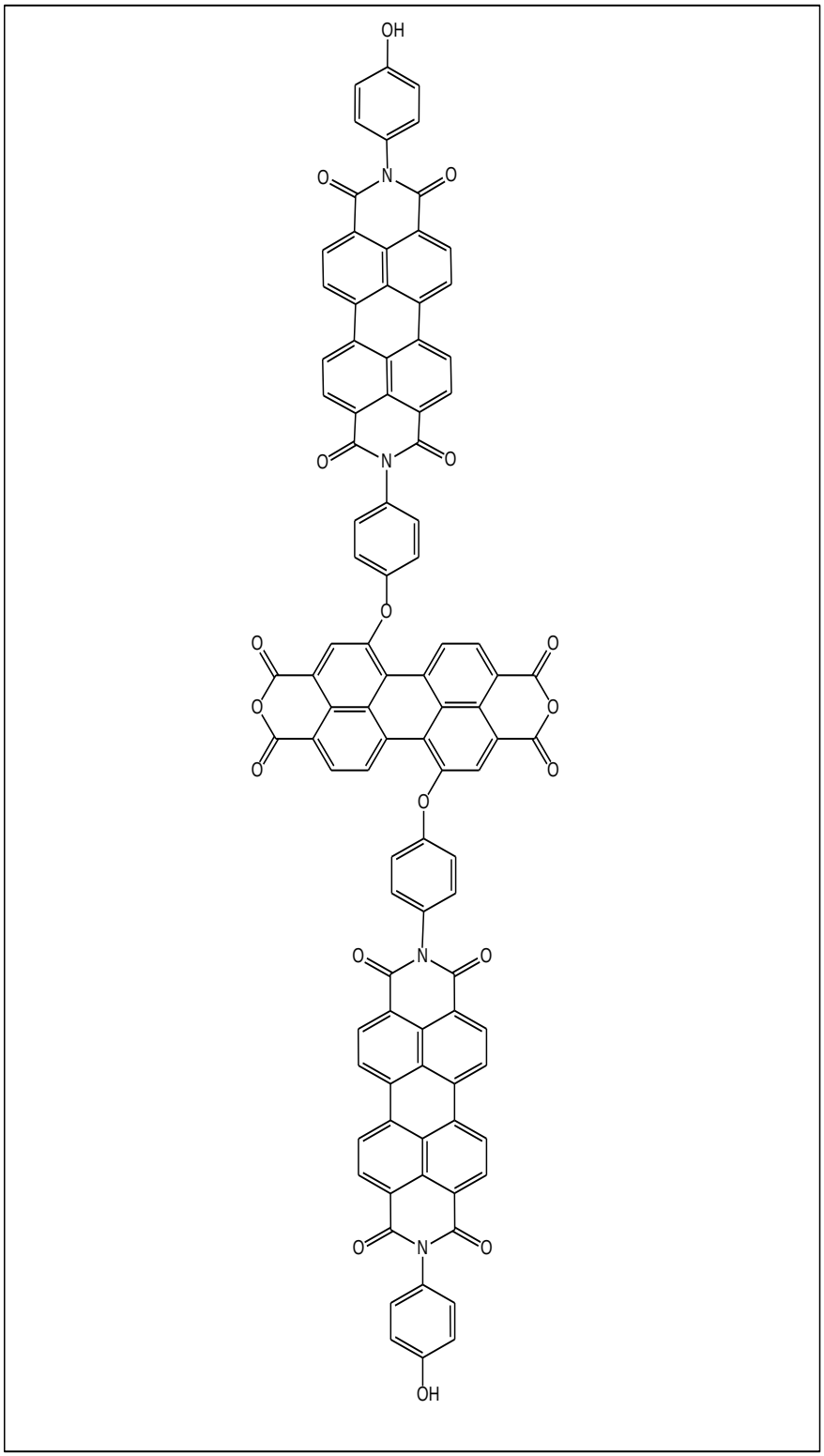

Figure 1.5: 1, 7-(Diphenoxyperylene Perylene-3, 4:9, 10-Tetracarboxylic Acid Dicarboximide)-3,4:9,10-Tetracarboxylic Anhydride (BPDA-PDA)

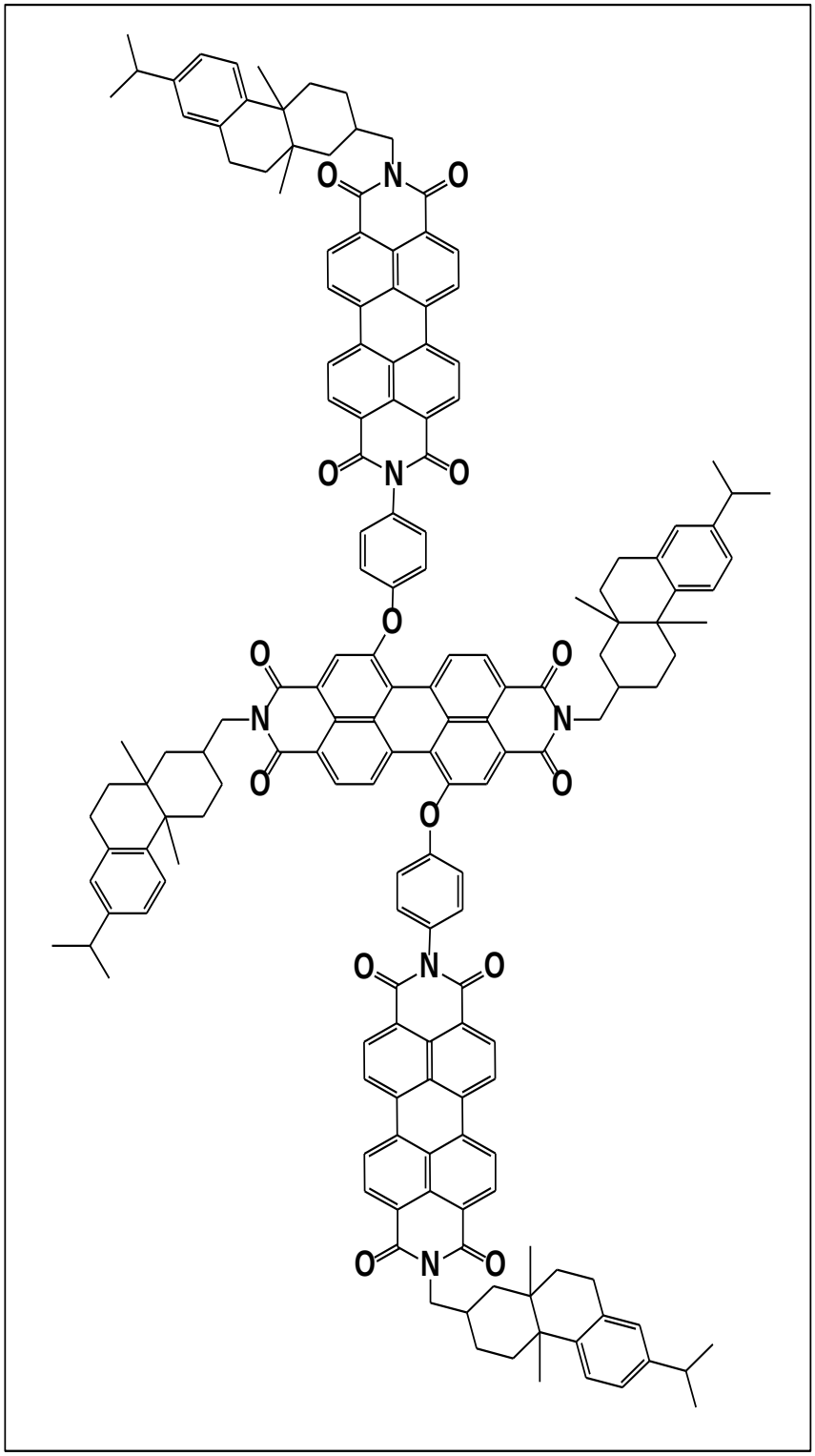

Figure 1.6: N,N′-Dehydroabiethyl -1,7-Di((N`-dehydroabiethyl, N- phenoxy) Perylene-3,4,9,10-Tetracarboxylic Acid Diimide) Perylene-3,4,9,10-Tetracarboxylic Acid Diimide (BPDI-PDI)

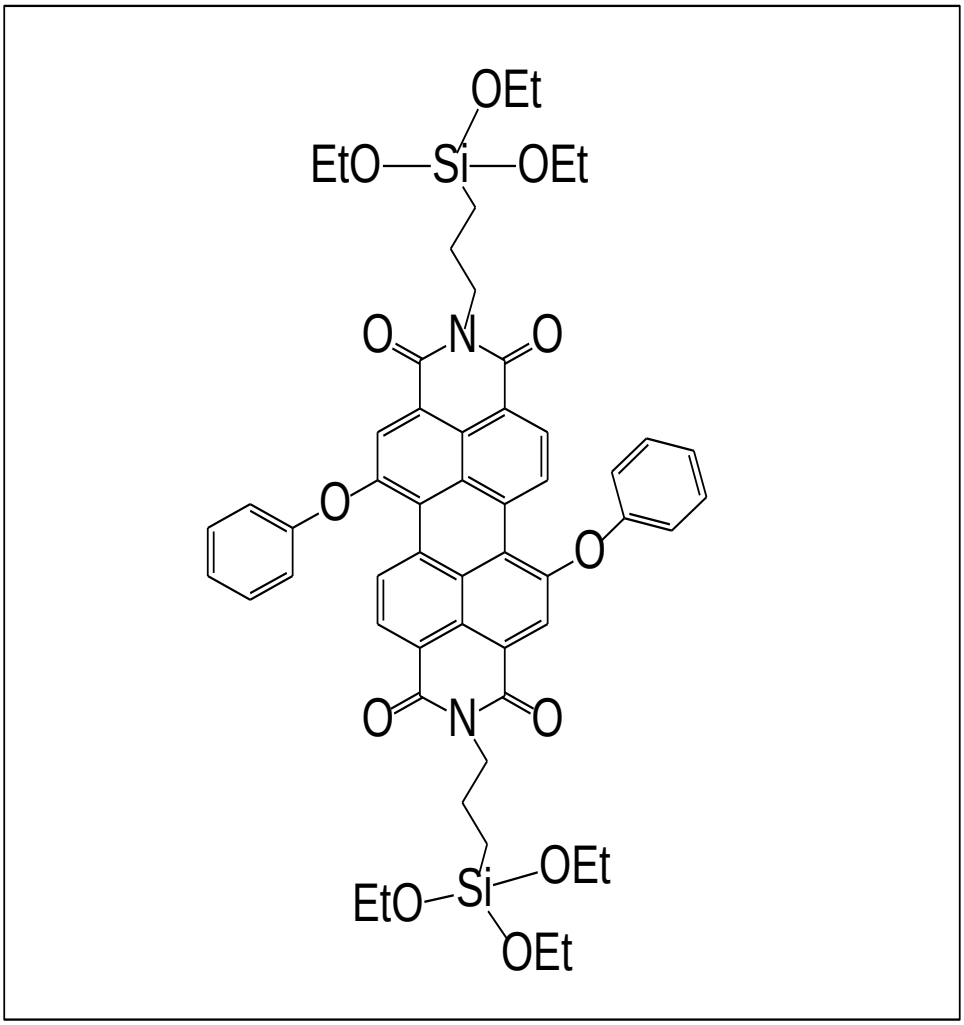

Figure 1.7: N,N´-Bis(3-Triethoxysilylpropyl)-1,7-Dipheno-xyperylene-3,4:9,10-Tetracaboxdiimide (BP-PDISi)

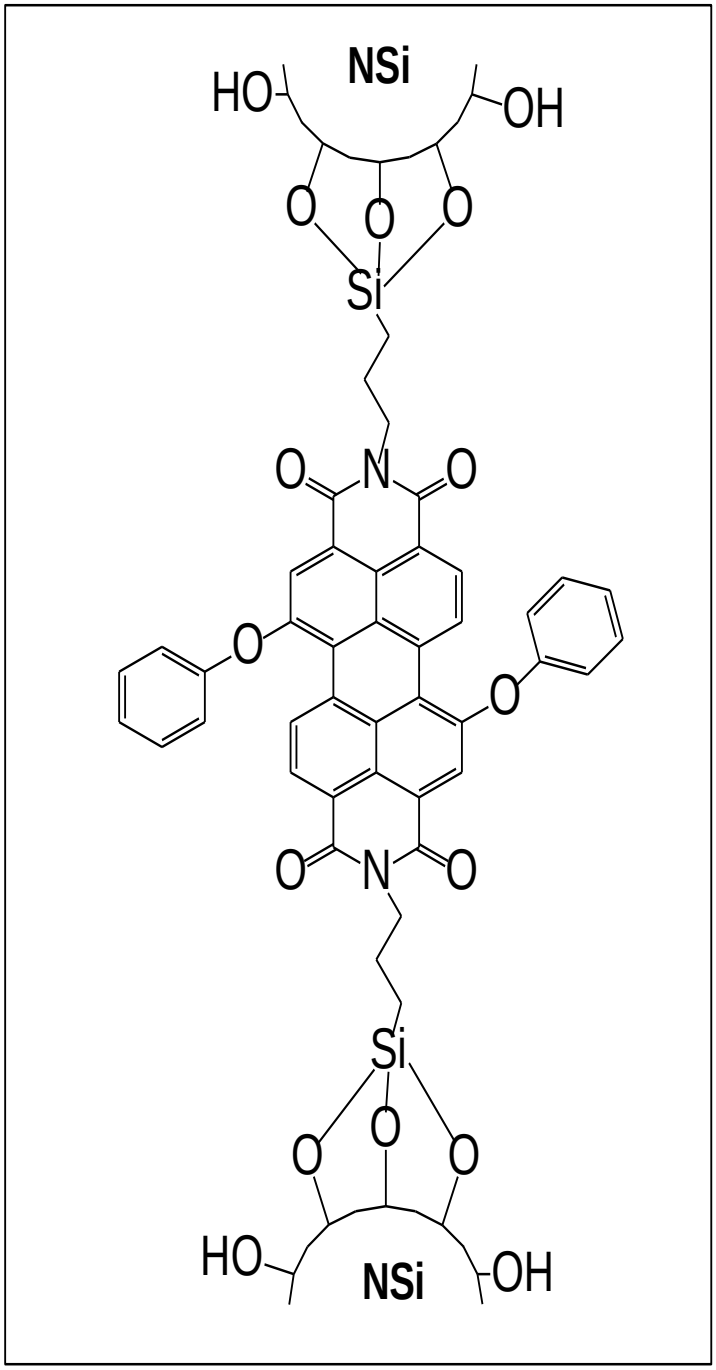

Figure 1.8: Nano-N,N´-Bis(3-Triethoxysilylpropyl)-1,7 -Di-Phenoxyperylene-3,4:9,10-Tetracaboxdiimide (BP-PPDSi)

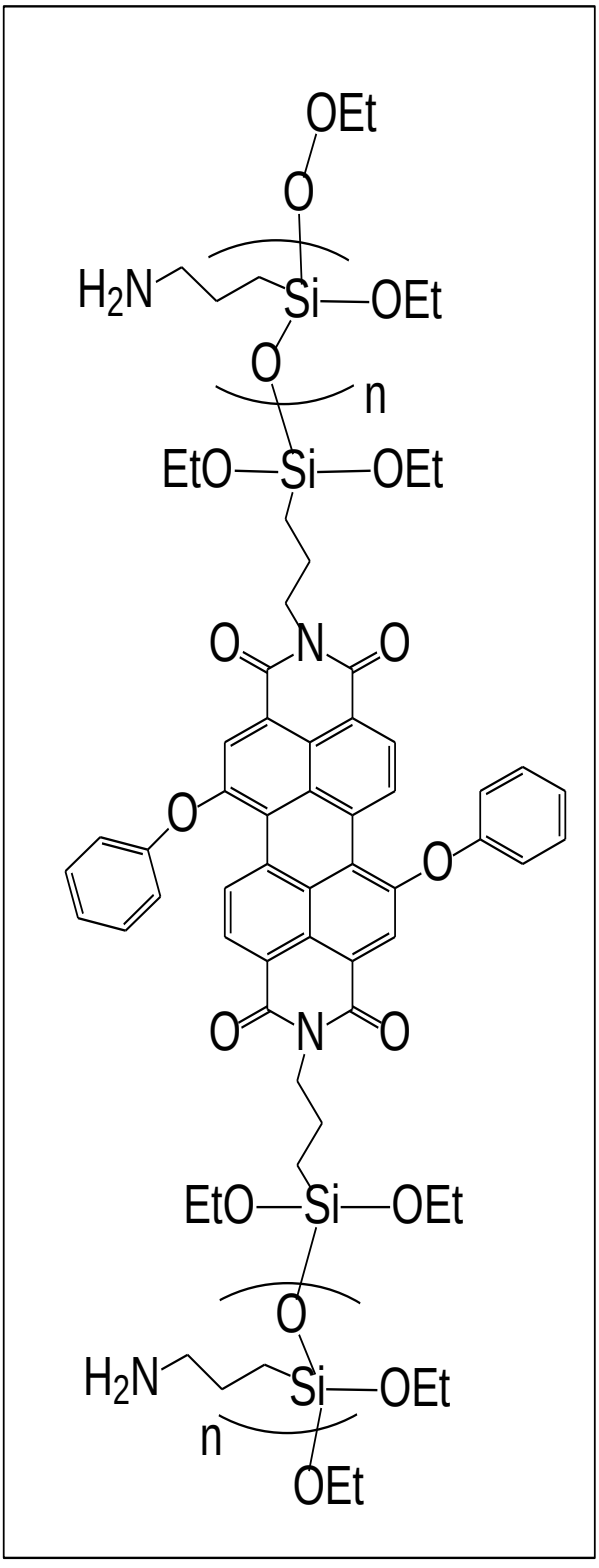

Figure 1.9: Poly-N,N′-Bis(3-Triethoxysily lpropyl)-1,7-Diphenoxyperylene-3,4:9,10 -Tetracaboxdiimide (BP-PPDSi)

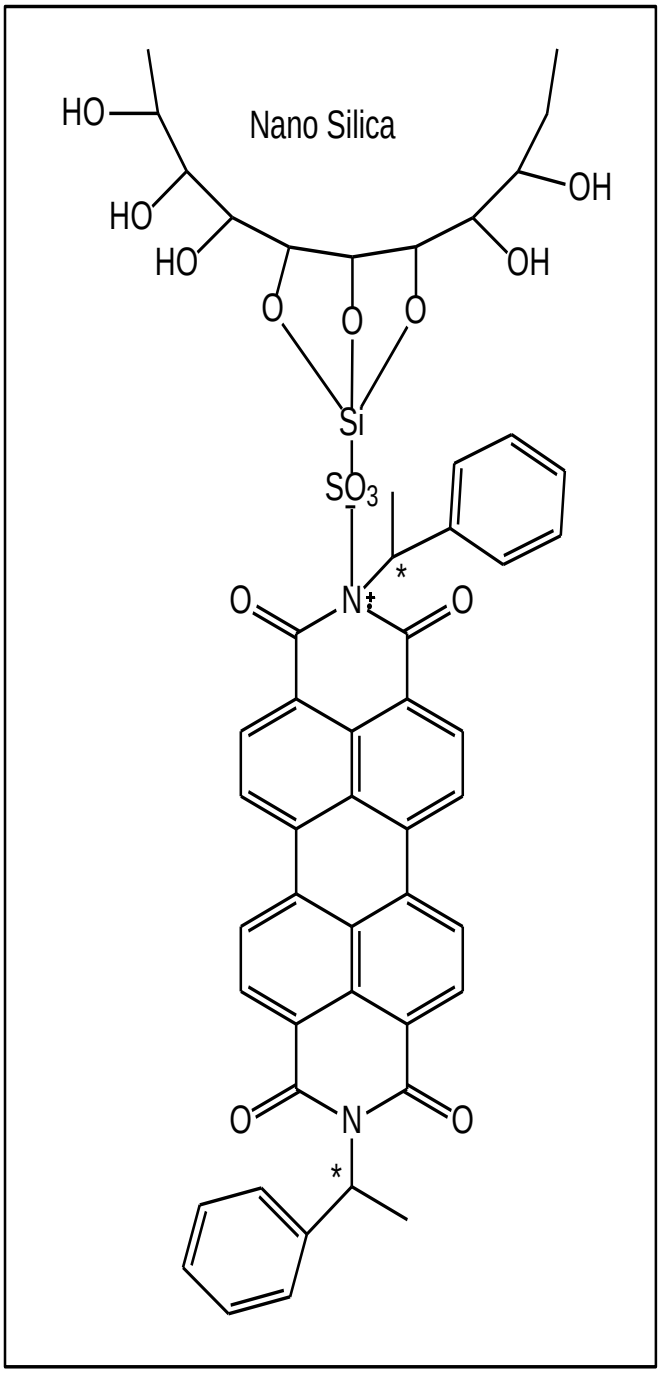

Figure 1.10: Nanosilica-N, N-Bis((S)-(−)-1 -Phenylethyl)-3,4,9,10- Perylene (NSPDI)

Chapter 2

THEORETICAL

2.1 Polyimides

Polyimides are important group of polymers with simple manufacturing and with essentially high heat and chemical resistance. Their great properties causes to apply them in the wide range of industrial and functional fields. Generally polyimides are produced in bulk, or thin film sedimentation also mostly by conventional dry etching techniques. The strong dynamo-mechanical, elasticity and electrical identity of polyimides is the main reason for its utilization in the industry[4-9].

2.1.1 Perylene

Perylene derivatives are one of the most important organic electron-acceptor semiconductors and comprehensively are utilized as n-type semiconductor materials [36].

Perylene derivatives have exhibited excellent brilliant chemical, physical, thermal stabilities and optical properties due to the owning large conjugated aromatic system. Among all, perylene diimides (PDI) have exhibited high intensive electrical, photovoltaic, photochemical, optoelectronic, high absorbance and fluorescence properties, as far as in industry they are famous as fluorescence dyes. This type of polyimides has wide range of application areas such as transistors, light-emitting diodes and especially Dye sensitized solar cells.

Same properties of perylene dyes such as: solubility, aggregation, optic and electronic properties can be modify by changing selective substitutions significantly in imide and bay position of perylene diimide. Commonly to synthesize bay substituted perylene diimides materials, since perylene display poor processability in bay positions, there was extensive research to produce perylene tetra alkoxycarbonyl with a substituent connected to perylene core. Perylene diimdes by owning bay substituted functional groups exhibited more modified properties than perylene dimides[23, 27].

2.2 Solar Cells

Today the major current energy sources are petroleum, Coal and natural gas, which these resources are going to be extinct. Also they cause pollution and increasing the carbon dioxide levels in climate. In recent decades, the scientists have begun to concentrate on decreasing carbon dioxide levels in atmosphere by focusing on clean energy source for generating clean electrical energy. Photovoltaic (PV) solar cell without any limitation in charge are able to convert directly sun energy to electrical energy without producing Carbon dioxide[9-16].

2.2.1 Dye Sensitized Solar Cells

Dye-sensitized solar cells (DSSCs) have been extensively used to create electricity, due to their simple structure, low efficiency, flexibility, inexpensive method, and wide range of application.

The four main part of DSSCs are composed of: the thin electrode film layer of titanium dioxide to absorb solar energy, the conductive transparent oxide layer for charge transfer, Pt or C-layer as counter electrode; the dye molecules as a redox electrolyte layer.

Many scientist and researcher in this field mentioned that for achieving quantum yield approximately up to 90%, the dye layer should be attached directly into the semiconductor parts in the wide area. Therefor they focused intensively to improve the efficiency of DSSCs with adjustment of all of four component especially by improvement of dye layer. However they assumed that in DSSCs efficiencies cannot exceed more than 10- 12% even with the best progression and applying advanced materials[27-38].

2.3 Nanotechnology

2.3.1 Introduction and Definition of Nanotechnology

In 1995 Richard Feynman, by using physical laws talked about the controlling things on the small scale and succeed to get Nobel Prize at the California institute. Years later in 2000, William J. Clinton searched about Nano science and succeed to generated nano scale science. In 2001 it becomes one of the top objects of science and technology spatially they succeed to produced three dimensional nanostructure also self-assembly of simple reagent in solutions or biological molecules especially DNA was introduced. The nanosized materials are inserted into a matrix of standard material and are introduced as a Nanocomposites. Also by plasma chemistry technology and vacuum deposition, Nanotubes are produced. Nowadays there are intensive attempt to use and fabricate nanotechnology in experimental area in all of physical, chemical, and biological field.

Recently we have seen the importance of Nanotechnology in our world and its extreme effect on economy, society, industry and science. In assumption Nanotechnology causes huge revolution in manufacturing of materials, electronics, medicine, energy, information technology and biotechnology[39].

The metal particles between 1-50 nm are known as nanometals which are very attractive because of their size, shape-dependent properties and high surface areas. The materials composed of atoms in either a single- or poly-crystalline arrangement with at least one dimension smaller than 100 nm are known as a nanocrystals. The nanocrystals exhibited magnetic, electronic, and optical properties which are

extensively depended on size and structure of crystals. Nanocrystals aren't good conductors, they known as a paramagnetic materials because their electronic energy levels are separated but in bulk are continuous, therefor by inserting an extra electron to their structure, they can be charged[39, 40].

2.4 Effective Factors in Nanotechnology

2.4.1 Size Control

Nanocrystals are synthesized in three step consists of: nucleation, growth, and termination. Two basic factor for controlling the particle size during the reaction are temperature and concentrations of reactants. Elementary object in synthesizing nano crystals is controlling size distribution, because it is one of the main determinative factors in nanocrystals properties. Disability in control of reaction temperature is caused wide distribution of nanocrystals size. Generally precipitation of nanocrystals in the same size of extent is possible by using centrifuge or appropriate solvent

Scientists have extensively researched to modify and improve the reaction produce to obtain nanocrystals in same size of extent with different form of rods, elongated spheres, cubes, and hexagons.

2.4.2 Capping Agent

Capping agent is one of the dominate elements which has important role in nanocrystal properties. In during of synthesis capping agent normally are used for controlling shape and size by stopping growth of nanoparticles. Many years ago ions, polymers and surfactants are used as capping agents, while nowadays dyes with proper functional groups like silica, hydrogen-bonding fragments of protein and DNA have been used as capping agents.

2.5 Why Nano

Nowadays Nano-science and advanced nanostructures is reachable by developing of new synthesis technics and experimental procedures.

Nanotechnology by producing new materials with excellent chemical, physical optical, electrical and photovoltaic properties is getting attention of scientists to discover new methods and spots of synthesizing nanomaterial [40].

2.6 Nano Composites and Nano Grained Materials

Nowadays there are extensive interest to forward materials to nano scales for improving their chemical and physical properties. Nano composites are compounds with at least two phases, one distributed in another as a matrix. The physical properties of Nano composites are completely different from origin one. Nano composites are achieved by distribution approximately 20-60% nanoparticles in a polymeric matrix. The surface to volume ratio described as a most important characteristic of nanomaterial, is increased by shorting of diffusion distance. One of the simplest and fundamental methods in decreasing size of particles was attrition or milling but it causes damage and defects to the particle surface, also can bring impurities into the

particle surface. Sol-gel method produce pure nanoparticle with promotes surface of particles. According to Hall-Patch relationship square root of particle size increase inversely proportional with mechanical properties, therefore the most important factor in mechanical properties of nanoparticles is surface of particles.

Except sol-gel method, installation of a solid inside a porous substrate, by vapor chemical reactions, is the other method for synthesizing of Nano composites[39-41].

2.6.1 Nano Polymers

Development of Nanotechnology and Nano science has exhibited extensive tendency for the improvement of materials with unique and fascinating properties and applications. The Nano composites in comparison to virgin polymers, display notable and visible improvements. Polymer Nano composites are new corroboration of polymeric materials using organo–inorganic Nano fillers. Generally three types of nanofillers is used in nanocomposite structures:

1. Nano particles with all three dimensions in nanoscales
2. Nano particles with two dimensional nanofillers
3. nano particles with only one dimension on a nanolevel

The main group of organic-inorganic hybrids are polymeric Nano-composites which inorganic part consist of: nanoparticles, nanotubes and nanometers are dispersed in an organic polymeric matrix. The combination of inorganic and organic matrix produced polymer nanocomposites as a new generation of materials with both characteristic properties of organic polymer and inorganic nanoparticles. Generally in polymeric nanocomposites by reducing nanoparticle size, mechanical properties, specifically

elastic modulus is improved. There are three main procedure to produce polymeric nanocomposites:

1) Inserting of nanoparticles into a melted polymeric matrix or its solution

2) Pushing nanoparticles in a polymer matrix

3) Polymerization of organic part in Presence of nanoparticles

4) Simultaneous combination of polymerization and formation of nanoparticles

Silica glass as an inorganic materials, has wide attention due to the optical properties, transparency, brittleness and hardness. On the other hand, generally polymers doesn't have good hardness, which is one of the most important factors effects on their applications. Polymeric Nano composites with Organic and inorganic parts, have great interest due to the combination of both organic and inorganic properties, such as: conductivity, toughness, optical activity, catalytic activity, chemical selectivity[39-41].

2.6.2 Silicon and Silica

Silica is one of the most widely used inorganic material which is widely used to produce Nanostructured materials. The main characteristic properties of silica is easily producing by hydrolytic polycondensation of silicon compounds. The following reasons are another advantages of using silica in producing nanostructural materials.

1. Different types of basic silica are commercially available and silicon industry is extensively grow which having the wide variety of applications.

2. Characterization of polymeric nanocomposites are easily viable by series of analytical and spectroscopic methods like NMR, IR, MS, etc.

3. Si-C bonds has been exhibited good stability, however stability of Si-C sp^3 bonds are more than Si-C sp^2 and Si-C sp bonds.

4. The synthetic route for producing silica powder is hydrolysis and condensation of R-SiX_3 (X: OMe, OEt, OiPr, H, Cl, OCOR, NR_2, SR, etc.), which is economical and easily proceed.

5. The stability of polymeric nanohybrid depends on both silica and organic matrix. Generally they have exhibited high thermal stability and good resistance in acids.

6. Shaping produced silica is simply possible by varying the experimental conditions, therefor, the hydrophilicity, porosity, the exact surface area and the size of produced particles are modifiable.

7. Silica composites are normally transparent, which is important to uses in optics fiber.

8. Silica is one of the significant inorganic materials which shows wide compatibility with all chemical entities such as: organic, inorganic, polymeric and even biological[14-21].

2.6.2.1 Silicon

C. S. Smith in 1950 for the first time used silica as a basic material in sensor industry and published the piezoresistive effect in Ge and Si. He showed that the piezoresistive coefficients of silica was higher than conventional metals and its GPa Young's modulus was comparable with steel. He emphasized the mechanical advantageous properties of Si caused a broad range of its application such as a material for membranes, beams, and etc.

2.6.2.2 Nanosilica Properties

The microstructure of silica is the basic factor to determine their characteristic properties such as: thermal conductivity, electrical conductivity and residual stress. Nowadays biomedical science are extensively used Silicon dioxide nanoparticles, which known as silica nanoparticles or nanosilica, due to the easy processability, high thermal and mechanical stability, low toxicity and easy surface functionalization with a range of molecules and polymers[40-46].

2.6.2.3 Nanosilica Applications

Micro Electro Mechanical Systems (MEMS) generally manufactured on silica due to owning the high resistance, poor solubility and easy production process.

SiO_2 films are produced by thermal oxidation in the presence of oxygen or vapor at 900 ˚C -1200 ˚C. Quartz is one of crystalline forms of silica which is applied widely in manufacturing of MEMS. Quartz is one of the wide used material in MEMS and microfluidic devices due to the optically transparent, piezoelectric, and electrically insulating. SOG (Spin-On-Glass) is also polymeric form of silica which employed in MEMS.

2.7 Different Synthetic Methods of Nano-Materials

2.7.1 General Methods

Different methods have been applied to synthesize nanomaterials as a liquid, solid and gas. In fact, all the methods are classified in two main cluster which known as bottom-up and top-down approaches.

Bottom-up: produce of nanoparticles by assembling of molecules or atoms

Top-down: produce nanoparticles by decomposition of larger particles

Generally the most common technics in nanomaterials manufacturing in bottom-up cluster are: chemical vapor deposition (CVD), chemical vapor condensation (CVC), matrix-mediated (template-assisted) processing, laser pyrolysis, precipitation, plasma or flame spraying synthesis, reduction, sol-gel, solvothermal and self-assembly. In among of all this technics, Sol-gel due to the low temperature processing, is widely used in compare to other technics.

2.7.1.1 The Sol-Gel Method

Last decades numerous methods were used to synthesize organic-inorganic nanomaterials. “Sol-gel” process is one of the best used methods which can produce organic and inorganic hybrid nanoparticles with controlled defined shapes, nanoscale sizes and structure. The sol-gel process usually is consist of three steps: In First step, sol as a concentrated solution or colloidal suspension of the reactants is produced. In the second step sol is concentrated and prepared the ‘gel’. In the third step homogeneous gel is heat-treated to obtain easily nanoparticles. First time, in 19^{th} century sol-gel is considered by hydrolyzing an alkoxide to produce nanosilica particles[5].

Chapter 3

EXPERIMENTAL

3.1 Materials

Reagents and reactants were obtained from commercial sources. Below are listed the chemical name, company of purchase and purity of used materials. Some of solvent used were purified according to the standard purification procedures. For spectroscopic analyses all organic solvents were employed in spectroscopic grade without further purification.

Regents:

3-amino-9-ethylcarbazol, Aldrich

3-aminopropyltriethoxysilane, Aldrich

Bromine, Aldrich

Chlorosulfunic acid (98%), Aldrich

Dehyroabiethylamine (98%), Aldrich

Dodecylamine, Fluka 98%

Phenol, Aldrich

Potassium carbonate, Aldrich

Potassium hydroxide, Aldrich

Hydrochloric acid, Riedel deHaen 37 %

Iodine, Aldric

Perylene -3,4,9,10-tetracarboxylic dianhydride (PDA), Aldrich 98 %

Silica-gel-60 (0.063–0.20 mm), Aldrich

Sulfuric acid, Aldrich 98 %

Tetraethylorthosilicate (TEOS), Aldrich 99%

Zinc acetate dehydrate ACS 99%

Solvents:

Acetone, Aldrich (99%)

Chloroform, Aldrich (99%)

Ethanol, Aldrich (99%)

Dimethylesulfoxide, Aldrich (99%)

Isoquinoline, Aldrich (97%)

M-cresol, Aldrich (97%)

Methanol, Aldrich (99%)

N,N-Dimethylformamide, Aldrich (99%)

3.2 Instruments

In wavenumber range from 4000 cm^{-1}-400 cm^{-1}, FT-IR spectra have been recorded from KBr pellets in solid-state using Mattson Satellite FT-IR spectrophotometer. Ultraviolet Absorption Spectra in solutions were measured on a Varian Cary100 Spectrophotometer. For solid state UV spectra of compounds Perkin–Elmer UV-VIS/NIR Lambdas 19 spectrophotometer is used. The Varian Cary Eclipse Spectrophotometer at excitation wavelength, λ_{exc}=485 nm were used for emission and excitation spectra measurements of compounds.

NMR spectra were recorded by Broker/XWIN-NMR (400 MHz for ^{1}HNMR, 100.6 MHz for ^{13}CNMR) on Fourier transform mode. The chemical shift value were reported in δ units (ppm) by assigning TMS (Tetramethyl Silane) as internal standard. The coupling constants (*J*) for all compound are reported in hertz (Hz).

Finnigan MAT 311 A instrument at 70 eV ionization energy is used for recording mass spectra. Thermogravimetric thermograms were obtained from Perkin Elmer-TGA Pyris1, and the compounds were heated at a rate of 10 ^{o}C/min under N_2 atmosphere. Thermal analyses were measured by using Perkin Elmers-DSC Model, Jade. The compounds were heated at a rate of 10 ^{o}C/min under N_2 atmosphere.Cyclic voltammograms and square wave voltammograms were recorded with a computer controlled Gamry instrument equipped with Refrence 600 Potensiostat, Galvanostat, and ZRA system. Cyclic voltammograms in solutions were obtained in 10^{-3} M by three-electrode cell having glassy carbon as working-electrode and Pt as counter electrode and Ag/AgCl as a reference electrode. Ferrocene is used as internal

reference. 1 M HCl solution by immobilized voltammetry technique by scan-rate of 50-1000 (mVs^{-1}) and 60-150 Hz as frequency were used to record Solid state redox potential. Morphology of the samples was performed on S-360 scanning electron microscopy.

3.3 Methods of Syntheses

3.3.1 Syntheses of 1, 7-Dibromoperylene-3,4:9,10-Tetracarboxylic Dianhydride (Br-PDA)

Core-brominated perylene bisanhydride (Figure 3.1) were prepared by a slightly modified literature. Using bromine and a catalytic amount of Iodine in sulfuric acid.

5.7 g (14.54 mmol) of PDA were solved in 90 ml conc. H_2SO_4 for 24 h at 50 ^oC then 1.66 ml (32.4 mmol) Bromine was added dropwise over 2 h and stirred for 24 h at 85 ^oC. The excess bromine was removed by Argon gas then 200 mL of distilled water was added to product. The resulting precipitate was filtered by suction filtration through a filter paper after 24 h. 6.36 g brownish red Dibromoperylene-3,4:9,10-tetracarboxylic dianhydride (Br-PDA) is produced and washed with water. Yield: 79 % (6.36 g, 79%)

FTIR (KBr), (cm^{-1}): 3055 ($_{C–H\ Aromatice}$); 1777 and 1730 ($_{C=O\ anhydride}$); 1588 and 1499 ($_{C=C\ Stretching}$); 1036 ($_{C\text{-}O\text{-}C\ Stretching}$); 806 and 732 ($_{C\text{-}H\ bend}$) and 684 ($_{C\text{-}Br}$); cm^{-1}. UV-vis (DMF), (λ_{exc} = 485 [M^{-1} cm^{-1}]): 426, 487, 517 nm. Fluorescence (DMF), (λ_{exc} = 485 [M^{-1} cm^{-1}]): 552, 582 nm.

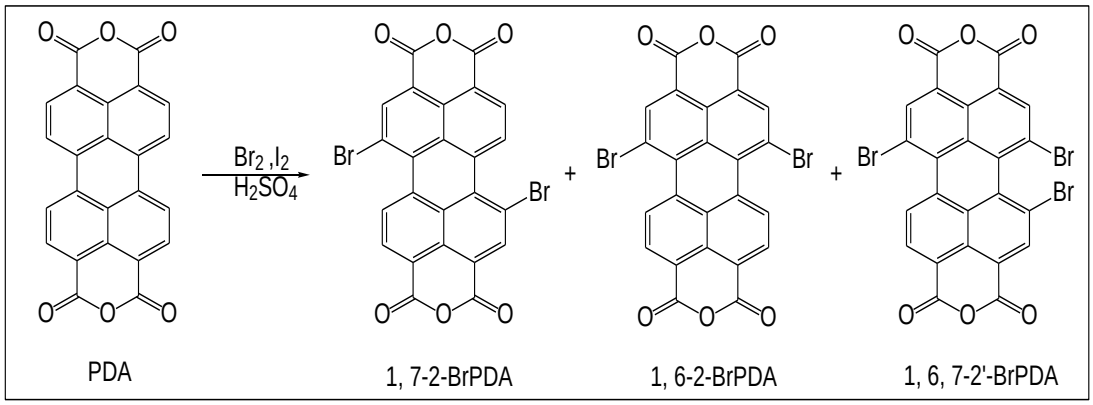

Figure 3.1: Synthetic Route of Isomeric Forming in the Bromination of Perylene Bisanhydride (Br-PDA)

3.3.2 Syntheses of 1, 7-diphenoxyperylene-3,4:9,10-tetracarboxylic dianhydride (BP-PDA)

3 gr (4.46 mmol) 1, 7-Diboromo -3, 4:9, 10-perylenetetracarboxylic dianhydride (Br-PDA) with 1.5 g (15.9 mmol) Phenol and 1.865g (13.5 mmol) K_2CO_3 was refluxed in 200 ml of DMF for 28 h under argon gas. The solution was cooled to room temperature and poured into mixture of acetic acid and cooled water (1:1) and the precipitate filtrated off after 24 h at -8 ^oC. The crude dark purple product was washed with water and methanol, then crystalized several times with DMF and methanol to obtain 2.1 g of 1,7-diphenoxyperylene perylene-3,4:9,10-tetracarboxylic acid dianhydride (BP-PDA). Yield: 81% (2.18 g, 81 %)

FTIR (Figure 4.6, KBr, thin film, cm^{-1}): 3065 (aromatic C-H stretch), 1768 and 1730 (anhydride C=O stretch), 1590 (aromatic C-C stretch), 1235−1158 (C=O stretching), 1014 (amide C-O-C stretch), 806 and 747 (aromatic C-H bend). 1HNMR, (500 MHz, DMSO-d6) Δh (ppm)=8.53 (d, J=5.0 Hz, 2 Ar-H, H-C(6), H-C(12)), 8.31 (d, J=5.0 Hz, 2 Ar-H, H-C(5), H-C(11)), 8.22 (s, 2 Ar-H, H-C(2), H-C(8)), 8.02 (m, 10 Ar-H, H-C(18–22), H-C(18′-22)); UV/Vis (DMF): λmax (nm) (ε)=387, 530, 653, 713.

Fluorescence (DMF, λexcit.=485 nm): λmax (nm)=572. Fluorescence quantum yield (DMF, reference dicarboxiimide with Φ_f=100%, λ_{excit}=485 nm)=60 %. Anal. Calcd. $C_{36}H_{16}O_8$ (Mw, 576.51); C, 75.00; H, 2.80. Found: C, 75.32; H, 2.96.

3.3.3 Syntheses of N,N´-Di(phenoxy)-1,7-Diphenoxyperylene-3,4,9,10-Perylenetetracarboxy Diimide (BP-PPI)

200 mg of "1,7-diphenoxyperylene perylene-3,4:9,10-tetracarboxylic acid dianhydride" (BP-PDA) (3.47 mmol) was mixed with 150 mg of 4-aminophenol (13.88 mmol) and 50 ml Isoquinoline were stirred at 80 ^oC over 2 h, 6 h at 150 **^oC** and 6h at 180^oC , under Argon gas. The reaction mixture was cooled to room temperature and poured dropwise into HCl 1 M (50 mL) after 24 h the resulting precipitate was precipitated then washed with water and methanol. The crude product was crystalized several times with mixture of DMF and n-Hexane and washed with water and Methanol (5:1) to obtain 3.13 g (4.13 mmol) of BP-PPI as a dark red solid. Yield: 77% (2.018 g, 77%)

FTIR (Figure 4.7, KBr, thin film, cm^{-1}): 3450 (O-H stretch), 3070 (aromatic C-H stretch), 1698 and 1654 (imide C=O stretch), 1594 (aromatic C=C stretch), 1357 (C=N stretching), 1199 (C−O−C ether), 1150 (C=O e C stretching), 846 and 758 (aromatic C-H bend).

^{1}HNMR, δH (ppm) (500 MHz, DMSO)=8.53 (d, J=5.0 Hz, 2 Ar-H, HC (6), H-C (12)), 8.31 (d, J=5.0 Hz, 2 Ar-H, H-C (5), H-C (11)), 8.22 (s, 2 Ar-H, H-C(2), H-C(8)), 8.02 (m, 10 Ar-H, H-C (17−21), HC (17'−21')). UV/Vis (DMF): λmax (nm) (ε_{max}) =300, 495. Fluorescence (DMF, λ_{excit}=485 nm): λ_{max} (nm) =576. Fluorescence quantum yield (DMF, reference (dicarboxiimide) with Φ_f=1%, λ_{exc}=485 nm) = 40%. Anal. Calcd.

for $C_{48}H_{26}N_2O_8$ (Mw, 758); C, 67.73; H, 4.11; N, 4.98; H. Found: C, 68.38; H, 3.45; N, 4.69.

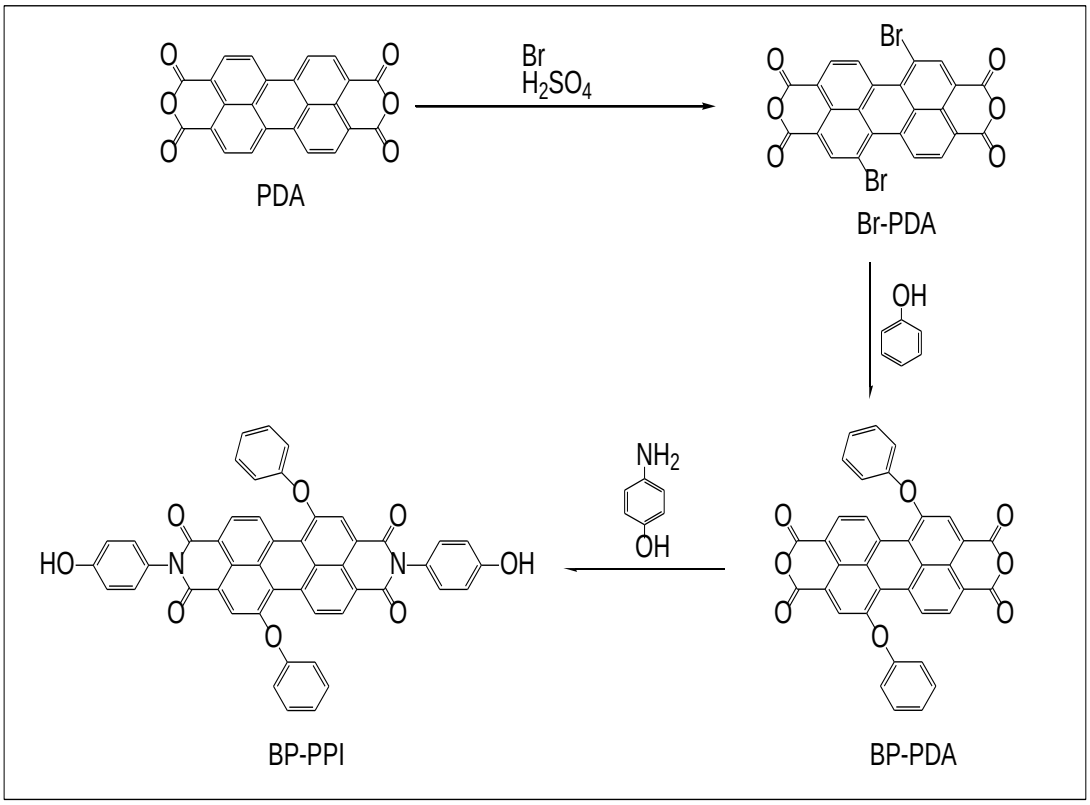

Figure 3.2: Synthetic Route of BP-PPI

3.3.4 Syntheses of N, N´-Di(dodecyl)-1,7-Di-3-Amino-9-Ethylcarbazol Perylene-3,4,9,10-Perylenetetracarboxy Diimide (BC-PDD)

BC-PDD were synthesized by a three step procedure as the details described below:

Bromination of PDA to produce Br-PDA as explained in 3.3.1

1. Imidization of Br-PDA to synthesize (Br-PDD)
2. Synthesize of (BC-PDD)

3.3.4.1 Synthesize of N,N´-Di(dodecyl)-1,7-Dibromo Perylene-3,4,9,10-Perylenetetracarboxy Diimide (Br-PDD)

A suspension of BrPDA (1.375 g, 2.5 mmol) obtained in the above reaction (section 3.3.1), Dodecylamine (0.93 g, 5 mmol) and Zn-acetate ($Zn(OAc)_2.2H_2O$) (0.55 g, 2.50 mmol) in 40 ml of isoquinoline were stirred under argon at 100 ^oC for 4h. The resulting mixture was heated at 170 ^oC for 6 h, at 190 ^oC for 2 h, and at 200 ^oC for 2 h during which time the progress of reaction was monitored by TLC. After cooling down to room temperature the resulting precipitate was filtered, and red crude product was purified via soxhlet extraction in methanol for 2 days. Yield: 85% (2.3 g, 85%).

FTIR (KBr), (cm^{-1}): 3058 ($_{C–H\ Aromatic}$), 2921- 2850 ($_{C–H\ Aliphatic}$), 1698- 1656 ($_{C=O\ imide}$), 1598 ($_{C=O\ Stretching}$), 1346 ($_{C\text{-}N\ Stretching}$), 748 ($_{C\text{-}H\ bend}$), 640 ($_{C\text{-}Br\ Stretching}$); cm^{-1}. UV-Vis (NMP): (λ_{exc} = 485 [M^{-1} cm^{-1}]): 426, 467, 694, 764 nm. Fluorescence (NMP): (λ_{exc} = 485 [M^{-1} cm^{-1}]): 485, 535, 574 nm.

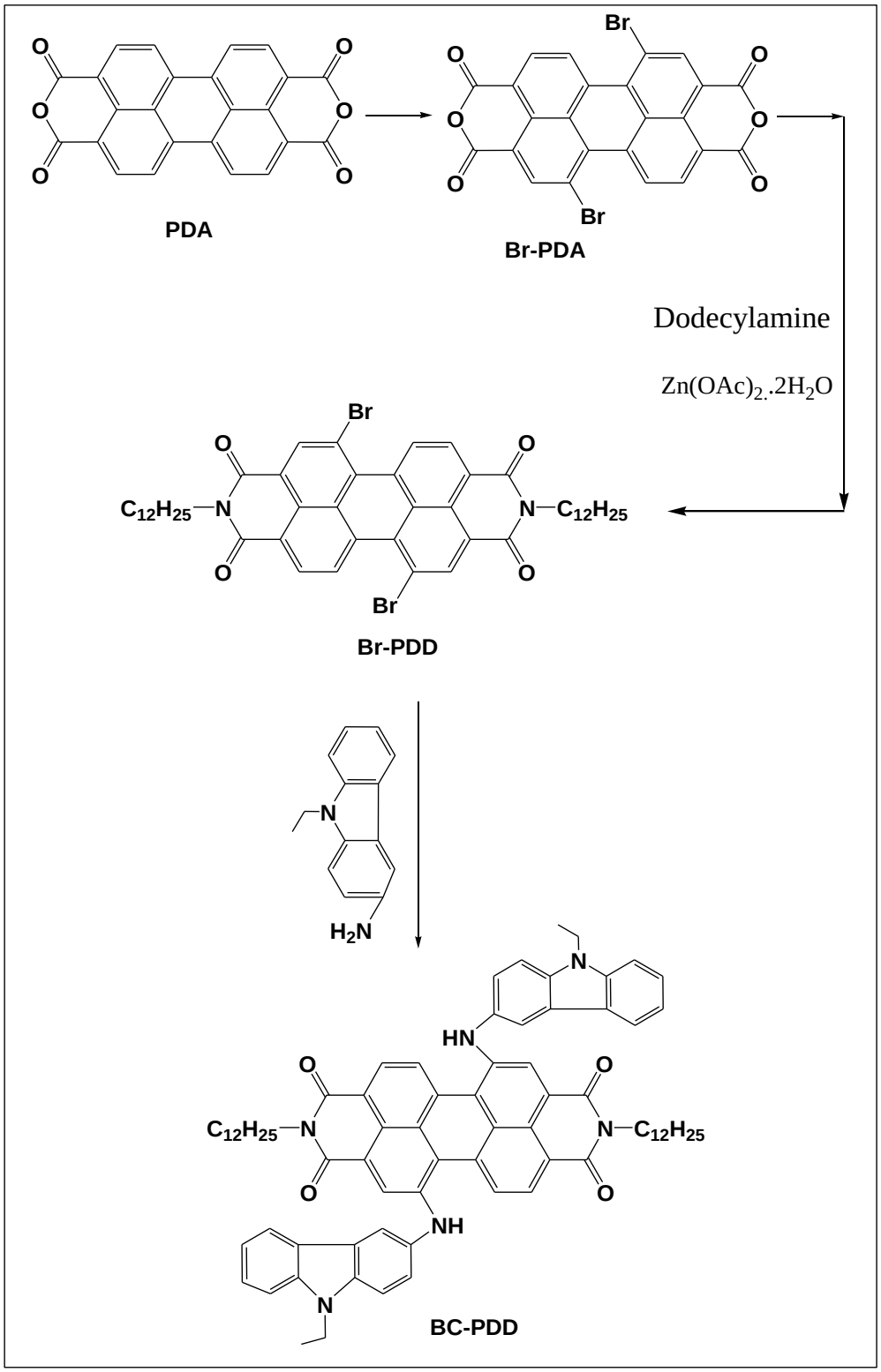

Figure 3.3: Synthetic Route of Production BC-PDD

3.3.4.2 Synthesize of N,N′-Didodecyl-1,7-Di(3-Amino-9-Ethylcarbazole) Perylene-3,4,9,10-Tetracarboxylic Acid Diimide (BC-PDD)

A mixture of 1 g (1.13 mmol) of Br-PDD and 0.952 g (4.52 mmol) of 3-amino-9ethylcarbazole in a mixture of 30 ml of isoquinoline and 10 ml of m-Cresol was stirred under Argon gas for 4 h at room temperature then 12h at 100 ^{o}C and for an additional 12 h at 190 ^{o}C. The resulting mixture was cooled to RT and 300ml of methanol was added. Resulting precipitate was collected by filtration and purified by soxhlet extraction with methanol for 2 days. Yield: 76% (1.29 g, 76%)

^{1}H NMR (400 MHz, $CHCl_3$), δ = 9.02 (d, 2H, *J*=8 Hz), 8.59 (d, 2H, *J*=8 Hz), 7.68 (s, 2H), 7.02 (t, 4H, *J*=8 Hz), 6.34 (t, 4H, *J*=8 Hz), 6.31 (d, 4H, *J*=8 Hz), 4.02 (d, 2H of NH, *J*=8 Hz), 3.29 (d, 4H, *J*=8 Hz), 1.59 (s, 2 OH), 1.28 (d, 4H, *J*=8 Hz), 0.96 (d, 4H, *J*=8 Hz). FTIR (KBr), (cm^{-1}): 3297 ($_{N–H\ Stretching}$), 3054 ($_{C–H\ Aromatic}$), 2922-2851 ($_{C–H\ Aliphatic}$), 1698- 1660 ($_{C=O\ imide}$), 1596 ($_{C=O\ Stretching}$), 1322 ($_{C-N\ Stretching}$), 812-745 ($_{C-H\ bend}$); cm^{-1}. UV-Vis (NMP): (λ_{exc} = 485 [M^{-1} cm^{-1}]): 698, 762 nm. Fluorescence (NMP): (λ_{exc} = 485 [M^{-1} cm^{-1}]): 536, 575 nm. Anal. Calcd for $C_{76}H_{82}N_6O_4$ (Mw, 1143); C: 76.81%, H: 5.37 %, N: 6.54%, O: 5.32%. Found: C: 79.83%, H: 7.23%, N: 7.35%, O: 5.06%.

3.3.5 Synthetize of 1, 7-(Diphenoxyperylene Perylene-3, 4:9, 10-Tetracarboxylic Acid Dicarboximide)-3,4:9,10-Tetracarboxylic Anhydride (BPDA-PDA)

The synthetic of BPDA-PDA was consisted of four step as follows: (figure 3.4)

1. Bromination of perylene dianhydride as described on 3. 3.1
2. Synthesize of N-(4-hydroxyphenyl)-3,4,9,10-perylenetetracarboxylic-3,4-anhydride-9,10-imide (PMI)
3. Synthetic of 7-(diphenoxyperylene perylene-3, 4:9, 10-tetracarboxylic acid dicarboximide)-3,4:9,10-tetracarboxylic anhydride (BPDA-PDA)

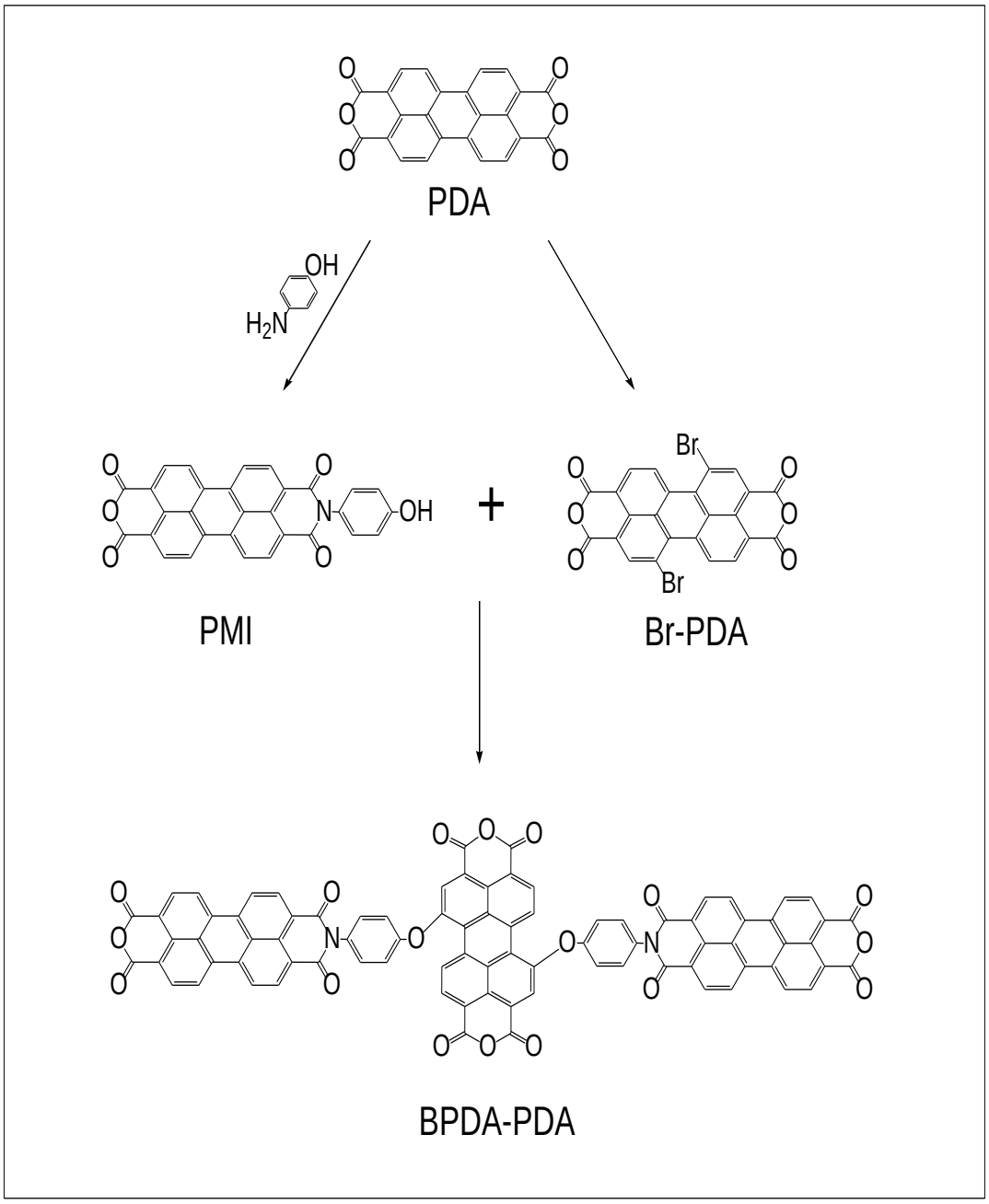

Figure 3.4: Synthetic Route of BPDA-PDA

3.3.5.1 Synthesis of N-(4-Hydroxyphenyl)-3,4,9,10-Perylenetetracarboxylic-3,4-Anhydride-9,10-Iimide (PMI)

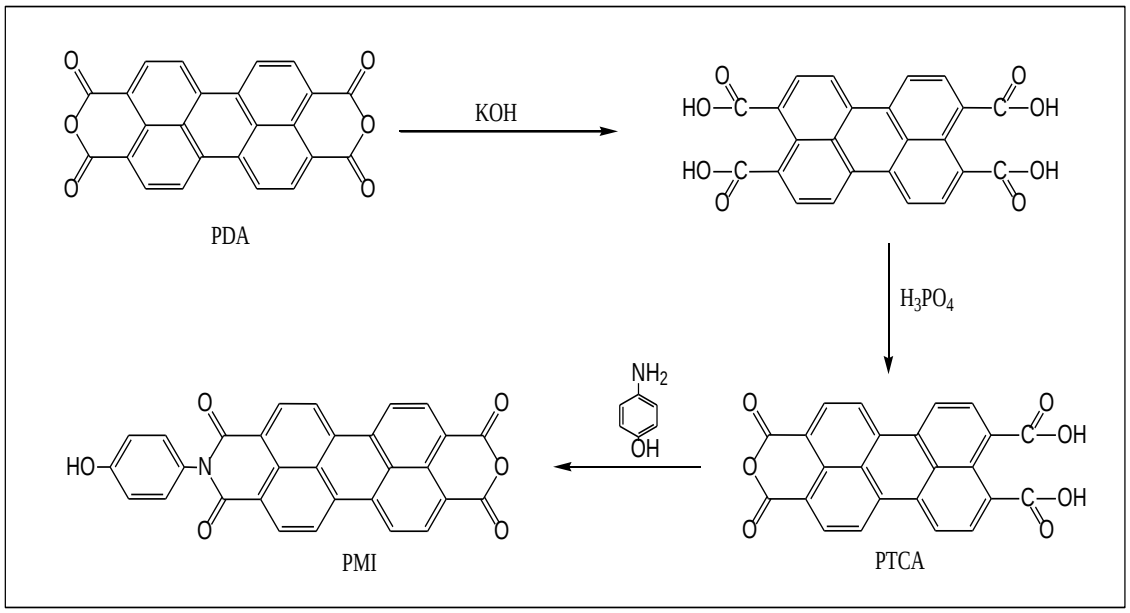

Figure 3.5: Synthetic Route of PMI

3.3.5.1. Synthesis of PTCA

3 g (7.6 mmol) of PDA was stirred in 35 mL of KOH solution (5%,) over 4 h at 90 ^{o}C after cooling to room temperature, 12.5 mL H_3PO_4 (10%) was added and stirred for 1 h at 90 ^{o}C. cured product was filtered and washed with water. Yield: 89% (3.1 g, 89%)

3.3.5.2 Synthesis of PMI

1 g (2.2 mmol) of PTCA and 4-aminophenol hydrochloride C_6H_7NO. HCl 3.17 g (8.8 mmol) with 50 mL water were stirred at 0-5 ^{o}C for 4 h then at 90 ^{o}C for 2 h, 12.5 mL potassium carbonate (25%,) was added and stirred for another 1 h at 90 ^{0}C. The precipitate was collected by vacuum filtration the washed with potassium carbonate (2%) and precipitate was dissolved in 100 mL KOH (3.5%), heated to 90 ^{0}C, kept at this temperature for 5 min and filtered while hot. After acidification with hydrochloric acid (10%), the precipitate was collected by vacuum filtration and dried in vacuum at

100 ^{o}C and washed with water until colorless then with ethanol. Yield: 98% (3.02 g, 98%).

FTIR (KBr), (cm^{-1}): 3432 ($_{O–H\ Stretching}$); 3104 ($_{C–H\ Aromatic}$); 1761, 1725 ($_{C=O\ Anhydride}$); 1720 ($_{C=O}$ imide); 1584 ($_{C=O\ Stretching}$); 1499, 1401 ($_{C\text{-}N\ Stretching}$); 1292 ($_{C\text{-}O\text{-}C\ ether}$); 800, 728 ($_{C\text{-}H\ bend}$). UV-Vis (DMF): ($\lambda_{exc}$ = 485 [M^{-1} cm^{-1}]): 453, 482, 518. Fluorescence (DMF): (λ_{exc} = 485 [M^{-1} cm^{-1}]): 532, 570, 618 nm.

3.3.5.3 Synthetic of 1, 7-(Diphenoxyperylene Perylene-3, 4:9, 10-Tetracarboxylic Acid Dicarboximide)-3,4:9,10-Tetracarboxylic Anhydride (BPDA-PDA)

1.06 g (2.2 mmol) of PMI with 0.549 g (1 mmol) of Br-PDA and 0.41 g (3 mmol) K_2CO_3 was refluxed in 200 ml of DMF for 28 h under argon gas. The solution was cooled to room temperature and poured into mixture of acetic acid and cooled water (1:1) and the precipitate filtrated off after 24 h at -8 ^oC. the crude dark purple product was washed with water and methanol, then washed several times with water and methanol. Yield: 77% (2.3 g, 77%).

FTIR (KBr), (cm^{-1}): 3096 ($_{C–H\ Aromatic}$); 1773, 1737 ($_{C=O\ anhydride}$); 1592 ($_{C=C\ Aromatic,\ Stretching}$); 1298 ($_{C-O-C\ ether}$); 1017 ($_{C-O-C\ Aromatic,\ Stretching}$); 806, 731 ($_{C–H\ bend}$); cm^{-1}. UV-Vis (DMF): (λ_{exc} = 485 [M^{-1} cm^{-1}]): 485, 518, 667. Fluorescence (DMF): (λ_{exc} = 485 [M^{-1} cm^{-1}]): 535, 570 nm. Anal. Calcd for $C_{96}H_{40}N_4O_{18}$ (Mw, 1537.23); C: 75.00%, H: 2.62%, N: 3.64%, O: 18.73%. Found: C: 65.84%, H: 3.26%, N: 3.33%, O: 27.57%.

3.3.6 Synthetic of N,N′-Didehydroabiethyl-1,7-Di((N`-Dehydroabiethyl,N-Phenoxy) Perylene-3,4,9,10-Tetracarboxylic Acid Diimide) Perylene-3,4,9,10-Tetracarboxylic Acid Diimide (BPDI-PDI)

0.5 g (0.37 mmol) of 2PDA with 0.527 g (1.84 mmol) of 4-dehyrdroebiethylamine and Zn-acetate (0.08 g, 0.37 mmol) in 60 ml of isoquinoline was stirred under argon at 100 ^{o}C for 4h. The resulting mixture was heated at 150 ^{o}C for 6 h, at 180 ^{o}C for 2 h. After cooling down, methanol is used to get precipitate product was. Brownish crude product was purified via soxhlet extraction in water and methanol. Yield 72% (0.62g, 72%) (Figure 3.5)

^{1}H NMR (400 MHz, $CHCl_3$), δ = 8.96 (d, 2H, *J*=8 Hz), 8.26 (d, 2H, *J*=8 Hz), 8.12 (s, 2H), 7.68 (t, 4H, *J*=8 Hz), 7.14 (t, 4H, *J*=8 Hz), 6.97 (d, 4H, *J*=8 Hz), 3.52 (d, 2H of NH, *J*=8 Hz), 3.03 (d, 4H, *J*=8 Hz), 2.26 (s, 2 OH), 1.54 (d, 4H, *J*=8 Hz), 1.26 (d, 4H, *J*=8 Hz), 1.07 (d, 4H, *J*=8 Hz), 0.92 (d, 4H, *J*=8 Hz). ^{13}C NMR (100 MHz, DMF, ppm): δ = 164.1, 147.6, 145.5, 135.1, 130.0, 127.2, 124.3, 46.4, 40.0 37.9, 33.4, 30.5, 26.2, 109.95. FTIR (KBr), (cm^{-1}): 3050 ($_{C–H\ Aromatic,\ Stretching}$); 2925, 2867 ($_{C\text{-}H\ aliphatic}$); 1698, 1656 ($_{C=O\ imide}$); 1594 ($_{C=C\ Aromatic,\ Stretching}$); 1251 ($_{C\text{-}O\text{-}C\ ether}$); 806, 752 ($_{C–H\ bend}$); cm^{-1}. UV-Vis (DMF): (λ_{exc} = 485 [M^{-1} cm^{-1}]): 458, 487, 524. Fluorescence (DMF): (λ_{exc} = 485 [M^{-1} cm^{-1}]): 539, 574 nm.

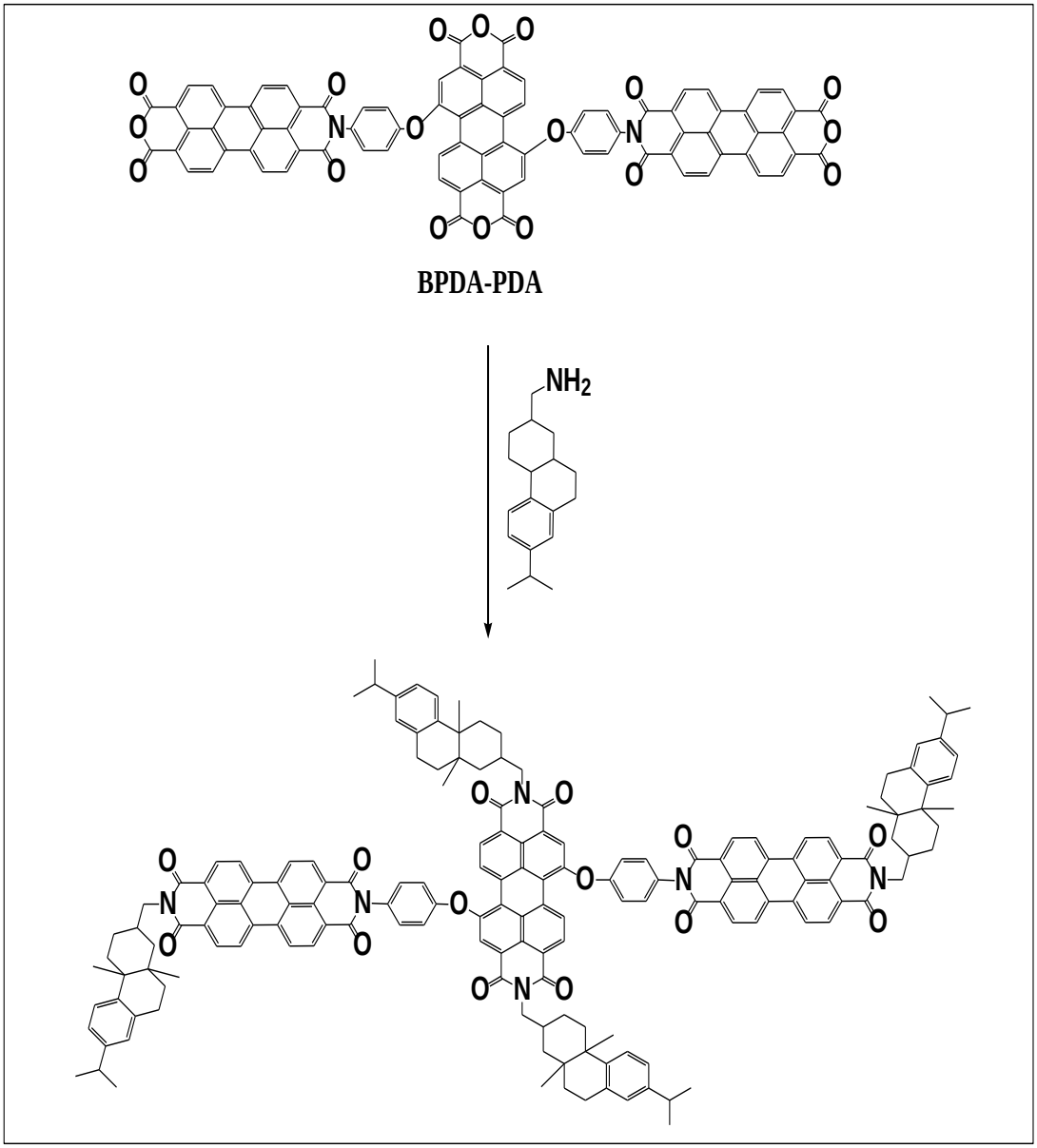

Figure 3.6: Synthetic Route of BPDI-PDI

3.3.7 Synthesize of N,N′-Didehyphenol-1,7Di(Propyltriethoxylsiline) Perylene-3,4,9,10-Tetracarboxylic Acid Diimide (BP-PDSi)

0.797 g (1.381 mmol) of BP-PDA and 0.7 ml (3.03 mmol) of 3-Aminopropyltriethoxysilane 99% (APTES) in 40 ml isoquinoline were stirred for 10 min into a Flask under argon area at room temperature. Then heated to 80 ^{o}C for 3h, 110 ^{o}C for 2 h and 130 ^{o}C for 3 h, after coming to room temperature the cold methanol is used to get precipitation and washed several times with methanol and acetone. Yield 68% (1.02 g, 68%)

^{13}C NMR (300 MHz, solid state, ppm): δ = 184.7, 156.4, 144.9, 103.9, 41.5, 23.8, 9.4, 4.5. FTIR (KBr), (cm^{-1}): 3355 ($_{O–H}$); 2931 ($_{C\text{-}H\ Aliphatic}$); 1690, 1655 ($_{C=O}$); 1440, 1342 ($_{C\text{-}N}$); 1122 ($_{C\text{-}Si}$); 1035 ($_{Si\text{-}O}$); 750, 804 ($_{C\text{-}H\ bend}$), cm^{-1}.

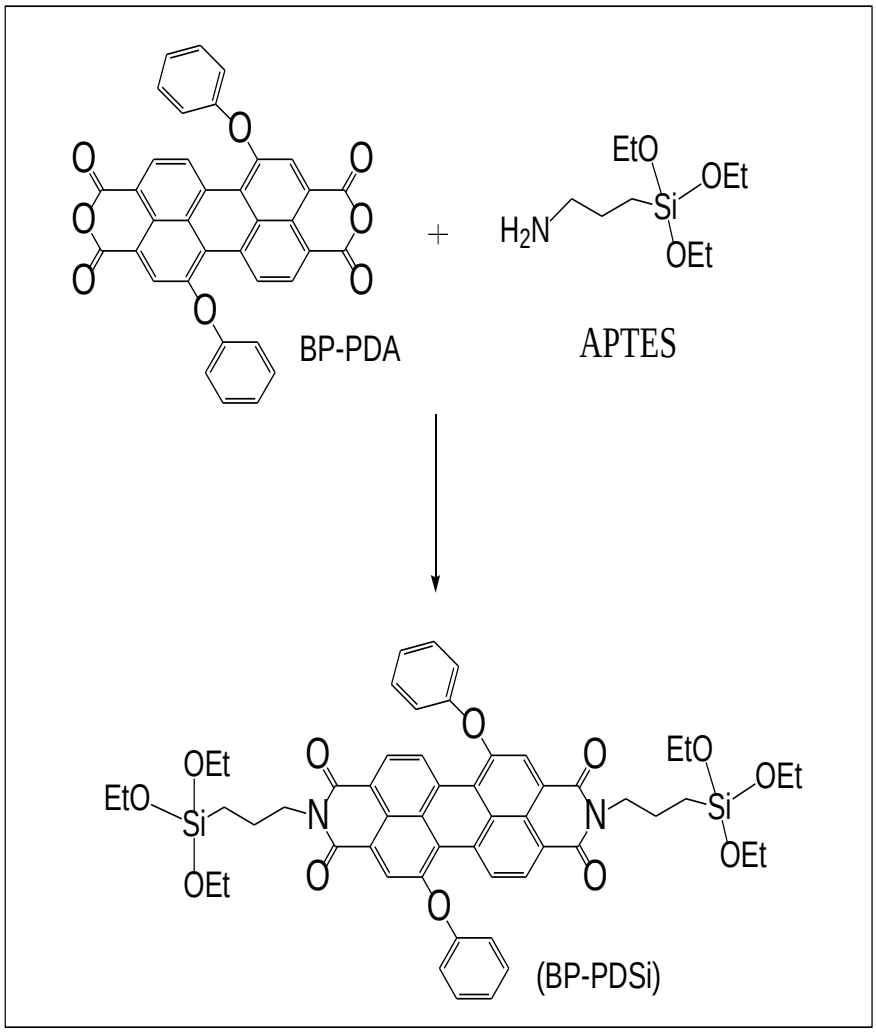

Figure 3.7: Synthetic Route of BP-PDSi

3.3.8 Synthesize of Nano-N,N′-Didehyphenol-1,7-Di(Propyltriethoxylsiline) Perylene-3,4,9,10-Tetracarboxylic Acid Diimide (Nano-BP-PDSi)

0.5 g of synthesized nanosilica (NSi) were completely dried was suspended in 60 ml of dried toluene, then 0.5 g (0.46 mmol) of BP-PDSi were added to reaction and refluxed for 24 h under argon atmosphere at 45 ^{o}C ,after coming to room precipitation were filtrated off and washed well with dichloromethane and hot water.

FTIR (KBr), (cm^{-1}): 3450 ($_{O–H}$); 2939 ($_{C\text{-}H\ Aliphatic}$); 1655, 1599 ($_{C=O}$); 1509 ($_{C\text{-}N}$); 1077 ($_{C\text{-}Si}$); 804 ($_{C\text{-}H\ bend}$), cm^{-1}.

3.3.9 Synthesize of Poly-N,N′-Didehyphenol-1,7-Di(Propyltriethoxylsiline) Perylene-3,4,9,10-Tetracarboxylic Acid Diimide (BP-PPDSi)

0.797 g (1.381 mmol) of BP-PDA and 6.55 ml (28 mmol) of 3-Aminopropyltriethoxysilane 99% (APTES) were stirred for 10 min into a Flask under argon area at room temperature. Then heated to 80 ^{o}C for 3 h, 110 ^{o}C for 2h and 130 ^{o}C for 3 h, after coming to room temperature the cold methanol is used to get precipitation and washed several times with methanol and acetone. Yield 68% (1.02g, 68%).

FTIR (KBr), (cm^{-1}): 3355 ($_{O–H}$); 2931 ($_{C\text{-}H\ Aliphatic}$); 1690, 1655 ($_{C=O}$); 1440, 1342 ($_{C\text{-}N}$); 1122 ($_{C\text{-}Si}$); 1035 ($_{Si\text{-}O}$); 750, 804 ($_{C\text{-}H\ bend}$), cm^{-1}.

3.3.10 Synthesis of Nano Silica and Study the Effect of Different Parameters on Silica Dimension

The Nanosilica particles were synthesized by hydrolysis of TEOS. 17.2 ml TEOS in 182 ml ethanol was drop-wise added (with 18 ml/min) into a mixture of ammonium hydroxide (0.08 mol), ethanol (163.54 ml) and water (1.94 mol) with continuous stirring for 6 h at 70 ^{o}C. After 24 h, white silica particles were gradually precipitated into flask and nanoparticles were separated from the solution with centrifugal separation. The separated particles were washed with deionized water and ethanol, and finally were dried at 80 ^{o}C for 4h in vacuum oven.

FTIR (KBr), (cm^{-1}): 3449 ($_{O–H}$); 1637-1706 ($_{O–H}$); 1105 ($_{Si–O–Si}$); 810 ($_{Si-O-Si}$); 467 ($_{Si–O}$); cm^{-1}.

In the next step, 0.6 g of Nanosilica in a neck flask with dropping funnel and gas inlet tube, in inert atmosphere of argon and 0.98g Chlorosulfuric acid (98%) was added in a period of 30 min drop-wise at room temperature. The mixture was stirred by using of magnetic stirrer for an hour, through the reaction content of inlet tube over water for adsorption HCl gas; 1.45g (white solids) of Nanosilica sulfonic acid was obtained. FT-IR (KBr): 3422 (υ O–H); 1638 (υ O–H); 1216 (υ O=S=O); 1072 (υ Si–O–Si); 614 (υ S-O);459 (υ Si–O); cm^{-1}.

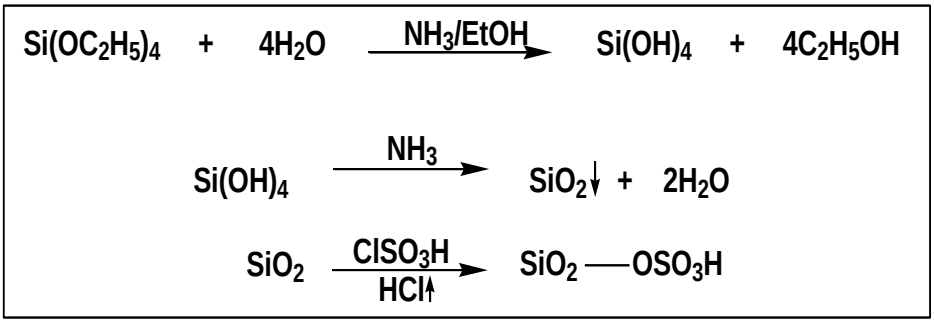

Figure 3.8: Synthetic Route of Nanosilica

3.3.11 Synthesis N, N-bis((S)-(−)-1-phenylethyl)-3,4,9,10- perylene diimide (PDI)

The (PDI-1) was synthesized as described in a previous paper. Perylene-3,4,9,10-tetracarboxylic dianhydride (1.00 g, 2.60 mmol),(S)-(−)-1-phenylethylamine (0.64 mL, 4.96 mmol) and $Zn(OAc)_2 \cdot 2H_2O$ (0.55 g, 2.50 mmol) were heated in a mixture of solvents (60 mL m-cresol and 8 mL isoquinoline) under N_2 atmosphere at 100 °C for 4 h, 160 °C for 6 h, 180 ◦C for 2 h and finally at 200 °C for 2 h. The precipitation was obtained by adding cooled solution into 300 ml aceton, then product was filtered off and dried at 100 °C under vacuum. In order to remove the unreacted amine the product was treated with methanol in a soxhlet extraction apparatus for 1 day and (PDI-1) was obtained as a red powder.

FT-IR (KBr): 3450 (υ_{O-H}); 3063 ($\upsilon_{C-H\ Ar}$); 2965 ($\upsilon_{O-H\ Aliphatic}$); 1697 ($\upsilon_{C=O}$); 1097 ($\upsilon_{Si-O-Si}$) cm^{-1}.

3.3.11.1 Synthesis Nanosilica-N, N-bis((S)-(−)-1-Phenylethyl)-3,4,9,10- Perylene Diimide (NSPDI)

The NSPDI was synthesized by a self-assembly method. According to this, 0.01443 g of (PDI -1) and 1.16 g of Nano silica sulfonic acid (NSSA), was mixed in solid state for 1h then was left for 24h.The product was washed well with deionized water and ethanol, respectively, and then dried in vacuum oven at 30 ^{o}C for 12h to obtain NSPDI as violet-black powder.

FTIR (KBr), (cm^{-1}): 3460 ($\upsilon_{O–H}$), 2856 ($\upsilon_{C–H\ aliphatic}$), 1686, 1638 ($\upsilon_{C=O}$), 1597 ($\upsilon_{C=C}$), 1577 ($\upsilon_{O-H}$), 1398 -1363 ($\upsilon_{C-N}$), 1226 ($\upsilon_{O=S=O}$), 1105 ($\upsilon_{Si–O–Si}$), 807 ($\upsilon_{Si–O–Si}$), 575 ($\upsilon_{S–O}$), 466 ($\upsilon_{Si–O}$); cm^{-1}. UV-Vis (H_2SO_4): (λ_{exc} = 485 [M^{-1} cm^{-1}]):518, 551, 559, (DMSO); 462, 489, 525, 581, (DMAc); 461, 487, 523, 580, (NMP); 461, 488, 524, 580. Fluorescence: (λ_{exc} = 485 [M^{-1} cm^{-1}]): (H_2SO_4); 630, 682, (DMSO); 537, 578, 621, (DMAc); 532, 572, 618, (NMP); 534, 574, 623.Excitation: (λ_{exc} = 650 [M^{-1} cm^{-1}]):

Chapter 4

DATA AND CALCULATION

4.1 Quantum-Yield

The quantity of reactant particles were creating identified principle products per photon of light is known as a quantum yield. These principle products do function as chain carriers and causes to more than one molecules. The general quantum-yield is the quantity of atoms responding per photons absorbed.

$$\boldsymbol{\Phi} = \frac{\text{number of moles (molecules)of product formed}}{\text{number of photons of radiation absorbed}}$$

The differential quantum-yield is;

$$\boldsymbol{\Phi} = \frac{\mathrm{d[x]/dt}}{\mathrm{n}}$$

d(x) / dt: measurable quantity rate change

(n): the photons number (mole or its equivalent Einstein) absorbed per unit time

Φ: Quantum-yield

4.2 Calculation of Optical Parametres

4.2.1 Maximum Extinction Co-efficients (λ_{max})

The Beer-Lambert's law expounded the relationship between absorbance and concentration of absorbing species, the following equation is used for calculation maximum extinction coefficients:

$\varepsilon_{max} = \frac{A}{cl}$

***A*:** Absorbance

***c*:** Concentration (mol L^{-1})

***l*:** Path length (cm)

ε_{max}**:** Maximum extinction co-efficient ($L.M^{-1}.cm^{-1}$)

ε_{max} calculation of BP-PPI:

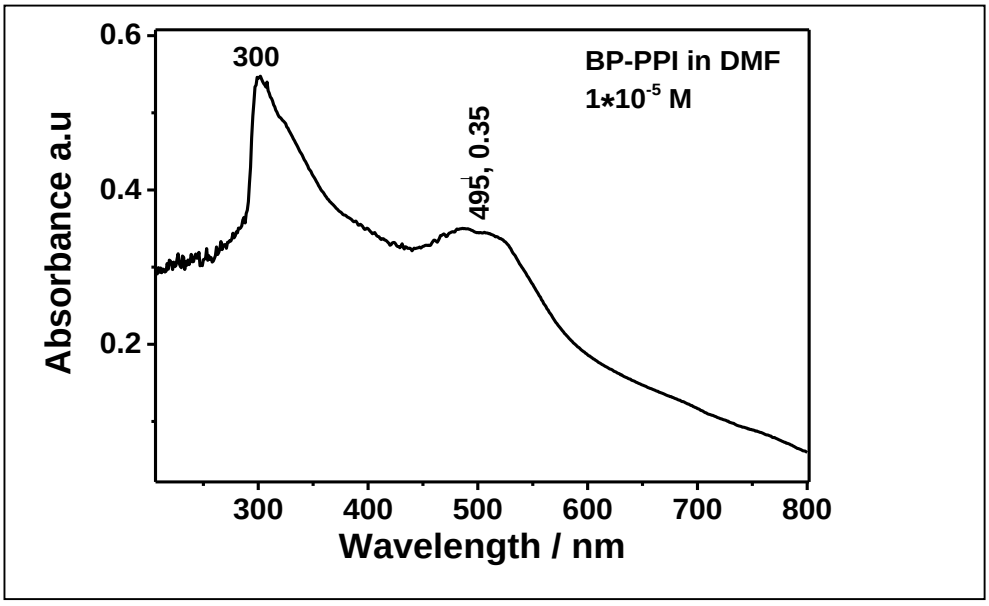

Figure 4.1: Absorbance-Spectrum of BP-PPI in DMF at $1\dot{x}10^{-5}$ M

Absorbance spectrum of BP-PPI (figure 4.1) in the concentration of $1*10^{-5}$ M, at wavelength 495 nm shows 0.42 absorbance.

$$\varepsilon_{max} = \frac{A}{cl} = \frac{0.35}{1\times10^{-5}\,M\times1cm} = 35000 \text{ L.} M^{-1}.cm^{-1}$$

The similar method is used to calculate Maximum extinction co-efficient of all synthesized compounds in different solvents and the result were shown in the following table (Table 4.1).

Table 4.1: Molar Absorptivity Data of BP-PDA, BP-PPI, BC-PDD, BPDA-PDA and BPDI-PDI

Compound	Solvent	Absorbance	λ_{max}	ε_{max}
BP-PDA	DMF	0.35	530	30700
	NMP	0.31	529	30900
	THF	0.32	516	33000
BP-PPI	DMF	0.35	495	35000
	NMP	0.30	487	30000
	THF	0.14	513	13800
BC-PDD	DMF	0.26	524	23000
	DMSO	0.36	526	33000
	NMP	0.22	518	20200
BPDA-PDA	DMF	0.51	518	38000
	DMSO	0.95	518	40900
	NMP	0.32	519	13000
BPDI-PDI	DMF	0.58	524	27300
	DMSO	0.24	527	10800
	NMP	0.93	527	42800

4.2.2 εmax Calculation of BP-PPI from the Plot of Absorbance vs. Concentration

According to Beer Lambert's Law, by the plotting of absorbance versus concentration, Maximum extinction co-efficient can be achieved. The slope of plot is determine the exact amount of the maximum molar absorption co-efficient.

Table 4.2: Different Concentration of BP-PPI and their Corresponding Absorbance Data at λ_{max}=485 nm

concentration	Absobance	λ_{max}
3×10^{-5}	0.72	496
2×10^{-5}	0.62	496
1×10^{-5}	0.35	495
5×10^{-6}	0.23	495
2×10^{-6}	0.09	495
1×10^{-6}	0.062	495

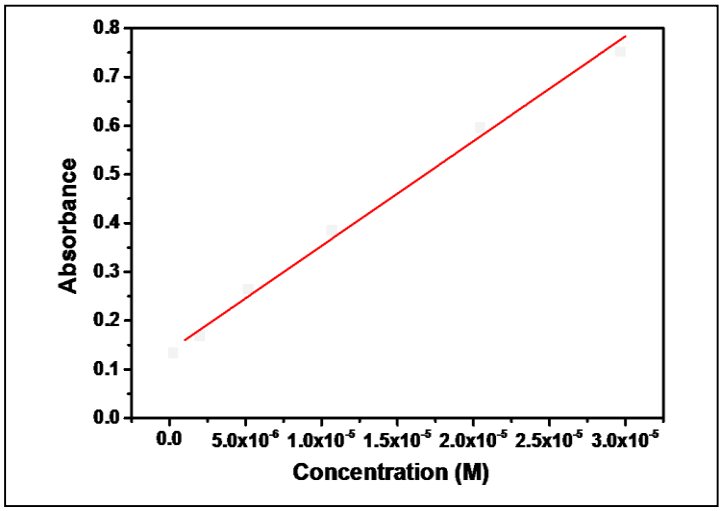

Figure 4.2: Graph of Absorbance Versus Concentration of BP-PPI in in DMF

The slope of the graph 4.2, ε_{max} of BP-PPI $= 32800$ L. $M^{-1}. cm^{-1}$

4.2.3 Fluorescence Quantum Yields (Φ_f)

The Fluorescence is absorbing a photon or light with enough energy by a compound, and then emits it such light which causes to form an energetically excited state. "Fluorescence quantum yield" through fluorescence process is showing the ratio of photons taken to the photons emitted**.**

$$\Phi_f = \frac{A_{std}}{A_u} \times \frac{S_u}{S_{std}} \times \left(\frac{n_u}{n_{std}}\right)^2 \times \Phi_{std}$$

Φ_f: Fluorescence quantum-yield

A_{std}: Absorbance of the reference (at the excitation wavelength)

A_u: Absorbance of the unknown (at the excitation wavelength)

S_{std}: The integrated emission-area across the band of reference

S_u: The integrated emission-area across the band of unknown

n_{std}: Refractive-index of reference solvent

n_u: Refractive-index of unknown solvent

Φ_{std}: Fluorescence quantum-yield of reference

In this research for calculation of fluorescence quantum yield, *N*,*N*_-bis(dodecyl)-3,4,9,10-perylenebis(dicarboximide) is used as a reference compound by reported Φ_f=1 in chloroform

The excited wavelength (λexc = 485 nm) for perylene dyes were similar to the reference.

Fluorescence Quantum Yield of BP-PPI:

The absorbance of BP-PPI in DMF and the reference compound in chloroform were recorded, also their fluorescence and corresponding integrated emission area is recorded.

Au = 0.0179, A_{std} = 0.1082, Sstd = 4100, Su = 317.93, n_{std} = 1.4429 at 20 ^{o}C, n_u =1.4305 at 20 ^{o}C, Φ_{std} = 1.0

$$\Phi_f = \frac{0.1082}{0.0179} \times \frac{317.93}{4100} \times \left(\frac{1.4305}{1.4429}\right)^2 \times 1 \qquad \Phi_f \text{of BP} - \text{PPI} = 0.49$$

The same method is used to measure fluorescence quantum yields of BP-PDA and BP-PPI in different solvents and they were tabulated below (Table 4.3).

Table 4.3: Fluorescence Quantum Yields of BP-PDA, BP-PPI, BC-PDD, BPDA-PDA and BPDI-PDI in Different Solvents

Compound	Solvent	λ_{max}	ε_{max}	Φ_f
BP-PDA	DMF	530	30700	0.61
	NMP	529	30900	0.22
	THF	516	33000	0.46
BP-PPI	DMF	495	35000	0.01
	NMP	487	30000	0.19
	THF	513	13800	0.32
BC-PDD	DMF	524	23000	0.4
	DMSO	526	33000	0.32
	NMP	518	20200	0.07
BPDA-PDA	DMF	518	38000	0.64
	DMSO	518	40900	0.29
	NMP	519	13000	0.06
BPDI-PDI	DMF	524	27300	0.73
	DMSO	527	10800	0.41
	NMP	527	42800	0.27

4.2.4 Half-width of the Selected Absorption $(\Delta\bar{\nu}_{1/2})$

The half-width of maximum absorption is known as full width at half maximum which is measured at half of the maximum intensity of absorbance spectrum as full or half-width of the curve.

$$\Delta\bar{\nu}_{1/2} = \bar{\nu}_{|} - \bar{\nu}_{\|}$$

$\bar{\nu}_{|}, \bar{\nu}_{\|}$ **:** The frequencies of absorption spectrum (cm^{-1})

$\Delta\bar{\nu}_{1/2}$**:** Half-width of maximum-absorption (cm^{-1})

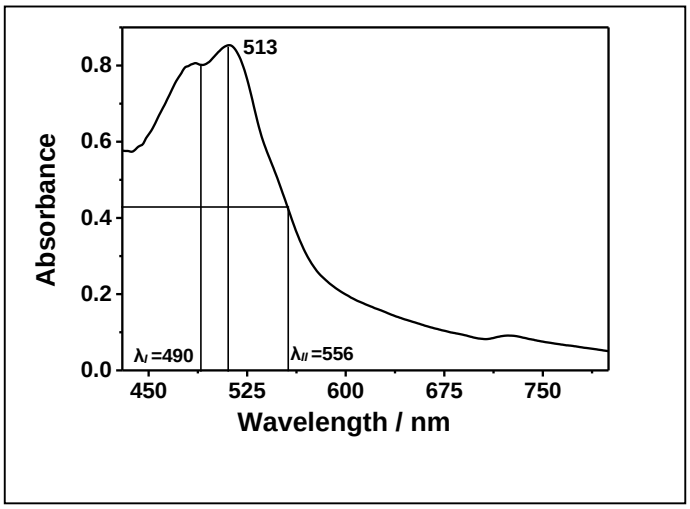

Figure 4.3: Absorption Spectrum of BP-PPI in THF

λ_{max} = 513 nm, λ_I = 490 nm, λ_{II} = 556 nm

$$\lambda_{max} = 513\ nm \times \frac{10^{-9}}{1nm} \times \frac{100\ cm}{1\ m} = 5.13\ \times\ 10^{-5}\ cm$$

$$\bar{\nu}_{max} = \frac{1}{\lambda_{max}} = \frac{1}{5.13\ \times 10^{-5}\ cm} = 18867.92\ cm^{-1}$$

$$\lambda_I = 490\ nm \times \frac{10^{-9}}{1nm} \times \frac{100\ cm}{1\ m} = 4.9\ \times\ 10^{-5}\ cm$$

$$\bar{\nu}_I = \frac{1}{\lambda_I} = \frac{1}{4.9 \times 10^{-5}\, cm} = 20408.16\, cm^{-1}$$

$$\lambda_{II} = 556\, nm \times \frac{10^{-9}}{1nm} \times \frac{100\, cm}{1\, m} = 5.56 \times 10^{-5}\, cm$$

$$\bar{\nu}_{II} = \frac{1}{\lambda_{II}} = \frac{1}{5.56 \times 10^{-5}\, cm} = 17985.61\, cm^{-1}$$

$$\Delta\bar{\nu}_{1/2} = \bar{\nu}_{|} - \bar{\nu}_{\|} = 20408.16 - 17985.61 = 2423\, cm^{-1}$$

4.2.5 Theoretical Radiative Lifetimes (τ_o)

To calculate the theoretical Radiative Lifetimes:

$$\tau_o = \frac{3 \times 10^8}{{V_{max}}^2 \times \varepsilon_{max} \times \Delta V_{1/2}}$$

τ_o **:** Lifetime of Theoretical radiative (ns)

V_{max} : Frequency of the maximum absorption band in cm^{-1}

ε_{max}: The maximum-extinction coefficient at the maximum-absorption wavelength (L mol^{-1} cm^{-1})

$\Delta V_{1/2}$**:** Half-width absorption (cm^{-1})

τ_o for BP-PPI in DMF:

$$\tau_o = \frac{3 \times 10^8}{(20202)^2 \times 35000 \times 7770.9}$$

$$\tau_o = 3.15 \times 10^{-9}\, sec$$

$$\tau_o = 3.15\, ns$$

The same method is used to calculate theoretical Radiative Lifetimes of BP-PDA and BP-PPI in different solvents and the results are tabled in table 4. 5

Table 4.4: Theoretical Radiative-Lifetimes of BP-PDA and BP-PPI in Different Solvents

Compound	Solvent	λ_{max}	ε_{max}	$\bar{V}^2_{max}(cm^{-2})$	$\Delta V_{1/2}\,(cm^{-1})$	τ_o
BP-PDA	DMF	530	30700	18867.92453	2858.808704	11.20
	NMP	529	30900	18903.59168	3532.295271	8.973
	THF	516	33000	19379.84496	2869.960576	9.839
BP-PPI	DMF	495	35000	20202.0202	7770.884251	3.153
	NMP	487	30000	20533.8809	6739.436037	4.105
	THF	513	13800	19493.17739	3819.709702	17.47

4.2.6 Theoretical Fluorescence Lifetimes (τ_f)

The theoretical fluorescence lifetime states the molecule theoretical average time which before fluorescence stays in the excited state. The theoretical fluorescence lifetime is calculates from the below equation.

$$\tau_f = \tau_o . \Phi_f$$

τ_f**:** Fluorescence lifetime in ns

τ_o**:** Theoretical radiative lifetime in ns

Φ_f**:** Fluorescence quantum yield

Theoretical Fluorescence Lifetime of BP-PPI in DMF:

$$\tau_f = \tau_o . \Phi_f$$

$$\tau_f = 3.15\,ns \times 0.01 = 0{,}032\,ns$$

The theoretical fluorescence lifetimes of the other compounds also were recorded using the same method. The results were summarized in table 4.6.

Table 4.5: The Theoretical Fluorescence Lifetimes of BP-PDA, BP-PPI, BC-PDD, BPDA-PDA and BPDI-PDI in Different Solvents

Compound	Solvent	λ_{max}	Φ_f	τ_o	τ_f
BP-PDA	DMF	530	0.61	11.20	6.83
	NMP	529	0.22	8.973	1.97
	THF	516	0.46	9.839	4.53
BP-PPI	DMF	495	0.01	3.153	0.03
	NMP	487	0.19	4.105	0.78
	THF	513	0.32	17.47	5.59
BC-PDD	DMF	524	0.4	6.565	2.10
	DMSO	526	0.32	33.09	2.31
	NMP	518	0.07	16.95	10.8
BPDA-PDA	DMF	518	0.64	16.59	4.81
	DMSO	518	0.29	44.83	2.69
	NMP	519	0.06	28.76	20.9
BPDI-PDI	DMF	524	0.73	60.53	24.2
	DMSO	527	0.41	19.32	5.22
	NMP	527	0.27	6.565	2.10

4.2.7 Fluorescence Rate Constants (k_f)

The speed of impulsive emission of molecule is known as a theoretical fluorescence rate constant. Fluorescence Rate-Constants is calculated by following process:

$$k_f = {}^{1}/_{\tau_o}$$

***k*f:** Rate constant of Fluorescence (s^{-1})

τ_o**:** Lifetime of Theoretical-Radiative in s

Fluorescence Rate Constant of BP-PPI in DMF

$$k_f = {}^{1}/_{3.15} \times 10^{-9}\, s^{-1} = 3.17 \times 10^{8}\ s^{-1}$$

The k_f of BP-PDA and BP-PPI are calculated by the same method and tabled in table 4. 6.

Table 4. 6: The Fluorescence Rate-Constant of BP-PDA and BP-PPI

Compound	Solvent	λ_{max}	τ_o	k_f
BP-PDA	DMF	530	11.20202	8.93×10^{7}
	NMP	529	8.973542	1.11×10^{8}
	THF	516	9.839603	1.02×10^{8}
BP-PPI	DMF	495	3.153116	3.17×10^{8}
	NMP	487	4.105643	2.44×10^{8}
	THF	513	17.47404	5.72×10^{7}

4.2.8. Rate Constants of Radiationless Deactivation (*k*d)

The below equation is used to calculate "the rate constants of radiationless deactivations" of the compounds.

$$\boldsymbol{k_d} = (\boldsymbol{k_f}/\Phi_f) - \boldsymbol{k_f}$$

***k*d:** Radiationless Deactivations Rate constant (s^{-1})

***k*f:** Rate constant of Fluorescence (s^{-1})

Φf**:** Fluorescence quantum-yield

Rate Constant of Radiationless Deactivation of BP-PPI in DMF:

$$\boldsymbol{k_d} = (\boldsymbol{k_f}/\Phi_f) - \boldsymbol{k_f}$$

$$\boldsymbol{k_d} = (3.17 \times 10^8/0.01) - 3.17 \times 10^8$$

$$\boldsymbol{k_d} = 3.14 \times 10^{10}\ s^{-1}$$

Table 4. 7. Rate Constant of Radiationless Deactivation of BP-PDA and BP-PPI in Different Solvents

Compound	Solvent	λ_{max}	Φ_f	$\boldsymbol{k_f}$	$\boldsymbol{k_d}$
BP-PDA	DMF	530	11.20202	8.93×10^7	5.71×10^7
	NMP	529	8.973542	1.11×10^8	3.95×10^8
	THF	516	9.839603	1.02×10^8	1.19×10^8
BP-PPI	DMF	495	3.153116	3.17×10^8	3.2×10^{10}
	NMP	487	4.105643	2.44×10^8	1.04×10^9
	THF	513	17.47404	5.72×10^7	1.22×10^8

4.2.9 Oscillator Strengths (*f*)

The oscillator-strength, states the electronic transition strength and is able to calculate by the following equation.

$$ƒ = \mathbf{4.32} \times \mathbf{10^{-9}} \ \boldsymbol{\Delta\bar{V}_{1/2}} \ \epsilon_{max}$$

***f*:** Oscillator strength

$\boldsymbol{\Delta\bar{V}_{1/2}}$: Half width in cm^{-1}

ϵ_{max}**:** At the maximum absorption-wavelength the maximum extinction-coefficient in $L \cdot mol^{-1} \cdot cm^{-1}$

Oscillator Strength of BP-PPI in DMF:

$ƒ = 4.32 \times 10^{-9} \ \Delta\bar{V}_{1/2} \ \epsilon_{max}$

$ƒ = 4.32 \times 10^{-9} \times 7771 \times 35000 = 1.17$

Table 4.8: Oscillator Strengths Data of BP-PDA and BP-PPI in Different Solvents

Compound	Solvent	λ_{max}	$\Delta\bar{V}_{1/2}$	ϵ_{max}	ƒ
BP-PDA	DMF	530	2858.8	30700	0.38
	NMP	529	3532.3	30900	0.47
	THF	516	2869.9	33000	0.41
BP-PPI	DMF	495	7770.9	35000	1.17
	NMP	487	6739.4	30000	0.87
	THF	513	3819.7	13800	0.23

4.2.10 Singlet Energies (*Es*)

Singlet-Energy is chromophore/fluorophorės lowest energy to get excited to an excited from ground state.

$$E_s = \frac{2.86 \times 10^5}{\lambda_{max}}$$

***Es*:** Single-Energy in kcal mol^{-1}

λ_{max}**:** The maximum Absorption-Wavelength

Singlet Energy of BP-PPI in DMF:

$$E_s = \frac{2.86 \times 10^5}{\lambda_{max}}$$

$$E_s = \frac{2.86 \times 10^5}{4950} = 57.8\ Kcal.mol^{-1}$$

Table 4.9: Singlet Energy of BP-PDA, BP-PPI, BC-PDD, BPDA-PDA and BPDI-PDI in Different Solvents

Compound	Solvent	λ_{max}	Φ_f	ε_{max}	f	Es
BP-PDA	DMF	530	0.61	34431	0.11	54.6
	NMP	529	0.22	66878	0.21	54.5
	THF	516	0.46	32089	0.12	55.1
BP-PPI	DMF	495	0.01	20347	0.68	57.8
	NMP	487	0.19	15161	0.44	58.7
	THF	513	0.32	5429	0.15	55.7
BC-PDD	DMF	524	0.4	23000	0.18	54.6
	DMSO	526	0.32	33000	0.64	54.4
	NMP	518	0.07	20200	0.12	55.2
BPDA-PDA	DMF	518	0.64	38000	0.24	55.2
	DMSO	518	0.29	40900	0.24	55.2
	NMP	519	0.06	13000	0.09	55.1
BPDI-PDI	DMF	524	0.73	27300	0.14	54.6
	DMSO	527	0.41	10800	0.06	54.3
	NMP	527	0.27	42800	0.21	54.3

4.3 Calculations of Electrochemical Parameters

Cyclic voltammetry is used for electrochemical characterization of synthesized materials by using 0.1 M $NaBF_4$ as a Supporting-Electrolyte in DMF solutions, also 1M HCl solution is used in solid state measurements.

4.3.1 Redox Potentials/Half Wave Potentials ($E_{1/2}$)

The average value of the anodic and cathodic peak potentials is known as a redox potential.

Redox potential can calculated from cyclic voltammetry with the internal reference by follow equation.

$$E_{1/2} = \frac{E_{pc} + E_{pa}}{2}$$

$E_{1/2}$: Half Wave potential

E_{pc} **:** Cathodic-Peak potential

E_{pa}**:** Anodic-Peak potential

Redox Potentials of EOPPI:

The cyclic voltammograms of BP-PPI is indicate one reversible symmetric redox processes in solution (Figure 4). The redox potential in DMF is calculated relative to the reference electrode below.

$$E_{1/2} = \frac{E_{pc} + E_{pa}}{2} = \frac{(-0.673) + (-0.595)}{2} = -0.634\ V$$

The peak potential separations for the redox processes by using the anodic and cathodic peak potentials, can be estimated by the following equation.

$$\boldsymbol{\Delta E_p = E_{pa} - E_{pc} = \frac{0.059}{n}\ V}$$

n is indicates the number of electrons transferred.

Peak-Potentials Separations of BP-PPI:

$\Delta E_p = E_{pa} - E_{pc}$

$\Delta E_p = (-0.595) - (-0.673)$

$\Delta E_p = 0.078\ V = 78\ mV$

"Ferrocene" is used as an internal reference and its oxidation potential is predicted as 0.623 V, therefore, *E*ox = 0.623 V

$E_{red^1/_2}\ vs.\ Fc = (E_{red^1/_2}\ vs.\ Ag/AgCl) - (E_{ox} vs.\ Ag/AgCl)$

$E_{red^1/_2}\ vs.\ Fc = (-0.634) - (0.623) = -1.257\ V$

$E_{red^1/_2}\ vs.\ Fc = -1.257\ V$

The redox-potentials of all synthesized compounds were calculated and the values were tabulated in Table 4.10.

Table 4.10: Electrochemical Information of BP-PDA, BP-PPI, BC-PDD, BPDA-PDA, BPDI-PDI, BP-PDSi, NanoBP-PDSi and BP-PPDSi in DMF

Compound	Epa / V	Epc / V	ΔE_p / mV	E1/2 (V) vs. (Ag/AgCl)	EFc (V) vs.	E1/2 vs. Fc / V
BP-PDA	-0.38	-0.47	90	-0.425	0.59	-1.02
	-0.22	-0.29	71	-0.255	0.59	-0.85
BP-PPI	-0.59	-0.67	78	-0.634	0.62	-1.26
	-0.34	-0.42	80	-0.379	0.62	-1.00
BC-PDD	-0.79	-0.78	-11	-0.785	0.60	-1.39
BPDA-PDA	0.819	0.25	565	0.5365	0.63	-0.10
PDI-PDI	-0.59	-0.67	72	-0.633	0.61	-1.24
	-0.34	-0.41	67	-0.377	0.61	-0.99
BP-PDISi	0.57	-0.47	1035	0.051	0.35	-0.30
	0.74	0.361	374	0.548	0.35	0.20
Nano-BP-PDISi	0.82	-0.31	1129	0.255	0.35	-0.1
BP-PPDISi	0.79	-0.49	1279	0.154	0.37	-0.22
	-	0.28	-	-	-	-

[a] E_{pc}: Cathodic-Potential.
[b] E_{pa}: Anodic-Potential.
[c] ΔE_p: Peak-Potential Separations.
[d] $E_{1/2}$: Half-Wave potential.
[e] Ag/AgCl: Reference Electrode of silver/silver chloride.

4.3.2 Energies of LUMO-Level

Energy levels of Lowest-Unoccupied Molecular Orbital (LUMO) with respect to the vacuum-level are calculated by using bellow equation.

$$E_{LUMO} = -(4.8 + E_{1/2})$$

E_{LUMO}: Energy of LUMO-levels in Ev

$E_{1/2}$: Redox-Potential of analyte (vs. Fc)

E_{LUMO} of BP-PPI

$E_{LUMO} = -(4.8 - 0.64) = -3.54\,V4$

$E_{LUMO} = -3.54\,V$

The LUMO-values of compounds were calculated by same method and tabled (table 4.12).

4.3.3 Energies of Optical-Band Gap (*E*g)

The optical-band gap energy of compounds were calculated by bellow equation, by using extrapolating of maximum absorbance wavelength of absorption spectrum to zero absorbance.

$$\mathrm{E_g} = \frac{1240\mathrm{eV\ nm}}{\lambda}$$

*E*g: Band-gap energy in eV

λ: Where Cut-off wavelength of the absorbance-band (nm)

***E*g of BP-PPI:**

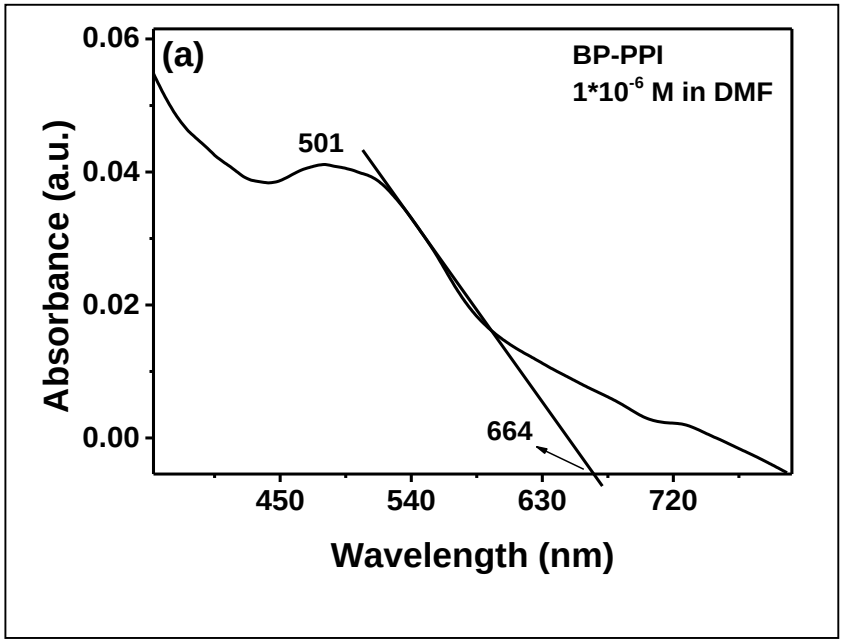

Figure 4.4: Absorption-Spectrum of BP-PPI in DMF

$$\mathrm{E_g} = \frac{1240\mathrm{eV\ nm}}{664\ \mathrm{nm}} = 1.86$$

$$\mathrm{E_g} = 1.86$$

4.3.4 Energies of HOMO Levels

The Highest-Occupied Molecular Orbital (HOMO) energy values were calculated from the LUMO and *E*g Values followed by the equation given below.

$$\mathbf{E_{HOMO} = E_{LUMO} - E_g}$$

***E*g:** Band gap energy in eV

***E*HOMO:** Energy of HOMO level in eV

***E*LUMO:** Energy of LUMO level in eV

HOMO level Energy of BP-PPI

$E_{HOMO} = E_{LUMO} - E_g$

$E_{HOMO} = -3.54 - 1.86 = -5.40\ V$

$E_{HOMO} = -5.40\ V$

The HOMO values of all compounds were calculated by the same method reported and tabled in table 4.11.

Table 4.11: Electrochemical Information of BP-PDA, BP-PPI, BC-PDD, BPDA-PDA, BPDI-PDI, BP-PDSi, NanoBP-PDSi and BP-PPDSi in DMF Solution

Compound	E_{pa} / V	E_{pc} / V	ΔE_p / mV	E_{LUMO} / eV	E_g / eV	E_{HOMO} / eV
BP-PDA	-0.38	-0.47	90	-3.8	2.08	-5.9
	-0.22	-0.29	71	-3.9	2.08	-6.0
BP-PPI	-0.59	-0.67	78	-3.5	1.86	-5.4
	-0.34	-0.42	80	-3.8	1.86	-5.6
BC-PDD	-0.79	-0.78	-11	-3.4	1.55	-4.9
BPDA-PDA	0.819	0.25	565	-4.7	2.14	-6.8
BPDI-PDI	-0.59	-0.67	72	-3.6	1.68	-5.2
	-0.34	-0.41	67	-3.8	1.69	-5.5
BP-PDISi	0.57	-0.47	1035	-4.5	1.44	-5.9
	0.74	0.361	374	-4.9	1.44	-6.4
Nano-BP-PDISi	0.82	-0.31	1129	-4.7	1.86	-6.6
BP-PPDISi	0.79	-0.49	1279	-4.6	1.86	-6.4
	-	0.28	-	-		-

[a] E_{pc}: Cathodic-Potential.
[b] E_{pa}: Anodic-Potential.
[c] ΔE_p: Peak-Potential Separations.
[d] $E_{1/2}$: Potential Half-Wave
[e] Ag/AgCl: Reference-Electrode of silver/silver chloride
[f] E_{Fc}: oxidation potential of ferrocene (internal-reference).

4.3.5 Diffusion Constants (D)

The diffusion coefficients refer to the effect of scan rate on the peak current were calculated by below equation.

$$D = \frac{\left(\frac{IPc}{\sqrt{V}}\right)^2}{[(2.69 \times 10^5\ As\ mol^{-1}V^{-1/2})^2 \times (n^{3/2})^2 \times (Ac)^2]}$$

D: Diffusion constant in $cm2s^{-1}$

Ipc: The cathodic peak current from the cyclic voltammogram

V: Scan rate used to record the cyclic voltammogram

$\frac{IPc}{\sqrt{V}}$ **:** Slope of the plot ipc vs. in units of $[(\mu A)\times(mV)^{-1/2}\times(s)^{1/2}]$

n: Number of electrons

A: Working electrode area in cm^2

***C*:** Electro-active species concentration (mol cm^{-3})

Diffusion-constants of BP-PPI:

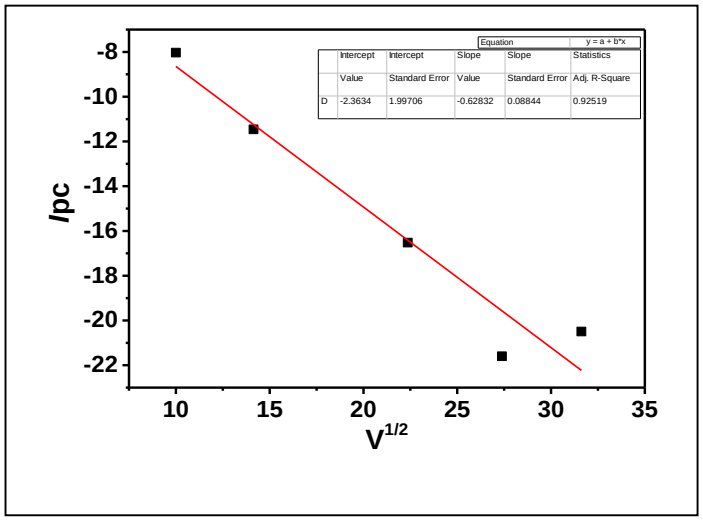

Fig 4.5: Plot of *i*pc vs $V^{1/2}$. Scan Rate of BP-PPI, Slope of the plot of ipc vs. $V^{1/2}$

IPc/$\sqrt{V}$, is determinated by drawing the plot of i_{pc} vs $V^{1/2}$ of BP-PPI and calculating plot slope

$$D=\frac{\left(-0.62832\left[(\mu A)\times(mV)^{-1/2}\times(s)^{1/2}\right]\right)^2}{\left[\left(2.69\times10^5\ As\ mol^{-1}V^{-1/2}\right)^2\times\left(4^{3/2}\right)^2\times\left(\left(3.14\times(0.1\ cm)\right)^2\times(1\times10^{-6}molcm^{-3})\right)^2\right]}$$

$$D_{BP-PPI}=8.65\times10^{-8}cm^2s^{-1}$$

The Diffusion constants of all compounds were calculated by same method and tabled in table 4. 12.

Table 4.12: Diffusion constants of of BP-PDA, BP-PPI, BC-PDD, BPDA-PDA, BPDI-PDI, BP-PDSi, NanoBP-PDSi and BP-PPDSi in DMF Solution

Compound	D (cm^2s^{-1})
BP-PDA	1.2953×10^{-8}
BP-PPI	8.65×10^{-8}
BC-PDD	1.62×10^{-8}
BPDA-PDA	6.39×10^{-5}
BPDI-PDI	1.07×10^{-7}
BP-PDISi	0.95×10^{-8}
Nano BP-PDISi	0.519×10^{-6}
BP-PPDISi	6.46×10^{-10}

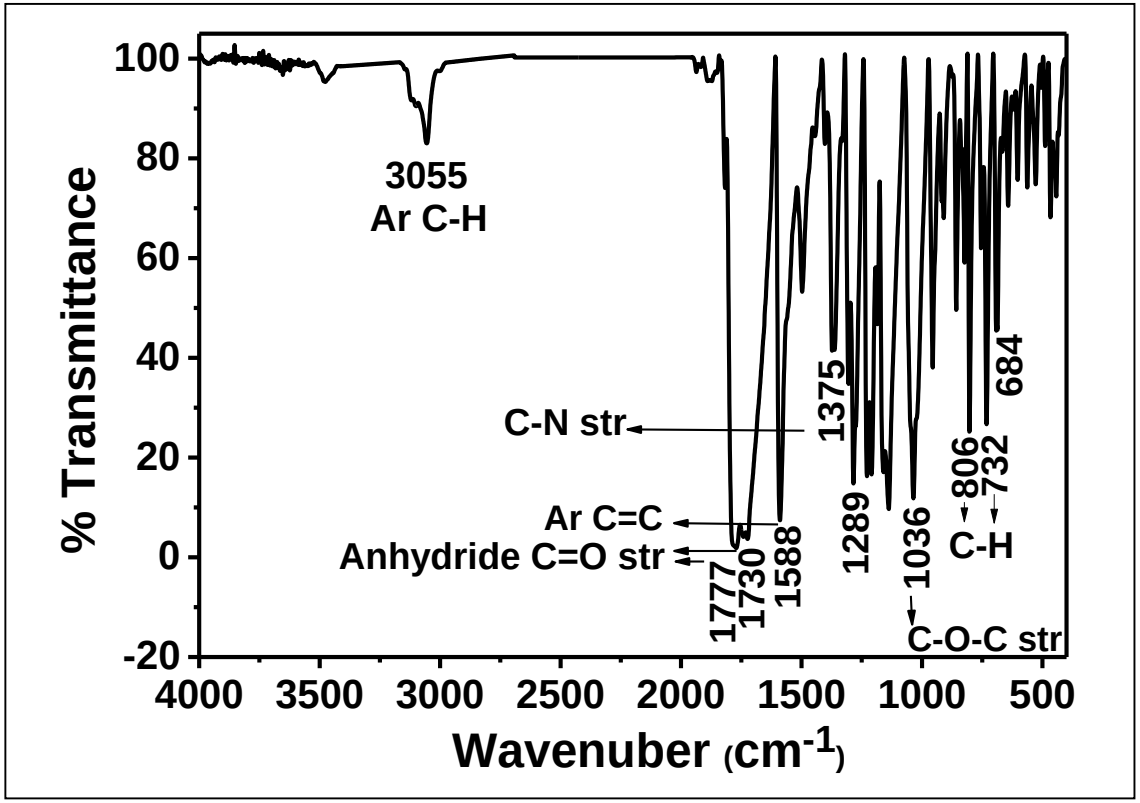

Figure 4.6: FT-IR Spectrum of BP-PDA (KBr Film)

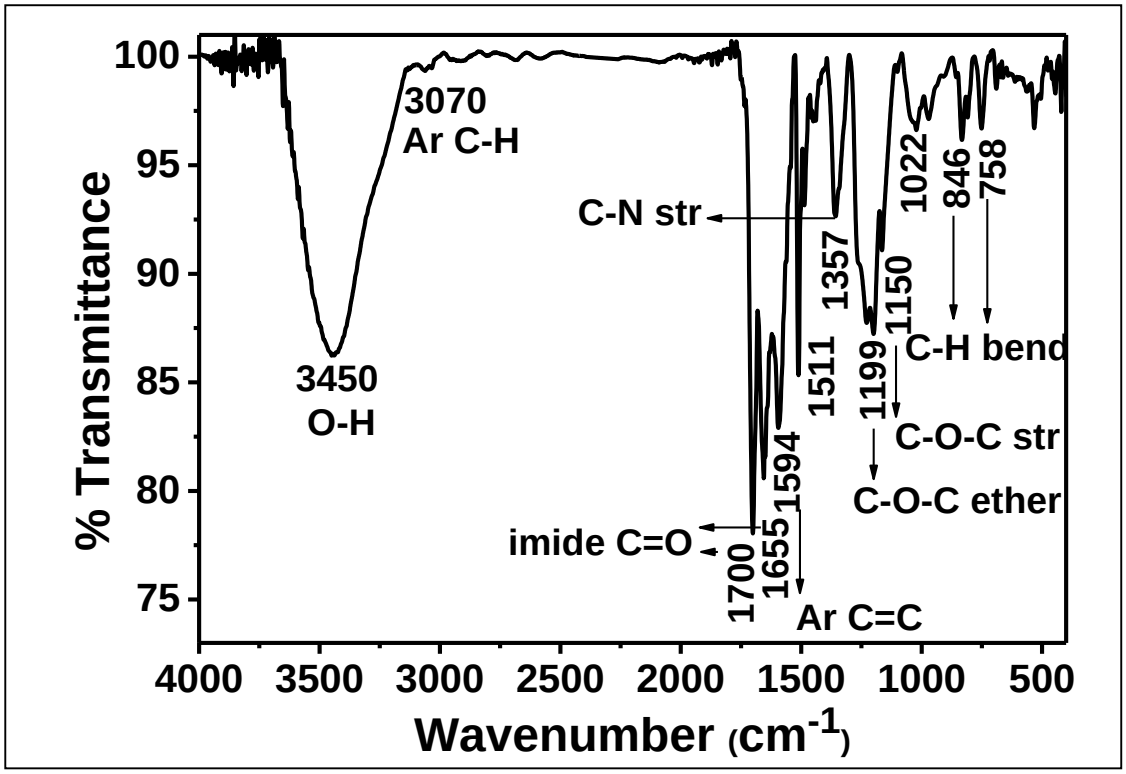

Figure 4.7: FT-IR Spectrum of BP-PPI (KBr Film)

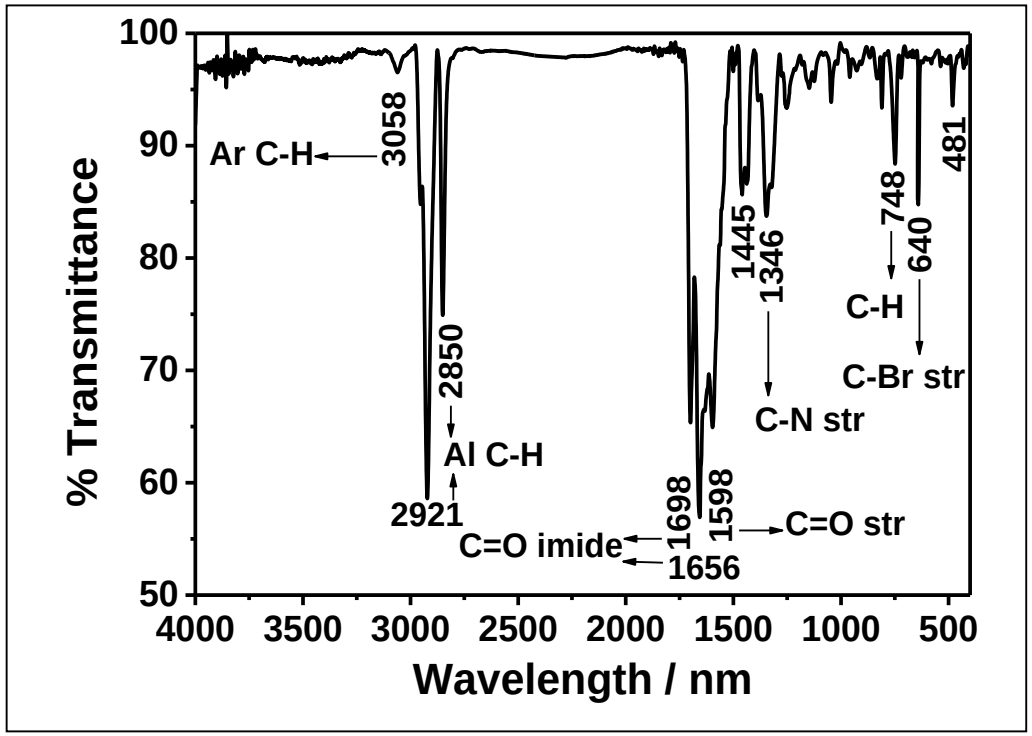

Figure 4.8: FT-IR Spectrum of Br-PDD (KBr Film)

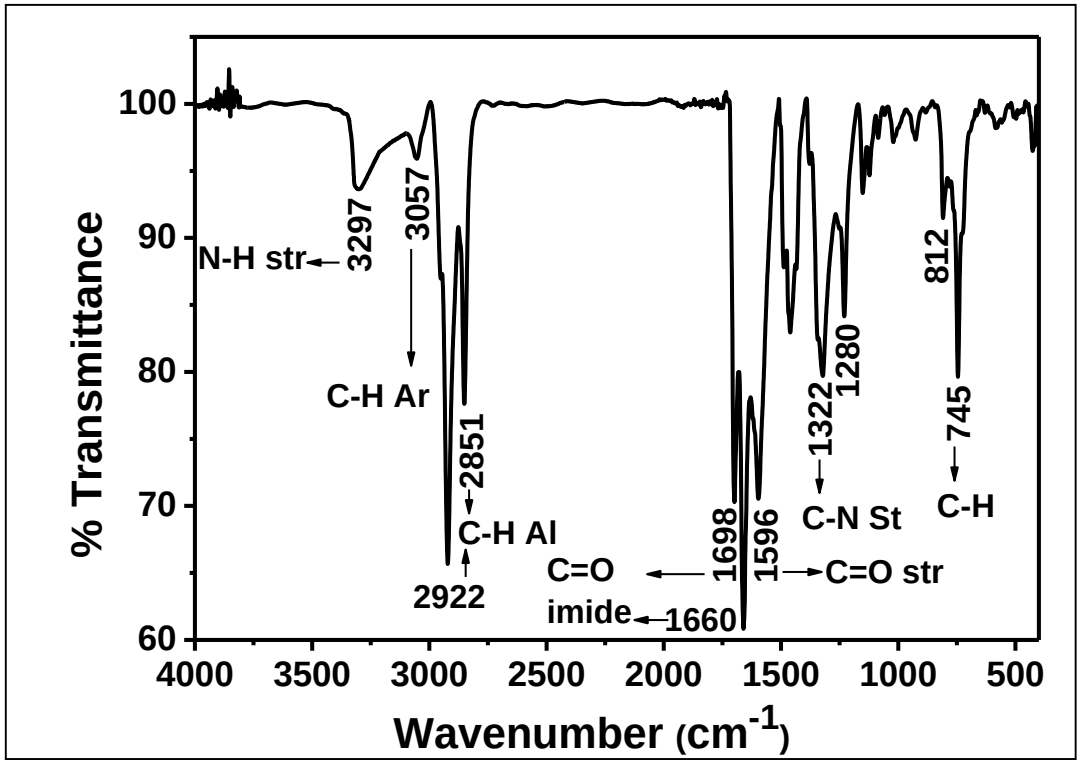

Figure 4.9: FT-IR Spectrum of BC-PDD (KBr Film)

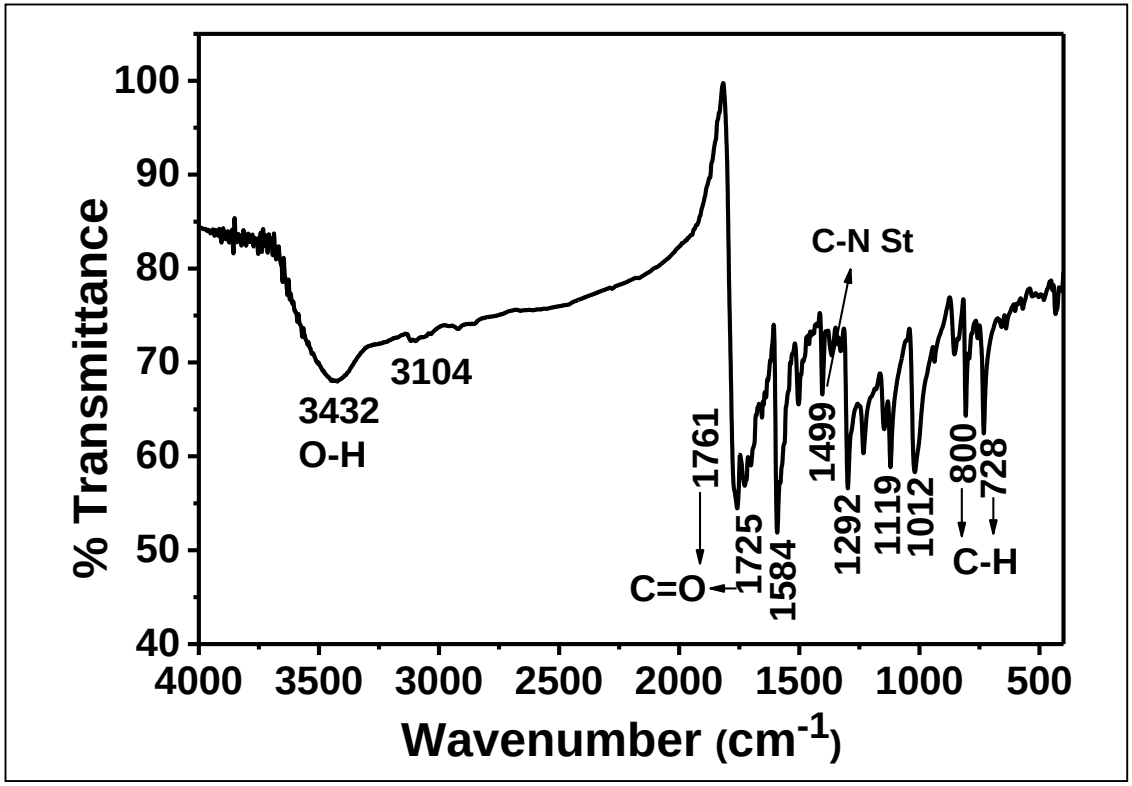

Figure 4.10: FT-IR Spectrum of PMI (KBr Film)

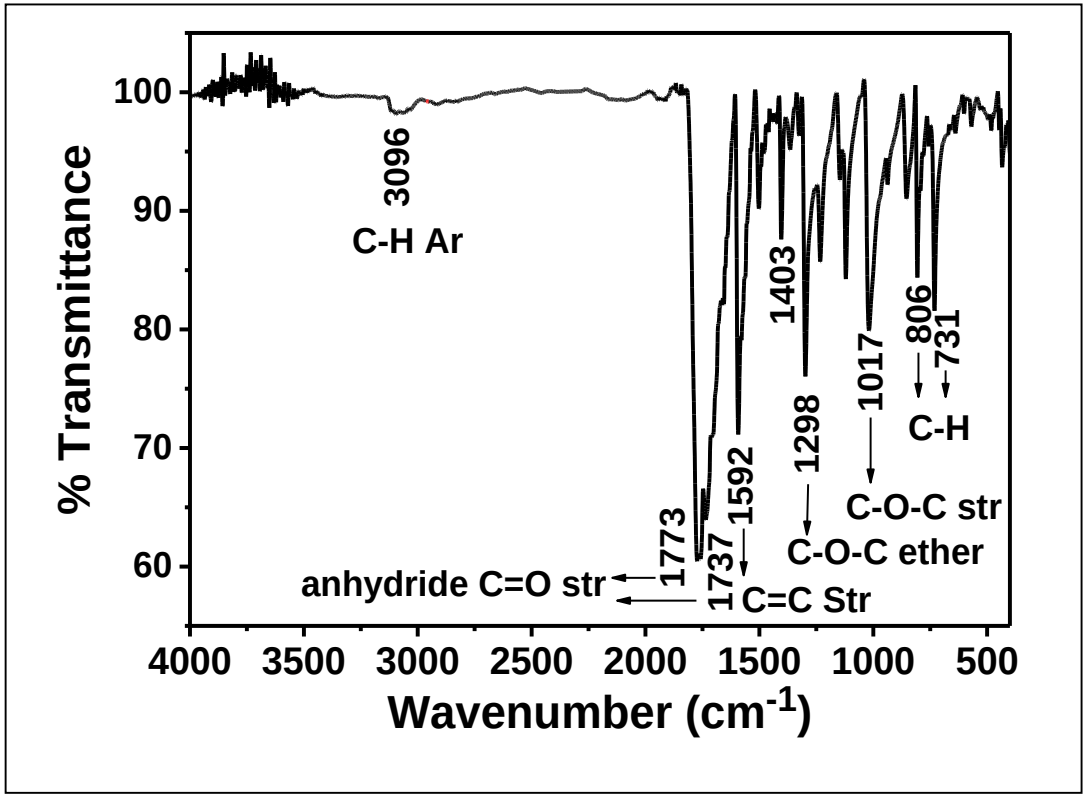

Figure 4.11: FT-IR Spectrum of BPDA-PDA (KBr Film)

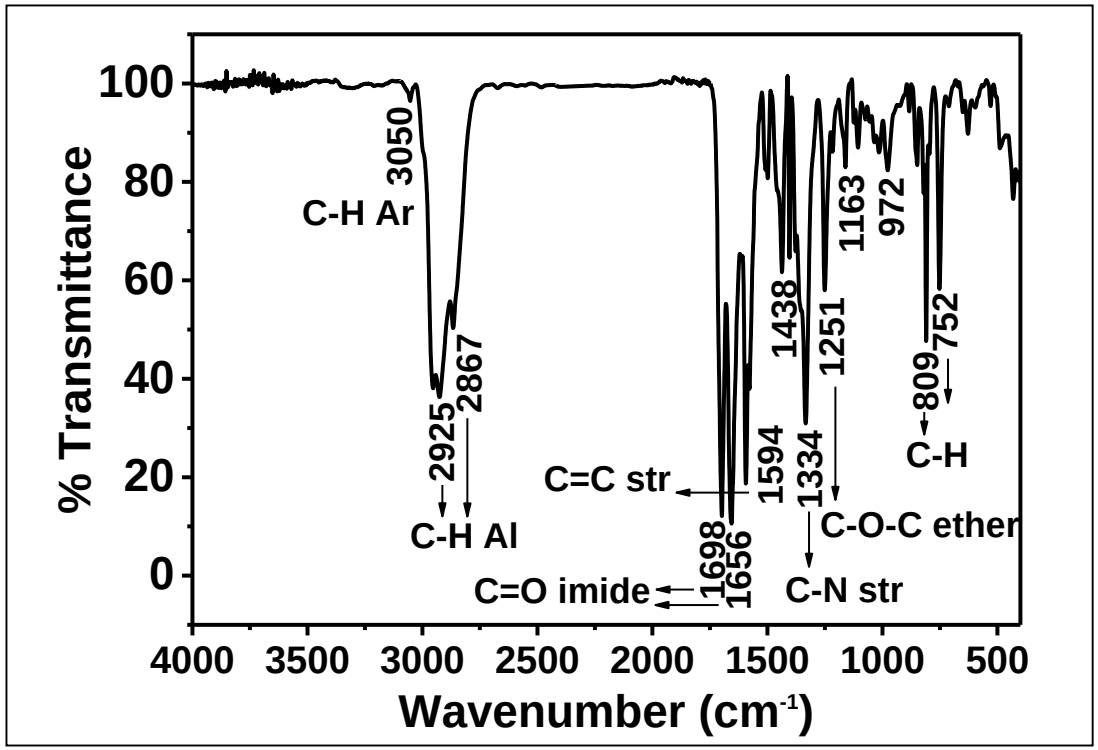

Figure 4.12: FT-IR Spectrum of BPDI-PDI (KBr Film)

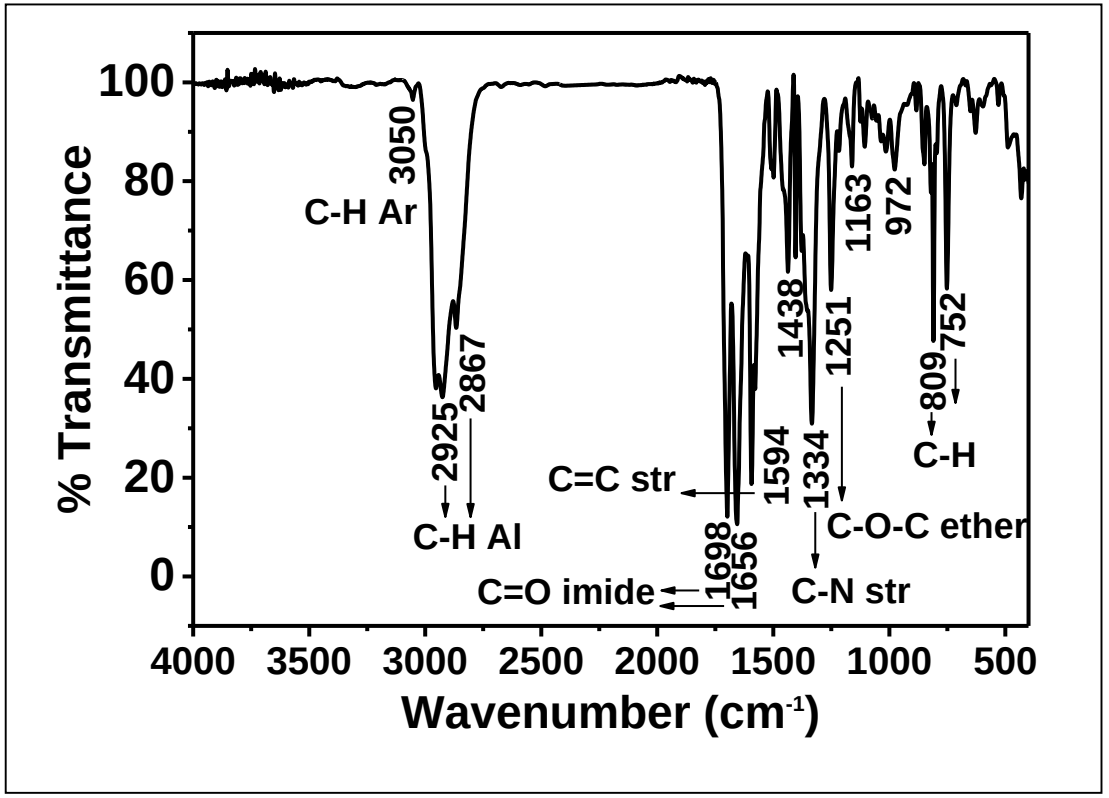

Figure 4.13: FT-IR Spectrum of BP-PDSi (KBr Film)

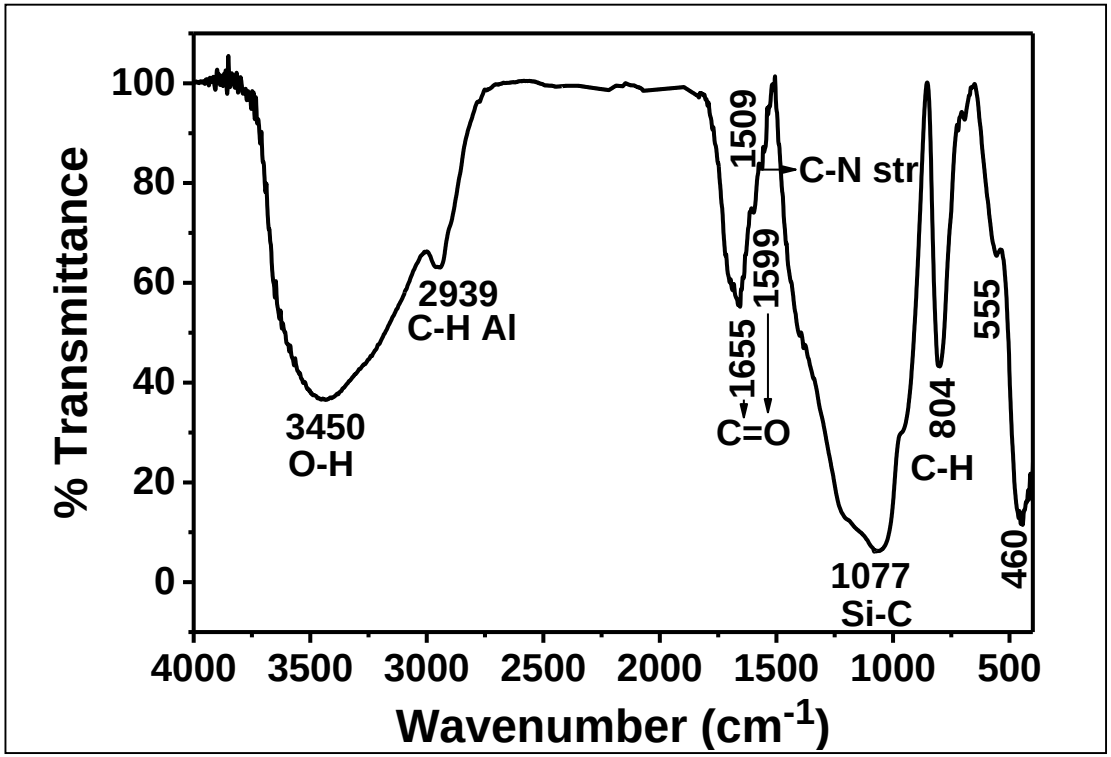

Figure 4.14: FT-IR Spectrum of BP-PDSi Nanocomposite (KBr Film)

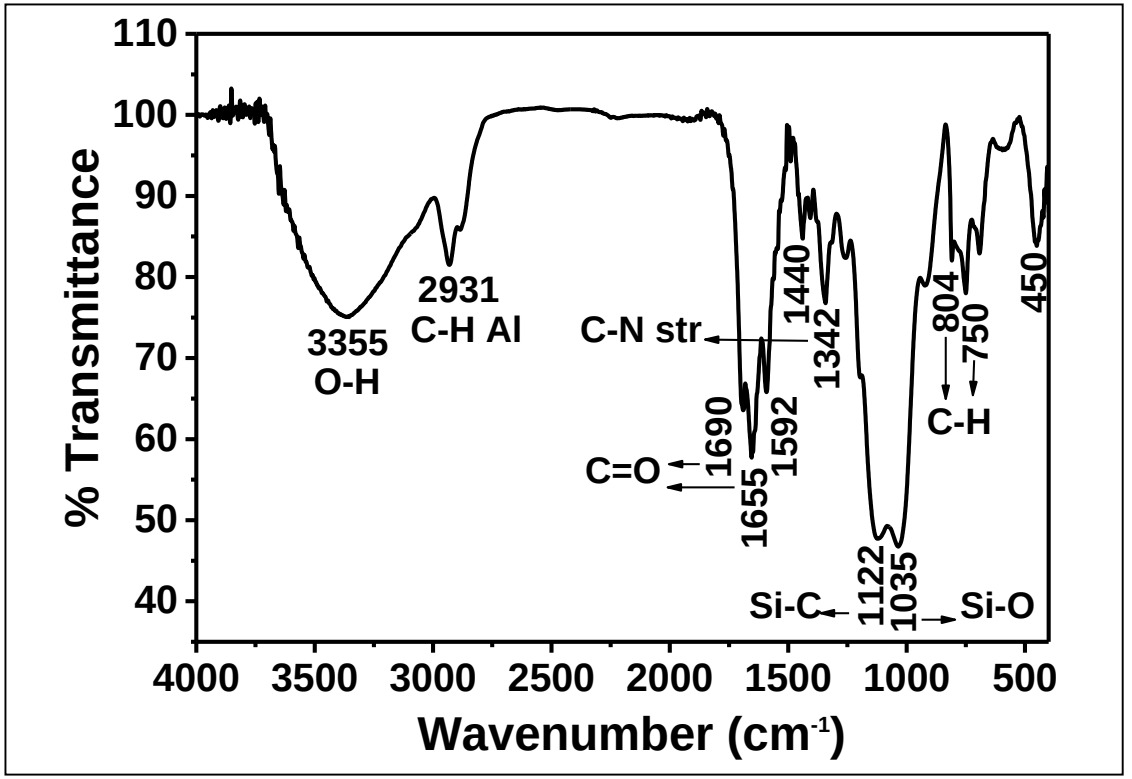

Figure 4.15: FT-IR Spectrum of BP-PPDSi (KBr Film)

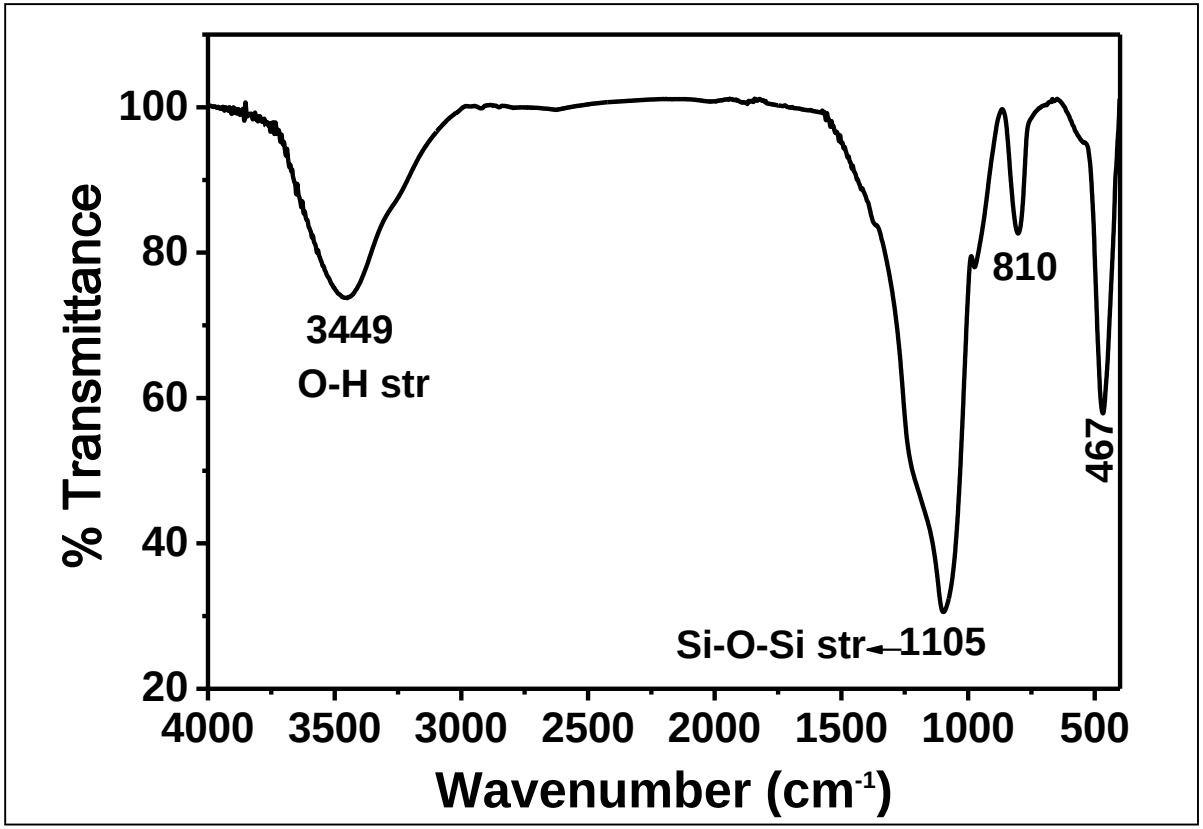

Figure 4.16: FT-IR Spectrum of Nanosilica (KBr Film)

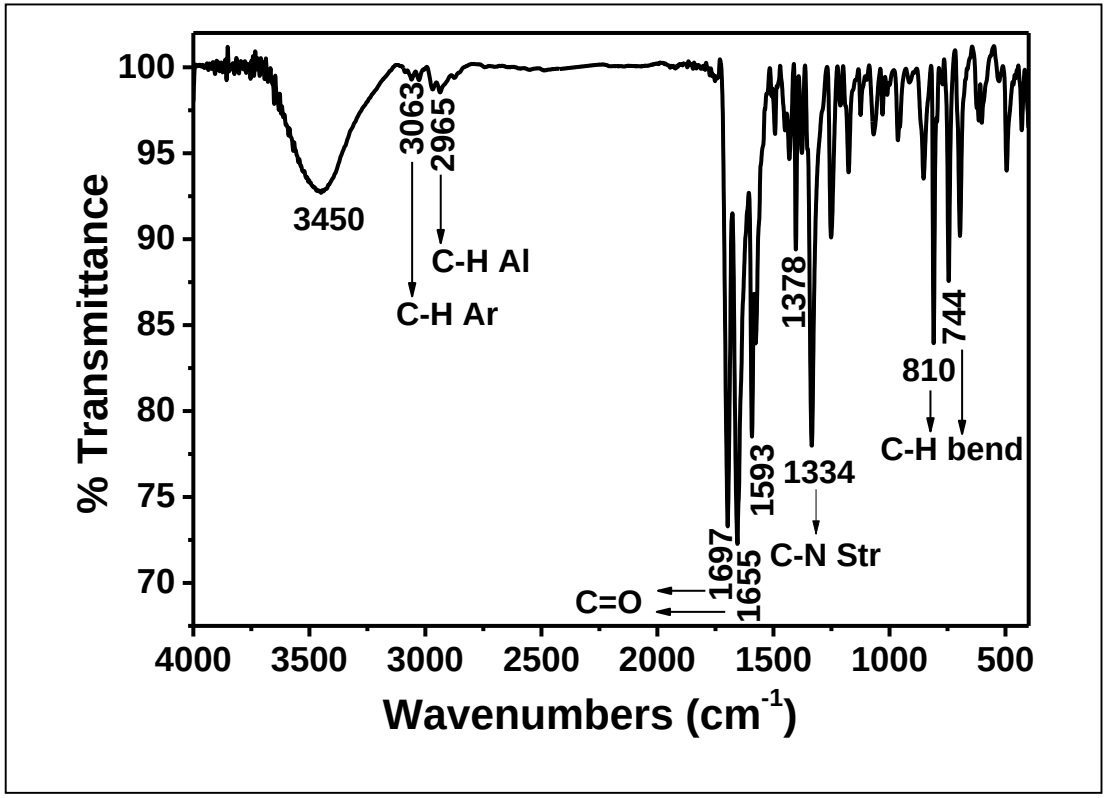

Figure 4.17: FT-IR Spectrum of PDI-1 (KBr Film)

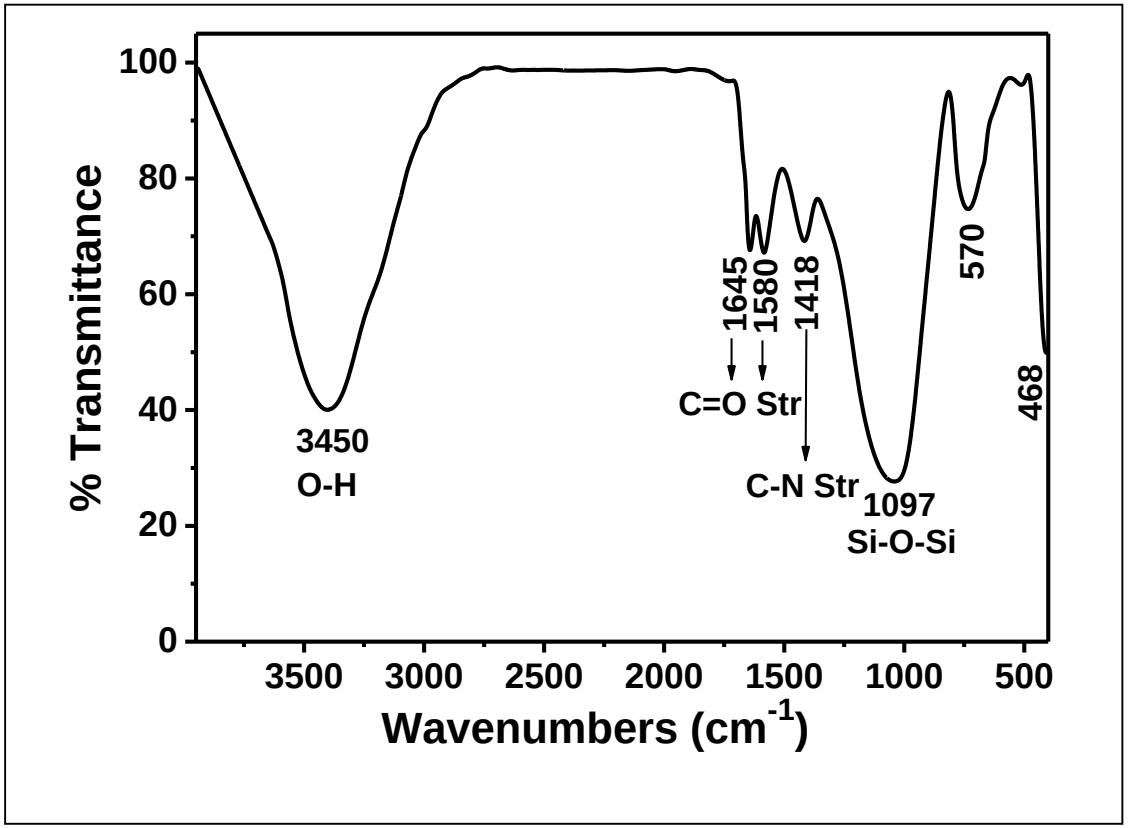

Figure 4.18: FT-IR Spectrum of NSPDI (KBr Film)

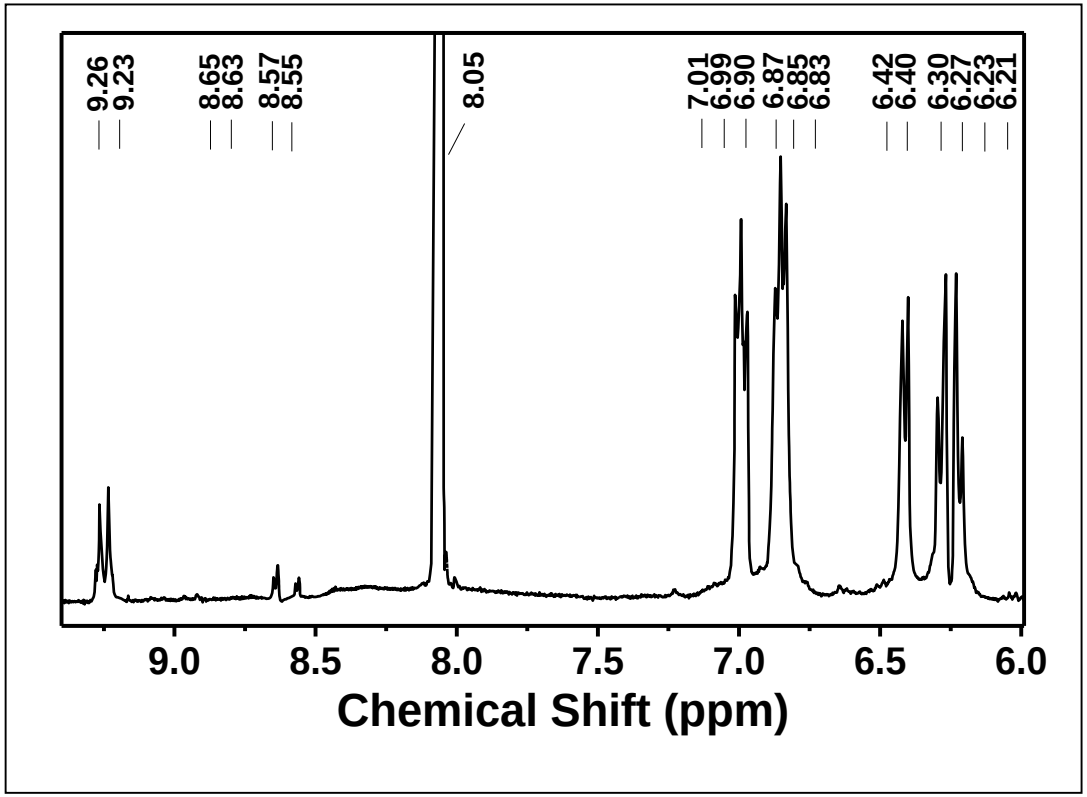

Figure 4.19: ^{1}H-NMR Spectrum of BP-PPI in Deuterated DMF

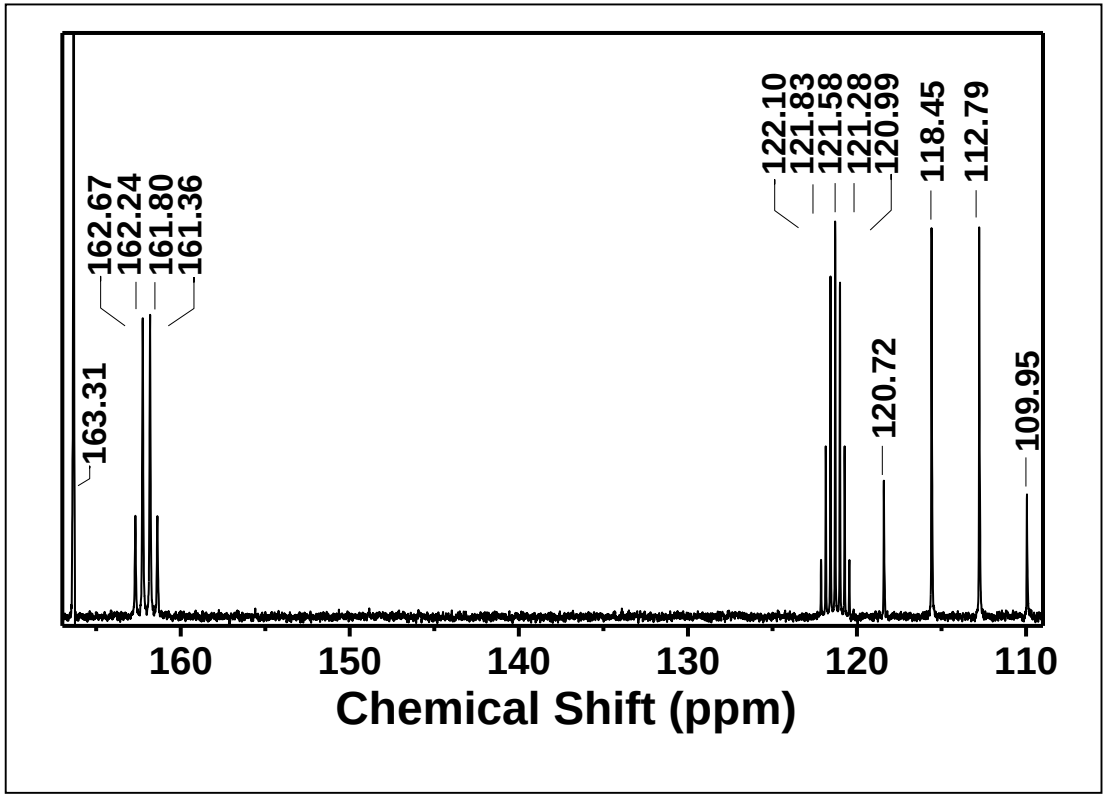

Figure 4.20: C^{13}NMR Spectrum of BP-PPI in Deuterated DMF

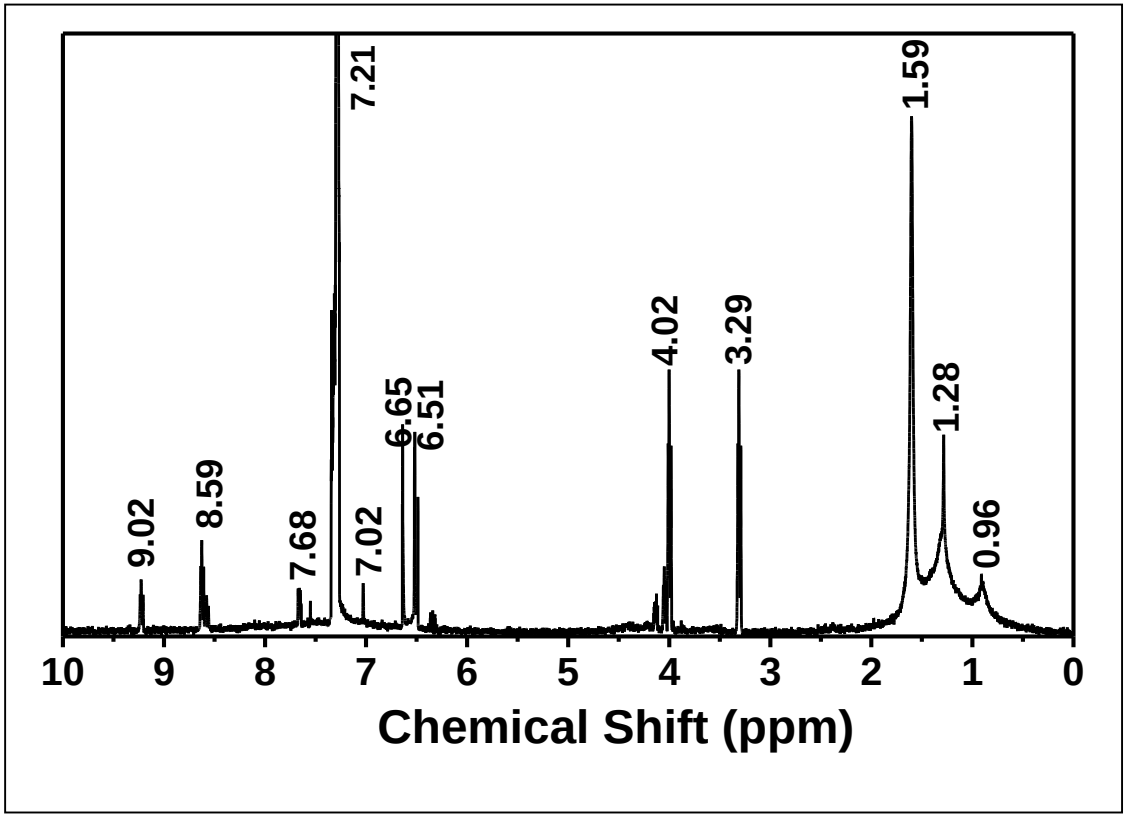

Figure 4.21: ^{1}H-NM Spectrum of BC-PDD in Deuterated CHl

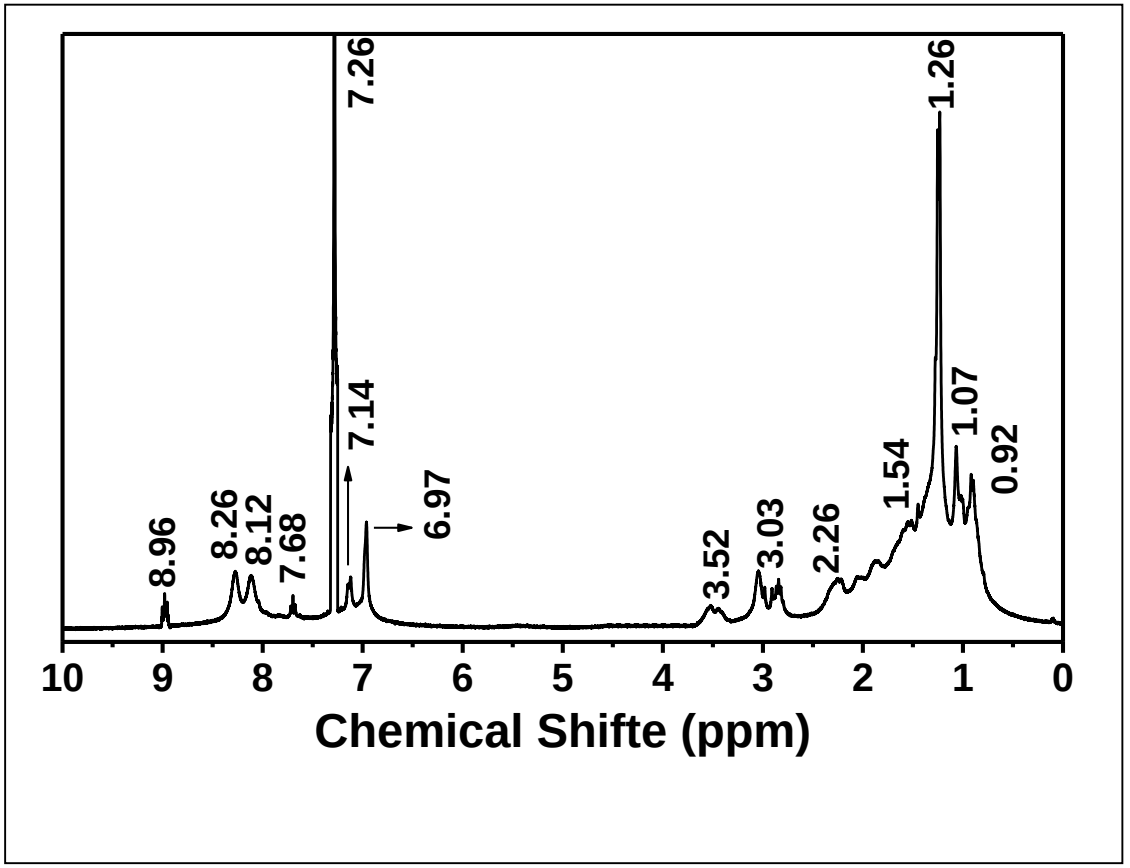

Figure 4.22: ^{1}H-NMR Spectrum of BPDI-PDI in Deuterated $CHCl_3$

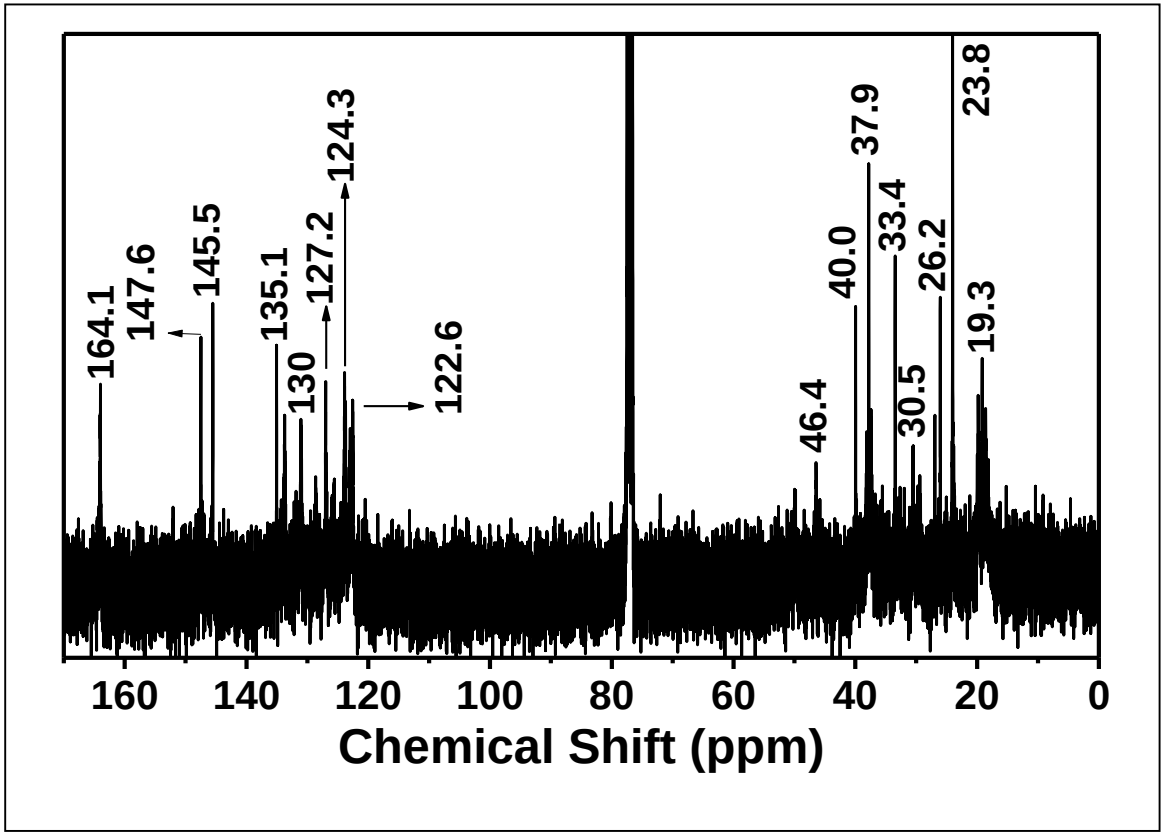

Figure 4.23: C^{13}NMR Spectrum of BPDI-PDI in Deuterated $CHCl_3$

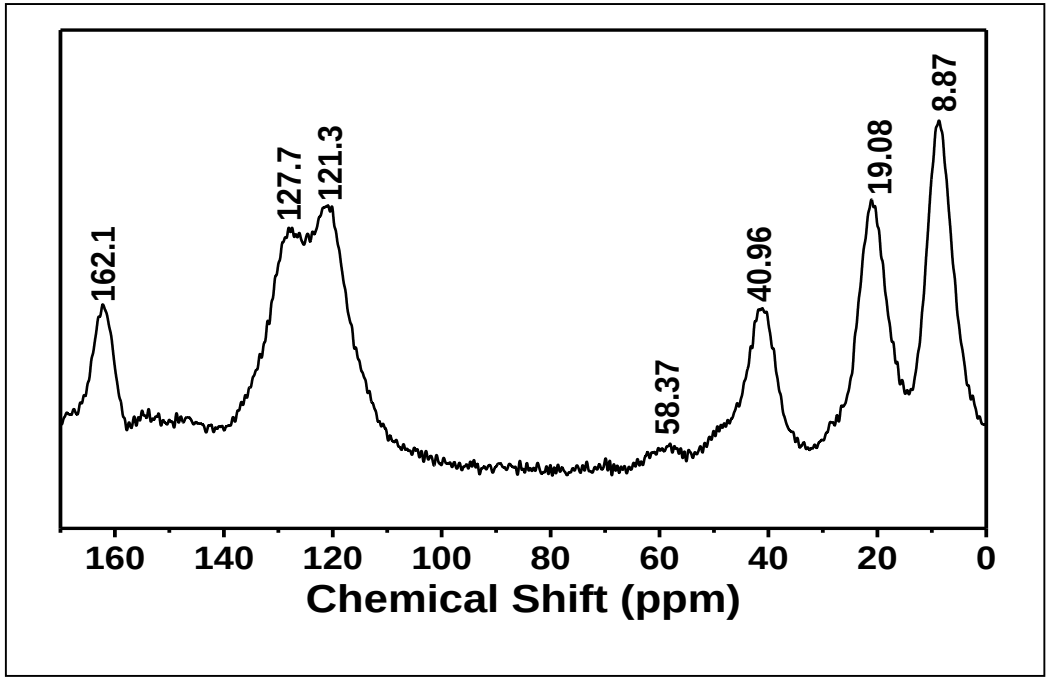

Figure 4.24: C^{13}NMR Spectrum of BP-PDSi in Solid State

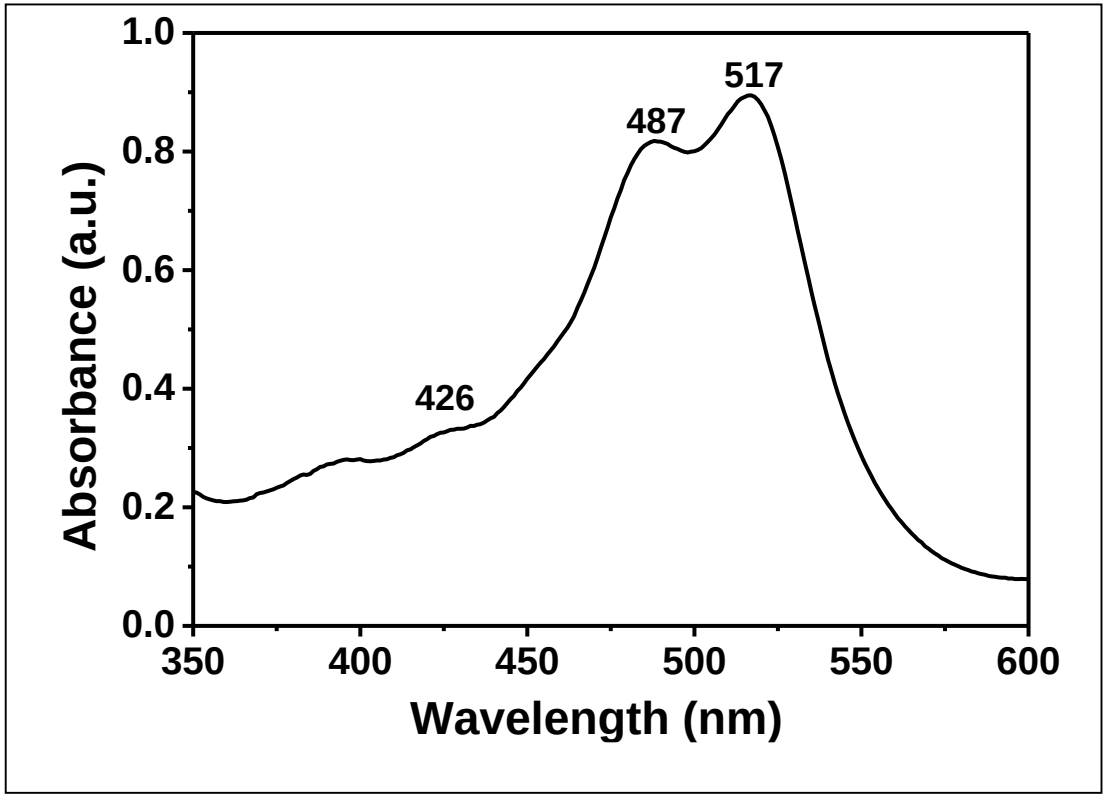

Figure 4.25: UV-Visible Absorption Spectra of Br-PDA in DMF

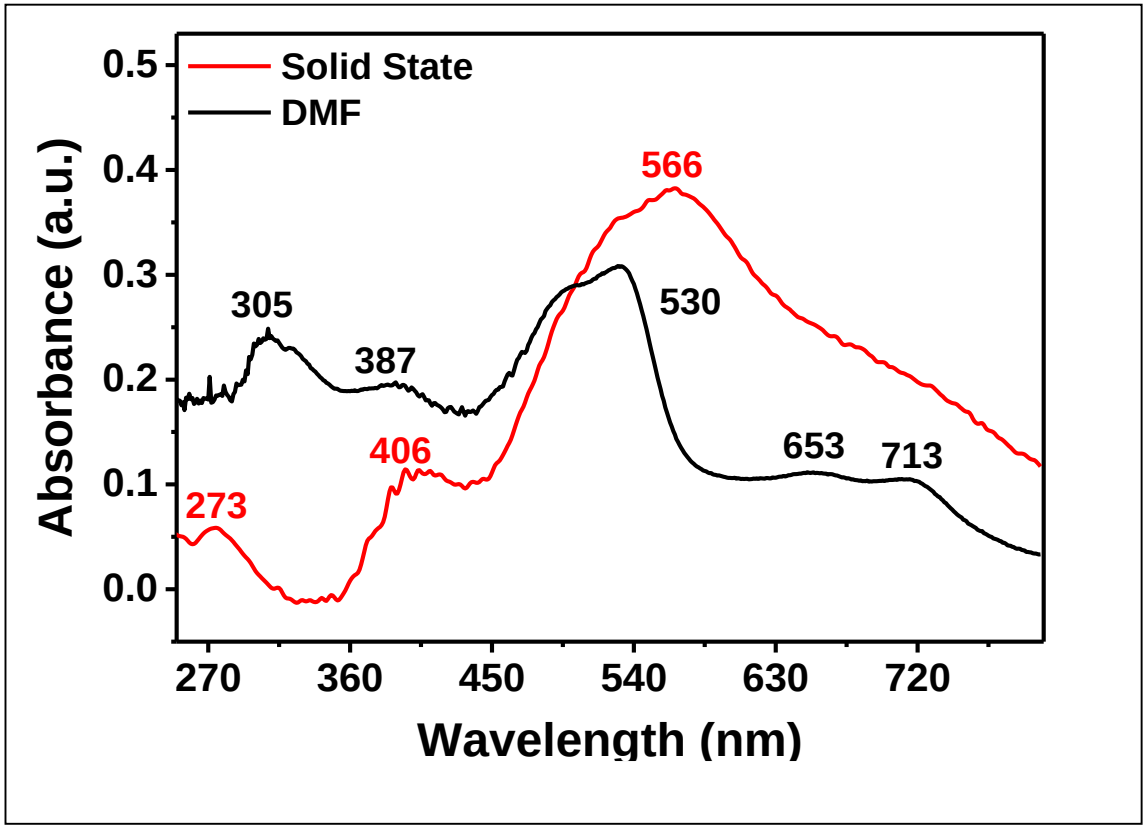

Figure 4.26: UV-Visible Absorption Spectra of Br-PDA in DMF and in Solid-State

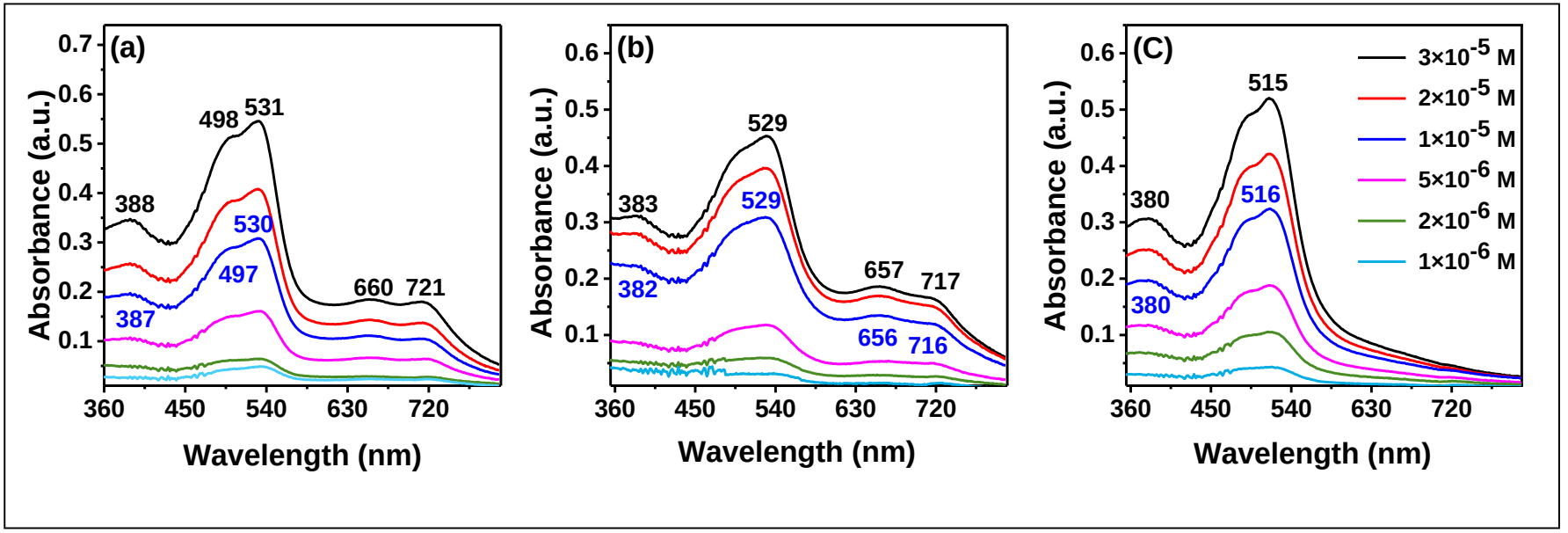

Figure 4.27: Concentration-Dependent Absorption (λexc = 485 nm) Spectra of BP-PDA in Different Solvents (DMF, NMP and THF at 3×10-5 M, 2×10-5 M, 1×10-5 M, 5×10-6 M, 2×10-6 M and1×10-^{6}M Concentrations) (a) Absorption in DMF, (b) Absorption in NMP and (c) Absorption in THF, Respectively

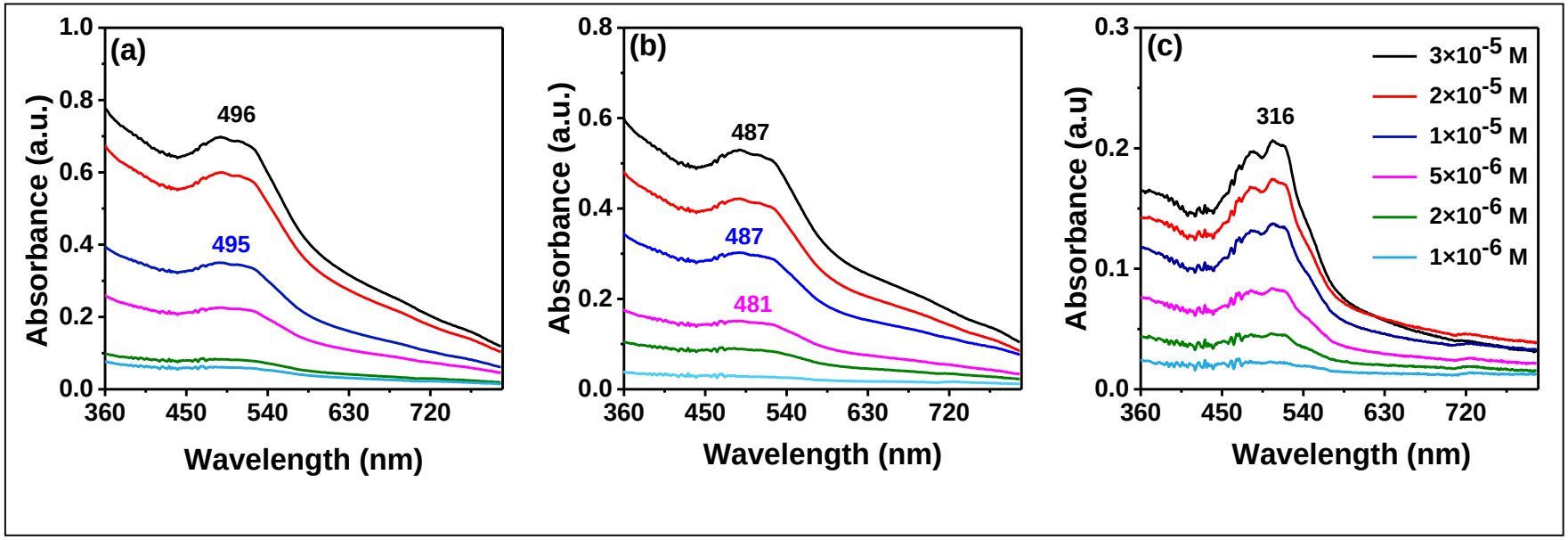

Figure 4.28: Concentration-Dependent Absorption (λ_{exc} = 485 nm) Spectra of BP-PPI in Different Solvents (DMF, NMP and THF at 3×10^{-5} M, 2×10^{-5} M, 1×10^{-5} M, 5×10^{-6} M, 2×10^{-6} M and1×10^{-6} M Concentrations) (a) Absorption in DMF, (b) Absorption in NMP and (c) Absorption in THF, Respectively

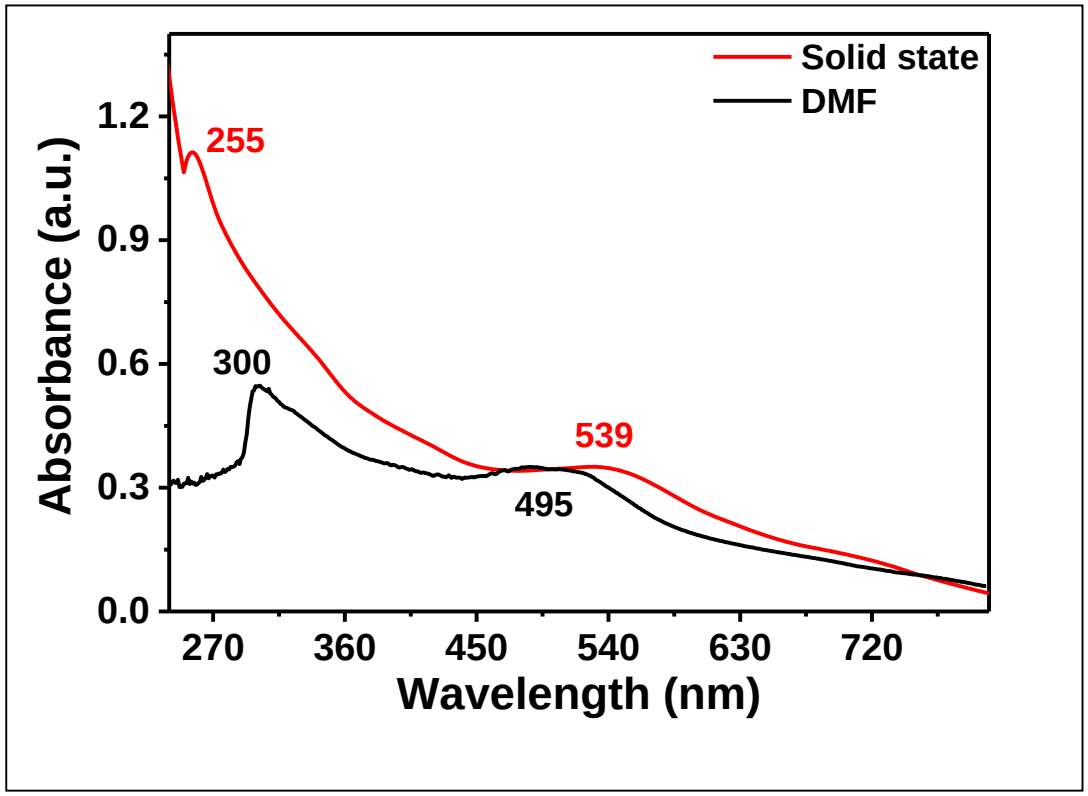

Figure 4.29: UV-Visible Absorption Spectra of BP-PPI in DMF and in Solid-State

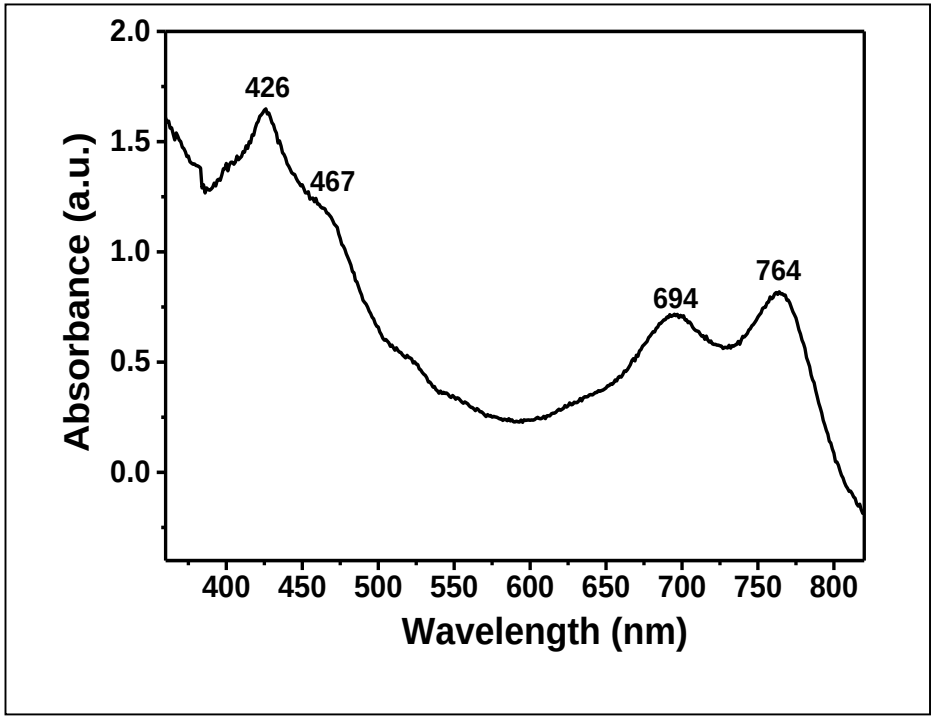

Figure 4.30: UV-Visible Absorption Spectra of Br-PDD in NMP

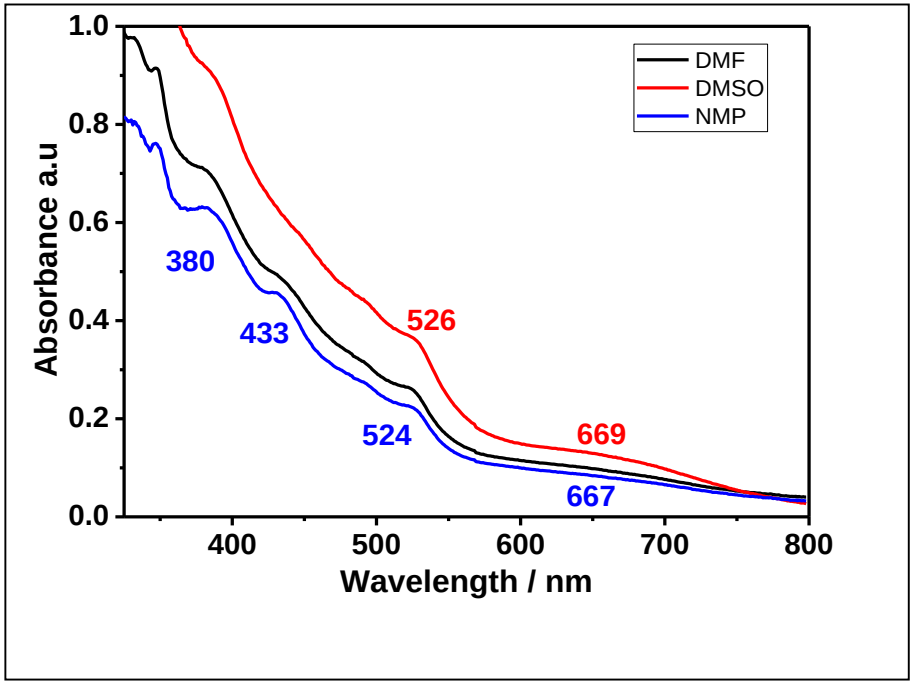

Figure 4.31: UV-Visible Absorption Spectra of BC-PDD in DMF, DMSO and NMP

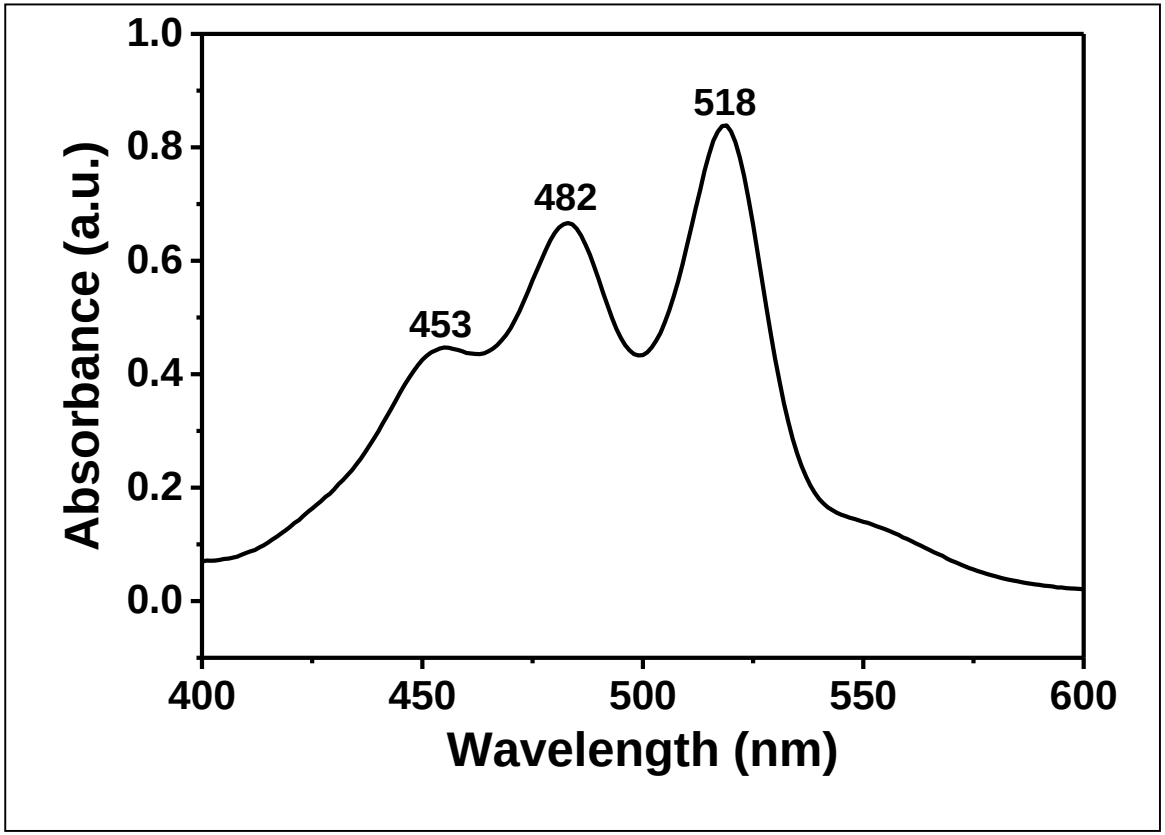

Figure 4.32: UV-Visible Absorbance of PMI in DMF

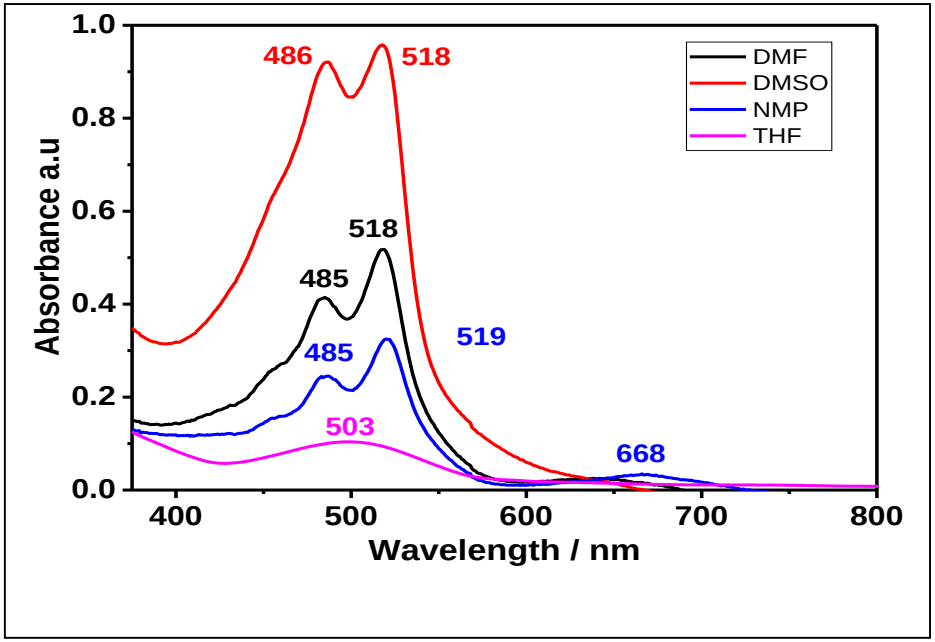

Figure 4.33: UV-Visible Absorbance of BPDA-PDA in DMF, DMSO, NMP and THF

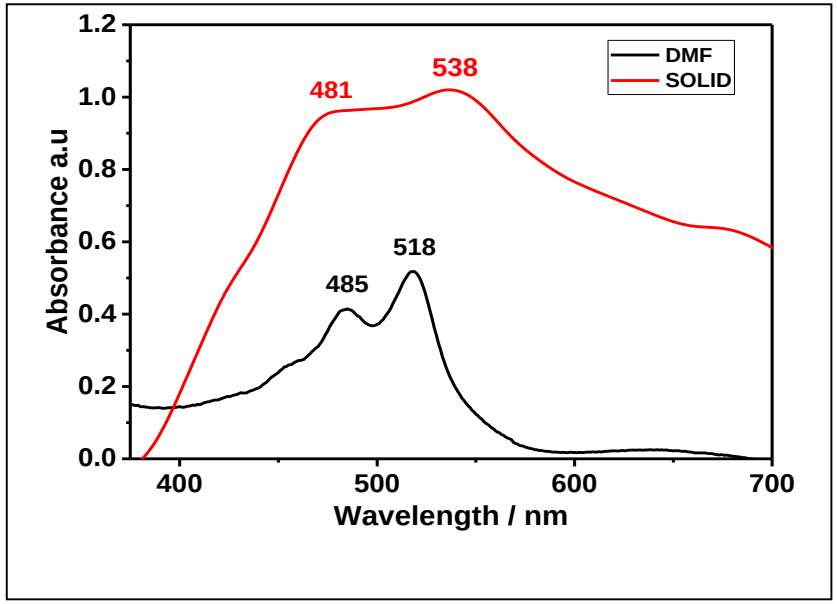

Figure 4.34: UV-Visible Absorbance of BPDA-PDA
in DMF and Solid State

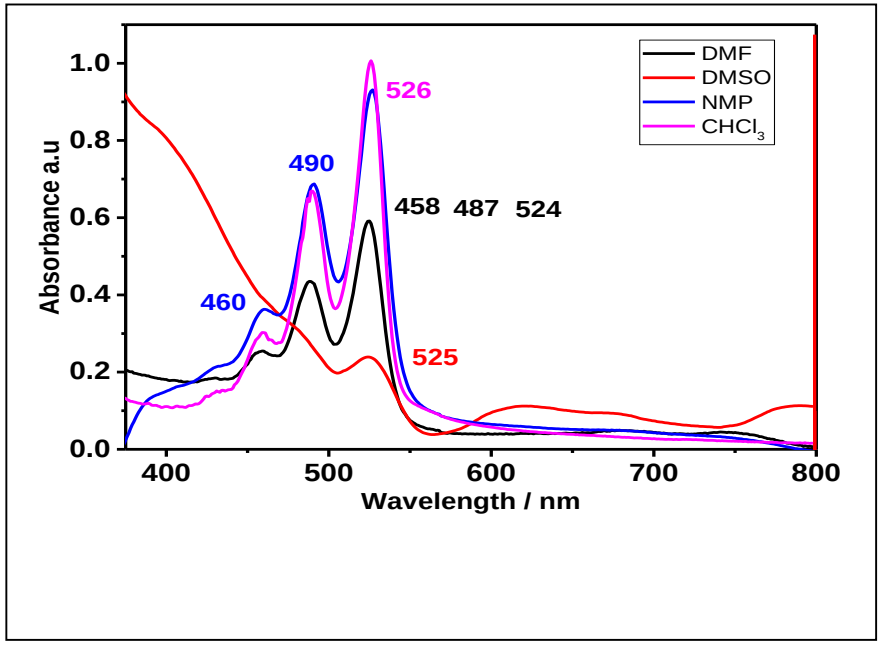

Figure 4.35: UV-visible Absorbance of BPDI-PDI
in DMF, DMSO, NMP and $CHCl_3$

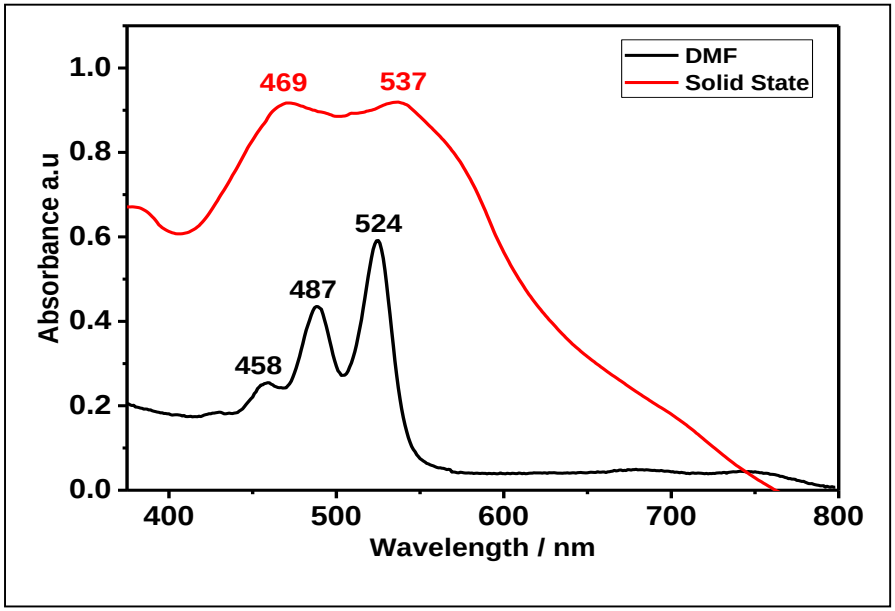

Figure 4.36: UV-Visible Absorbance of BPDI-PDI
in DMF, and Solid State

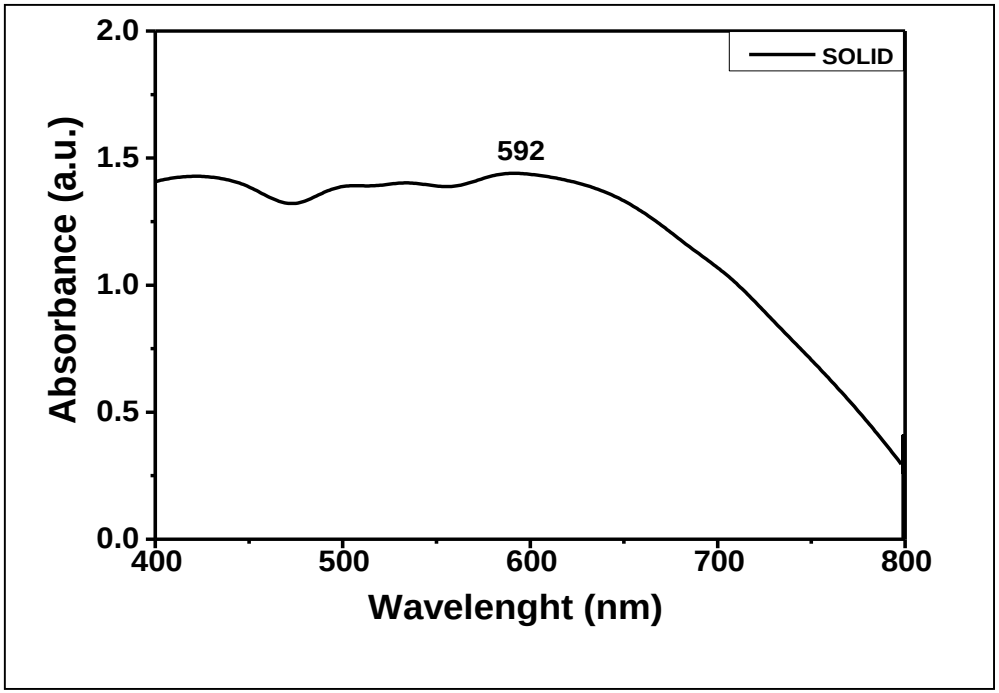

Figure 4.37: UV-Visible Absorbance of BP-PDSi in Solid State

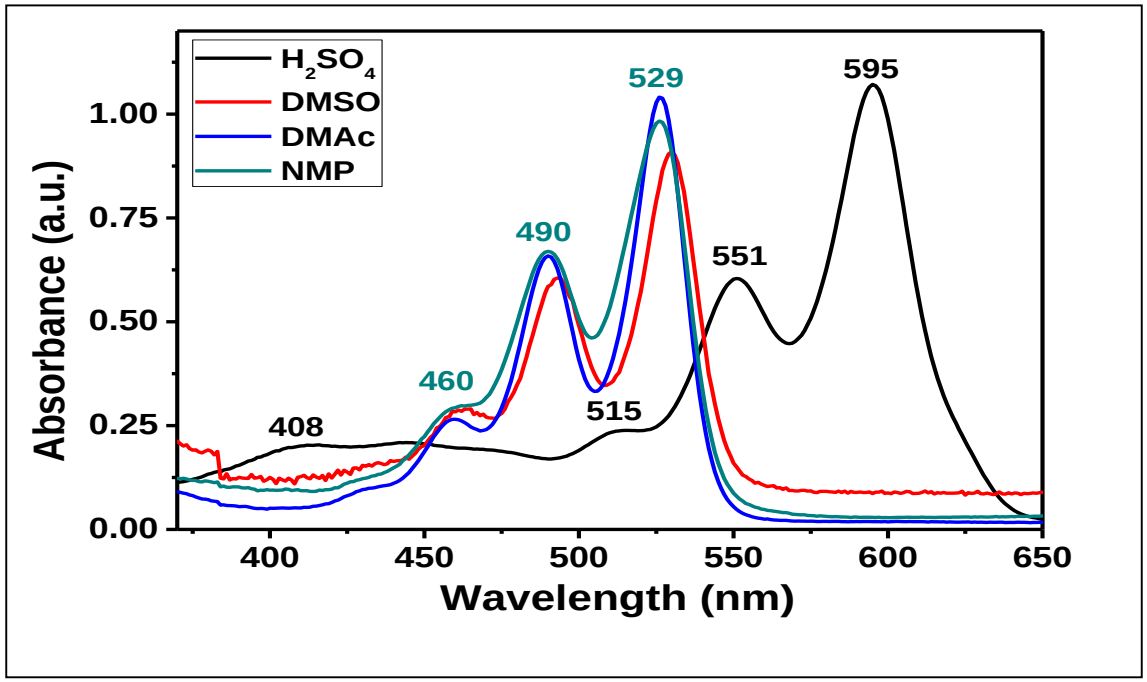

Figure 4.38: UV-Visible Absorbance of PDI-1 in H_2SO_4, DMSO, DMAc and NMP

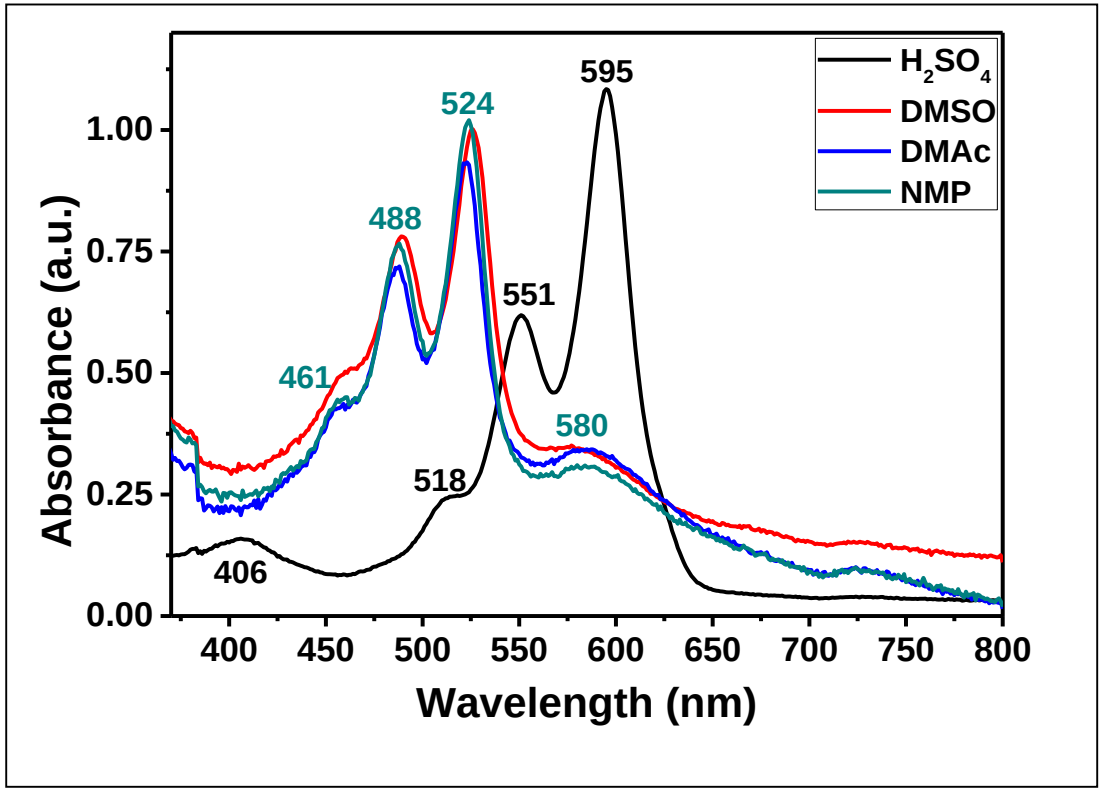

Figure 4.39: UV-Visible Absorbance of NSPDI in H_2SO_4, DMSO, DMAc and NMP

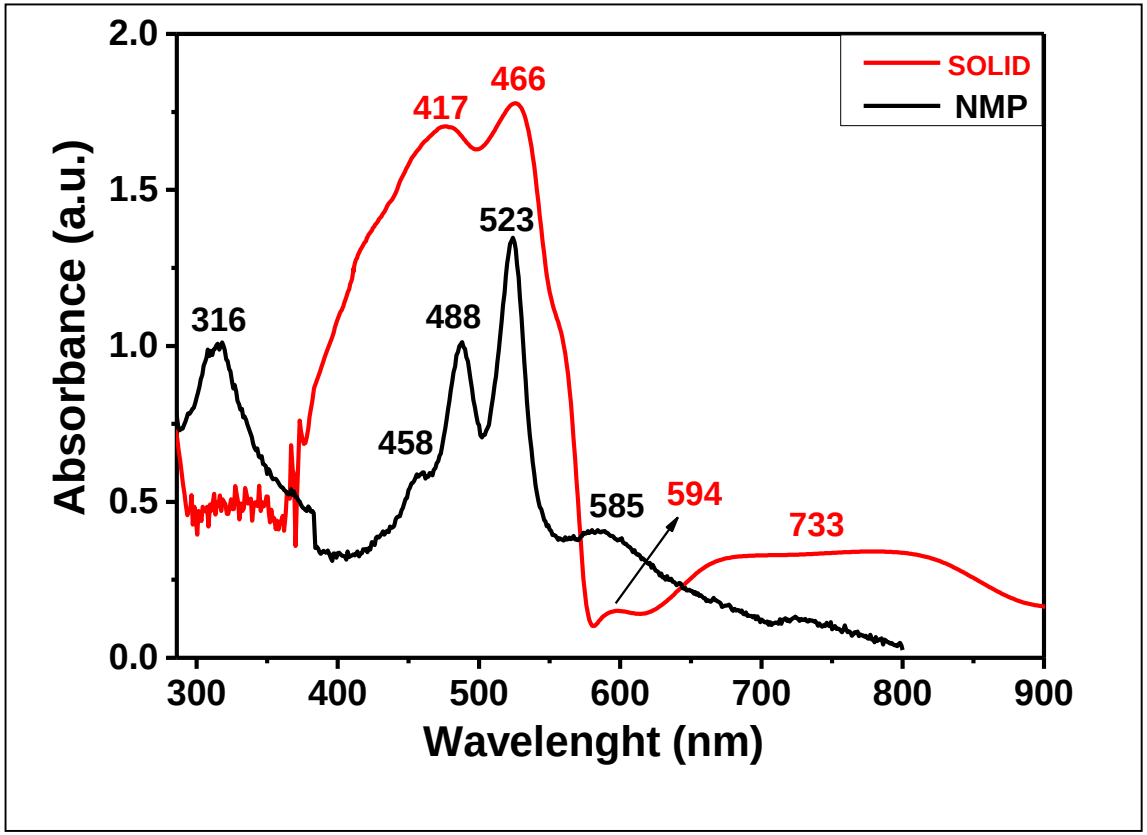

Figure 4.40: UV-Visible Absorbance of NSPDI in NMP Solution and in Solid-State

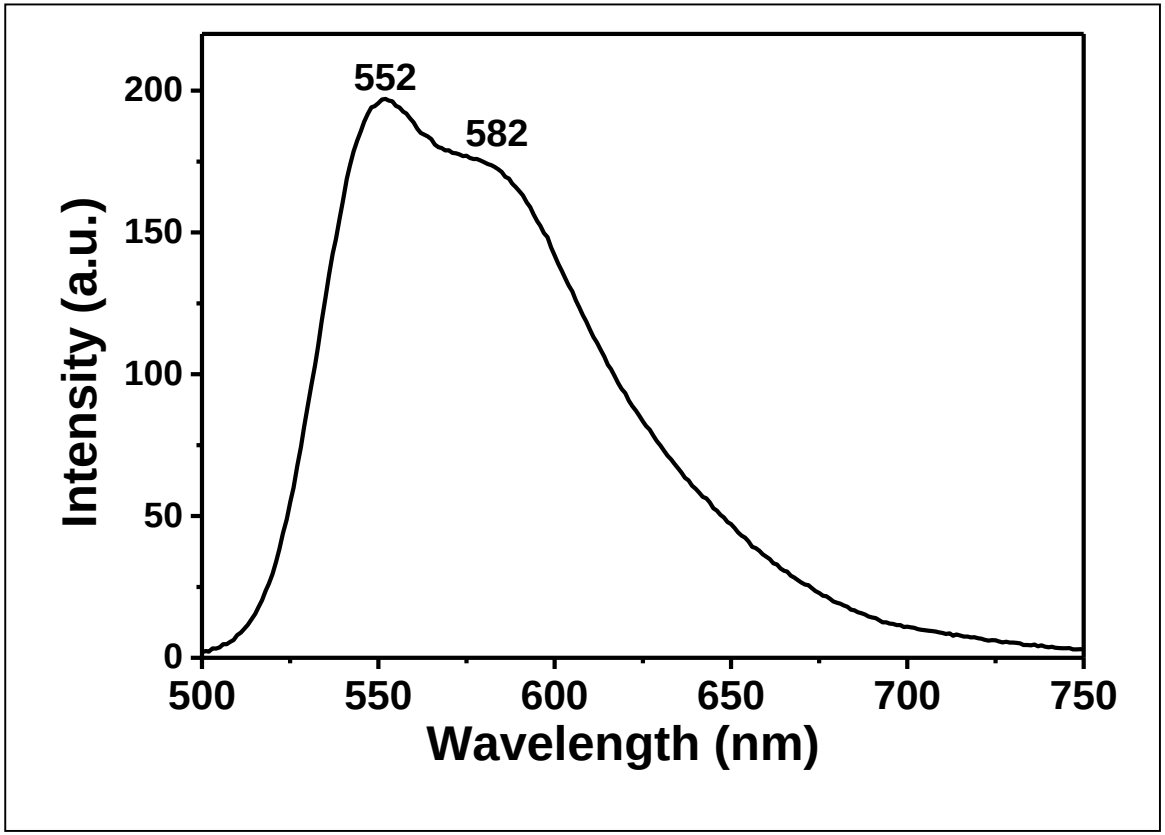

Figure 4.41: Emission-Spectra of Br-PDA in DMF

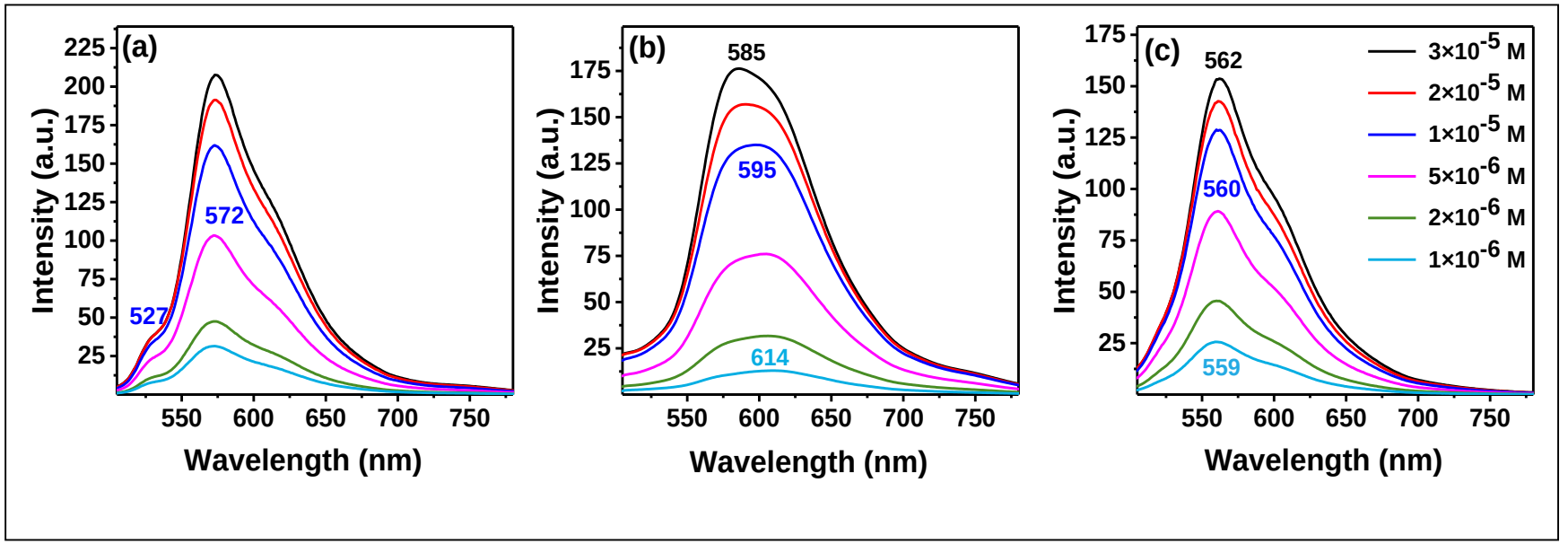

Figure 4.42: Concentration-Dependent-Emission (λ_{exc} = 485 nm) Spectra of BP-PDA in Different Solvents (DMF, NMP and THF at 3×10^{-5} M, 2×10^{-5} M, 1×10^{-5} M, 5×10^{-6} M, 2×10^{-6} M and 1×10^{-6} M Concentrations), (a) Emission in DMF, (b) Emission in NMP, (c) Emission in THF Respectively

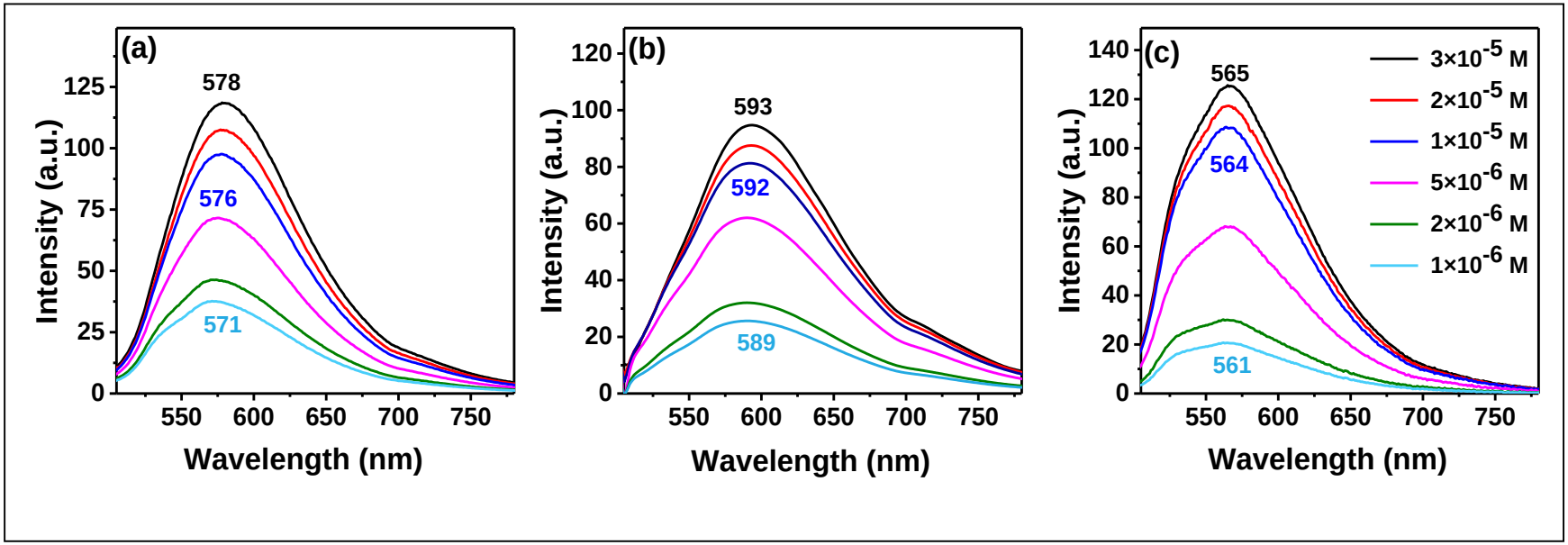

Figure 4. 43: Concentration-Dependent-Emission (λ_{exc} = 485 nm) Spectra of BP-PPI in Different Solvents (DMF, NMP and THF at 3×10^{-5} M, 2×10^{-5} M, 1×10^{-5} M, 5×10^{-6} M, 2×10^{-6} M and1×10^{-6} M Concentrations), (a) Emission in DMF, (b) Emission in NMP, (c) Emission in THF Respectively

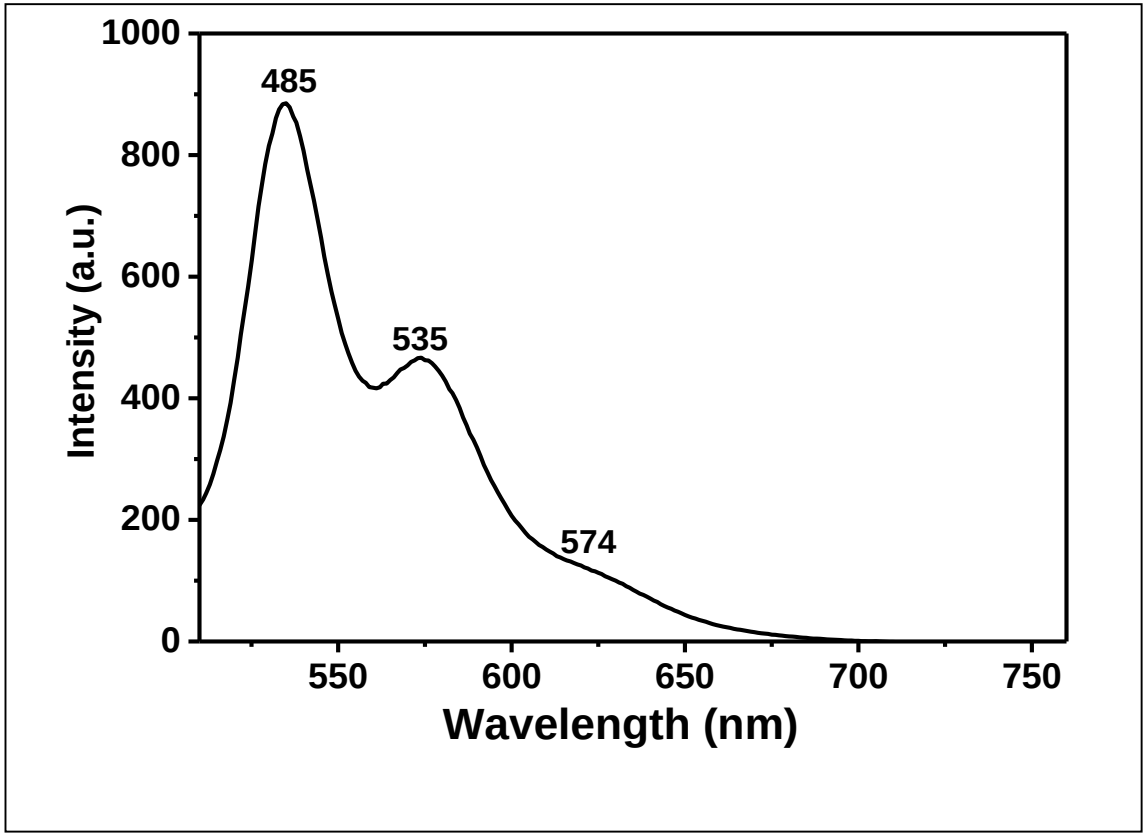

Figure 4.44: Emission-Spectra of Br-PDD in NMP

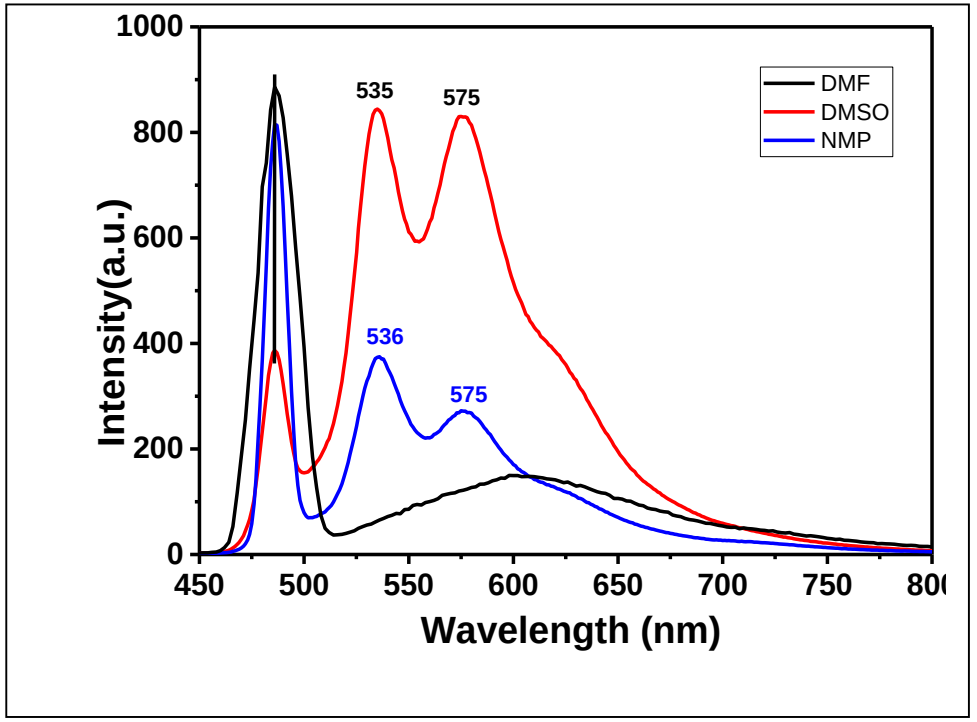

Figure 4.45: Emission-Spectra of BC-PDD in Different Solvent

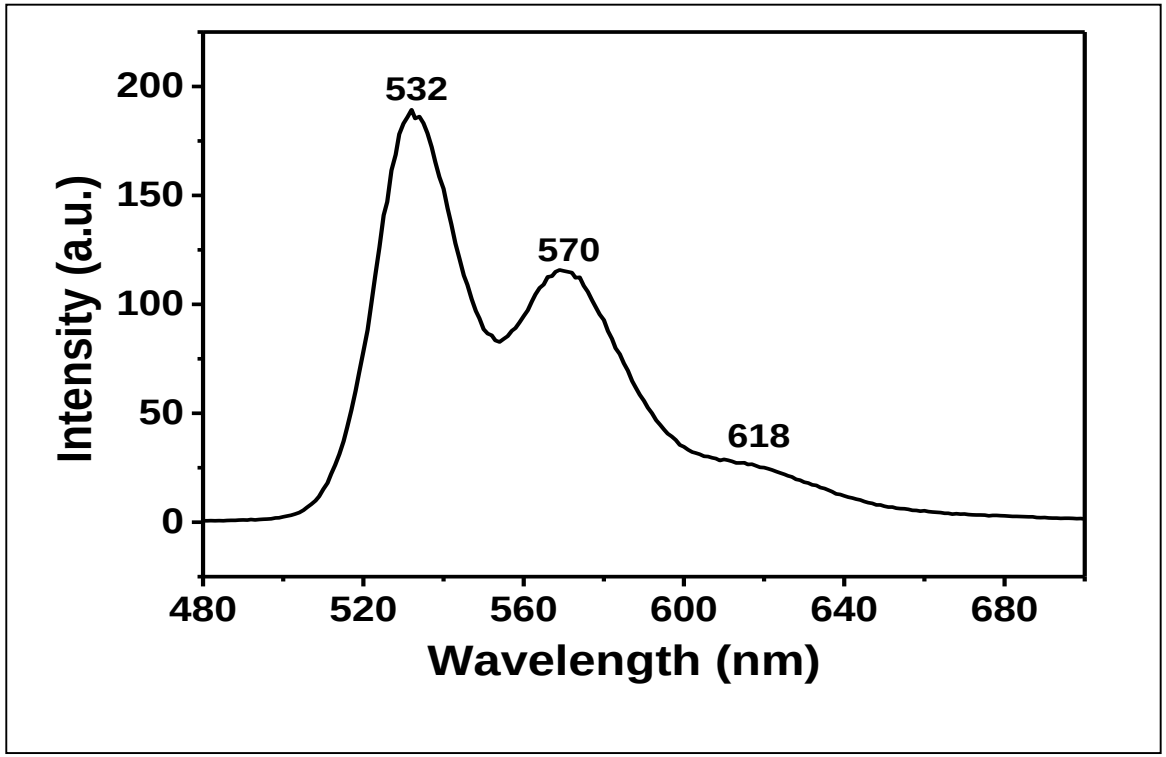

Figure 4.46: Emission-Spectra of PMI in DMF

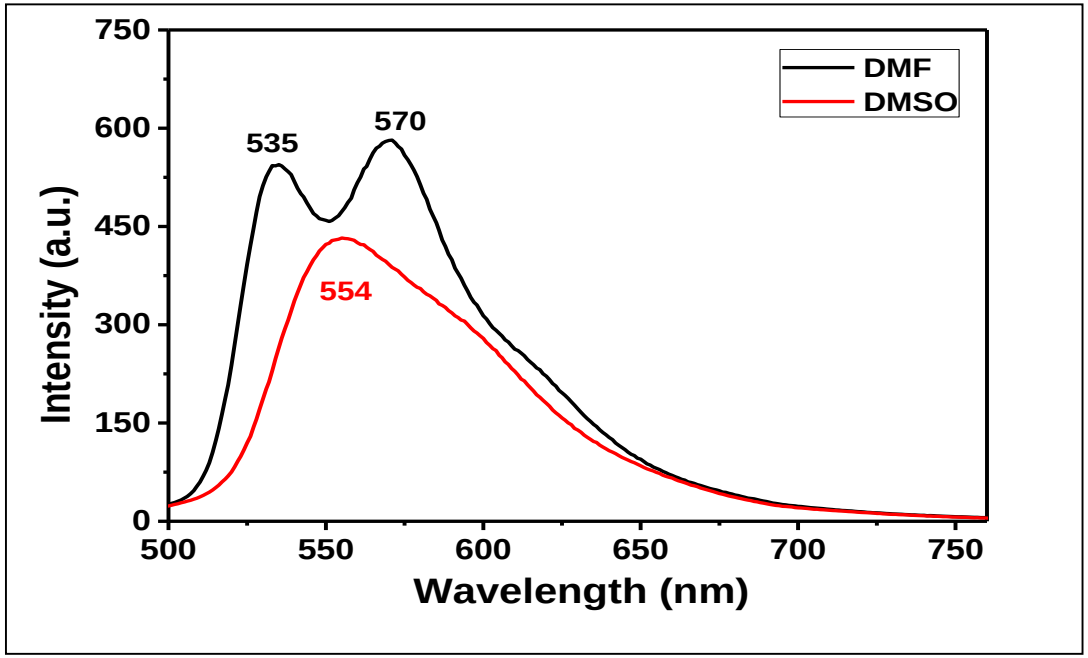

Figure 4.47: Emission-Spectra of BPDA-PDA in DMF and DMSO

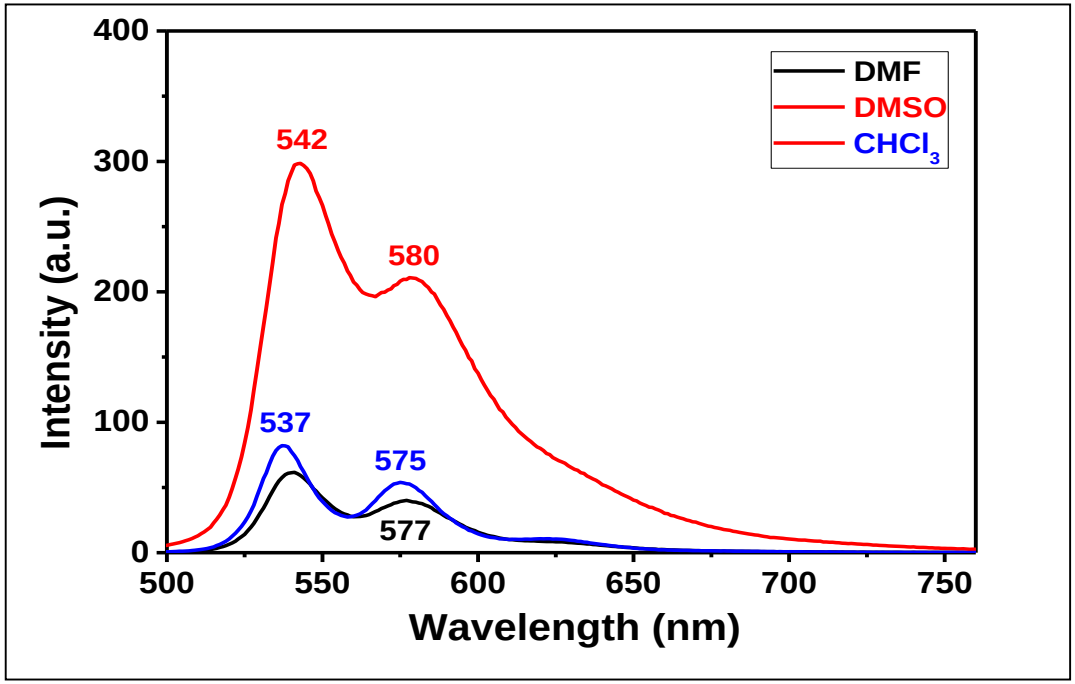

Figure 4.48: Emission-Spectra of BPDI-PDI in DMF, DMSO and $CHCl_3$

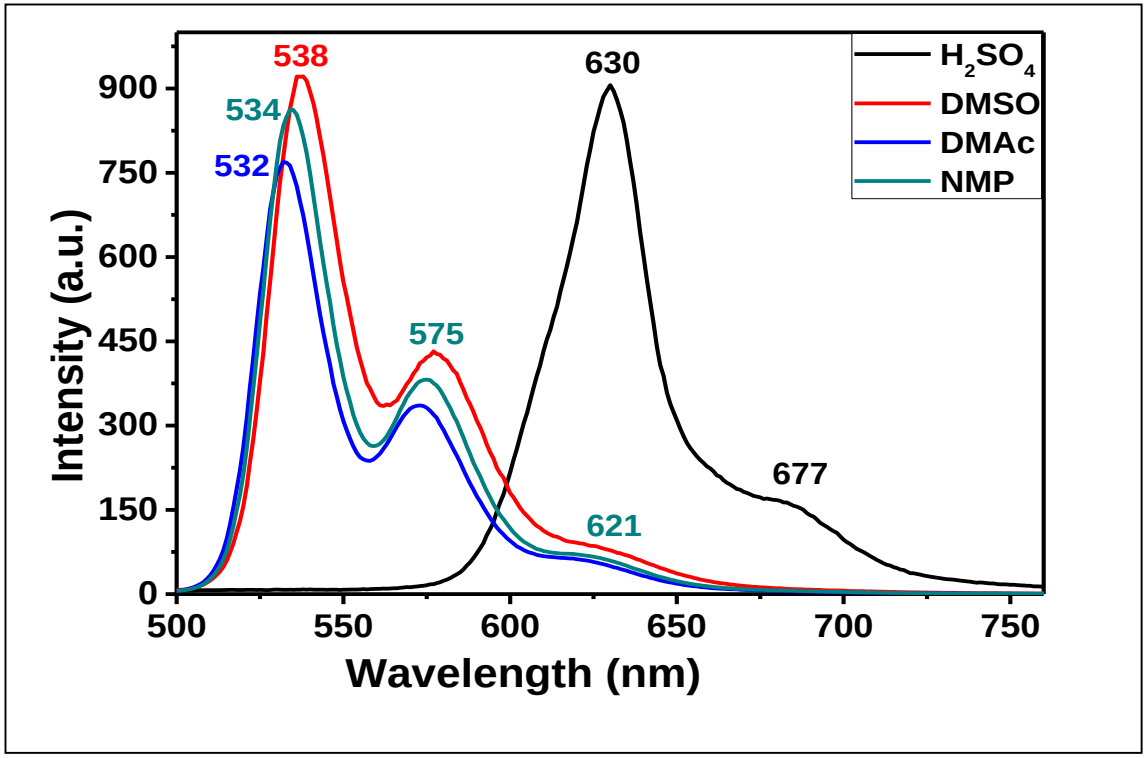

Figure 4.49: Emission (λ_{exc} = 560 nm) Spectra of PDI-1 in Different Solvents (H_2SO_4, DMSO, DMAc and NMP)

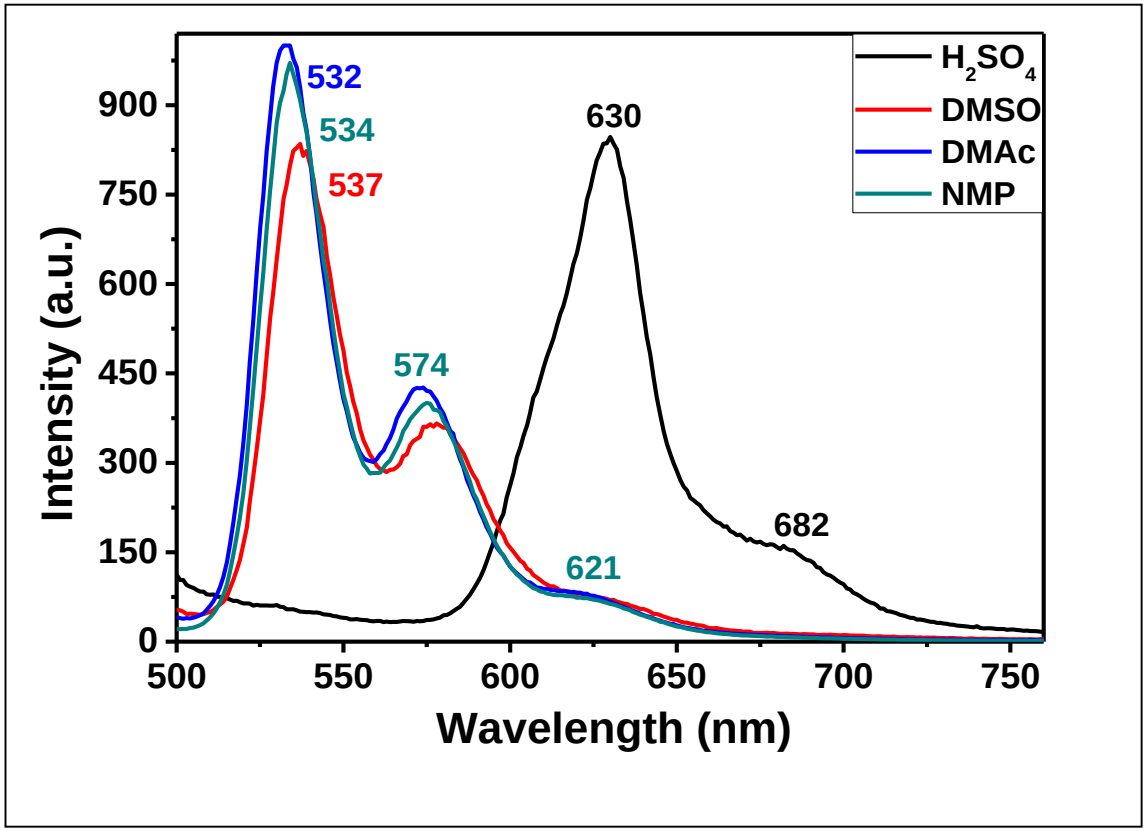

Figure 4.50: Emission-Spectra of NSPDI in Different Solvents
(H_2SO_4, DMSO, DMAc and NMP)

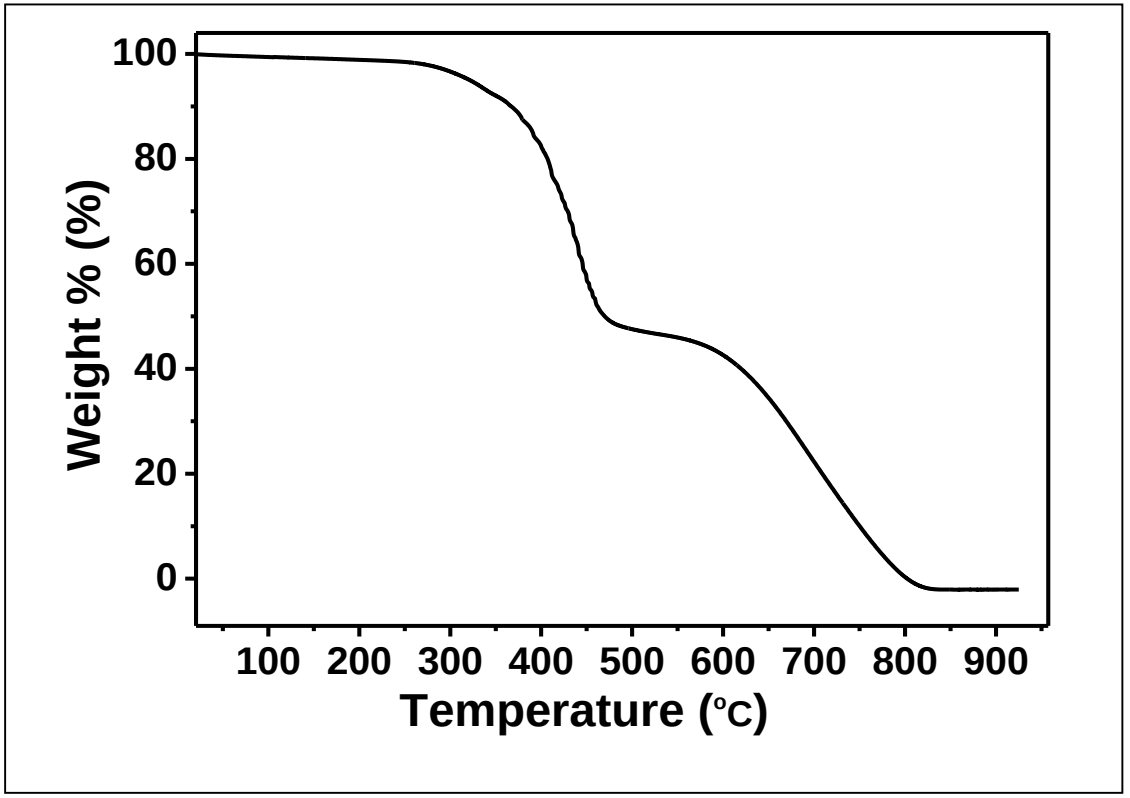

Figure 4.51: TGA-Thermograms of BP-PPI

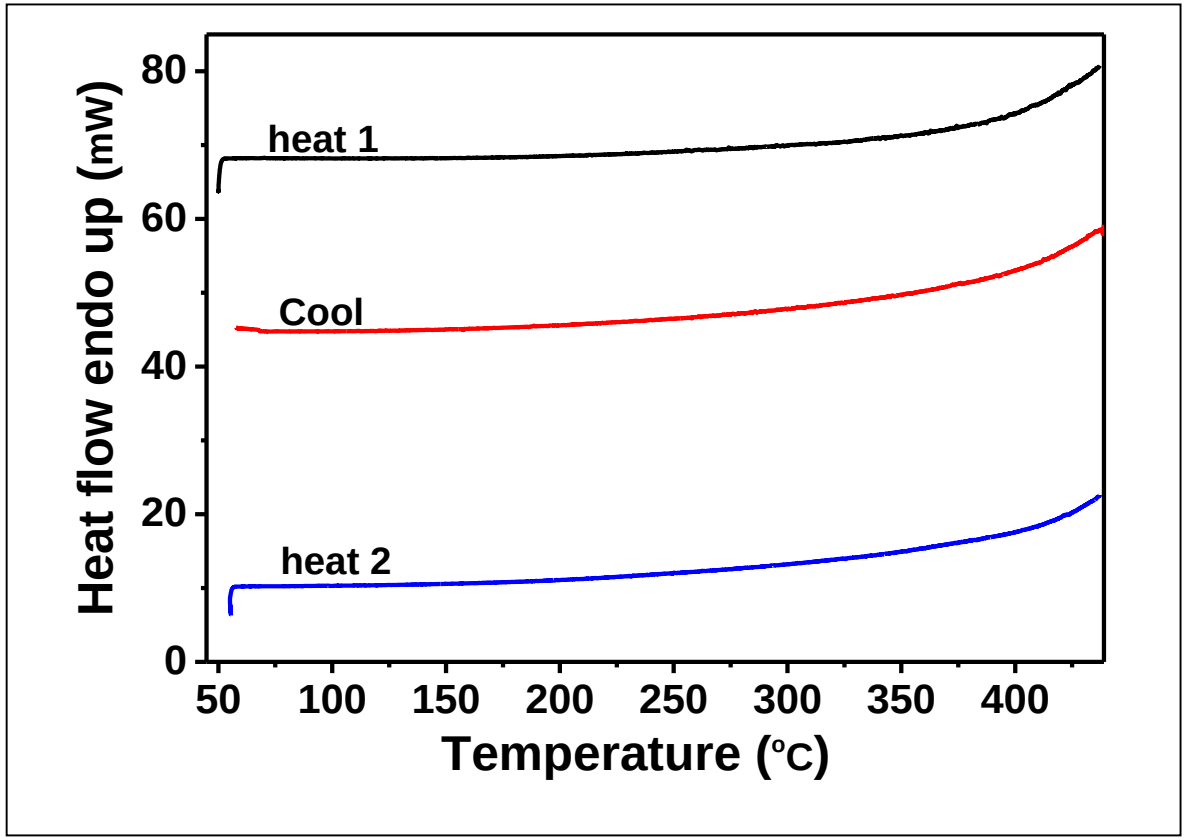

Figure 4.52: DSC-Diagram of BP-PPI

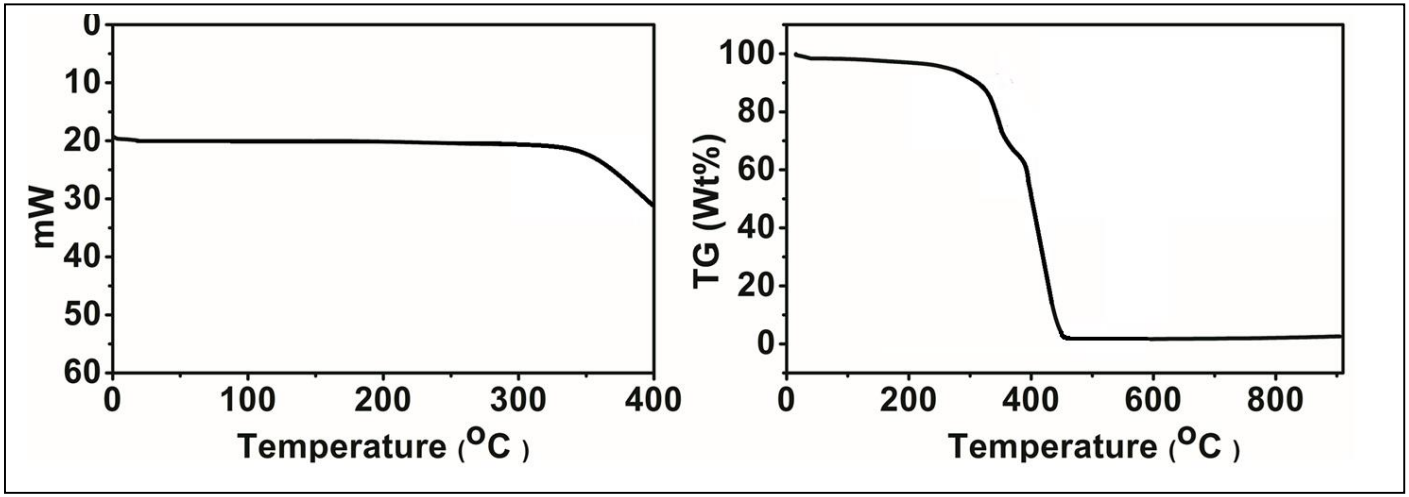

Figure 4.53: DSC-Diagram and TGA Thermograms of BC-PDD

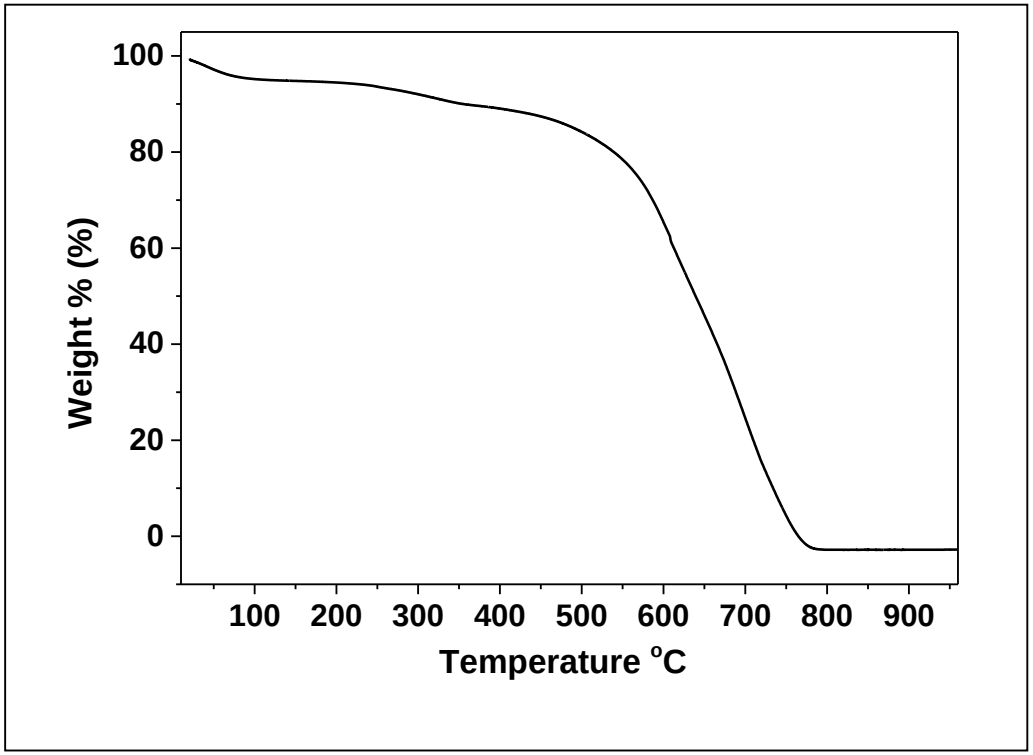

Figure 4.54: TGA-Thermograms of BPDA-PDA

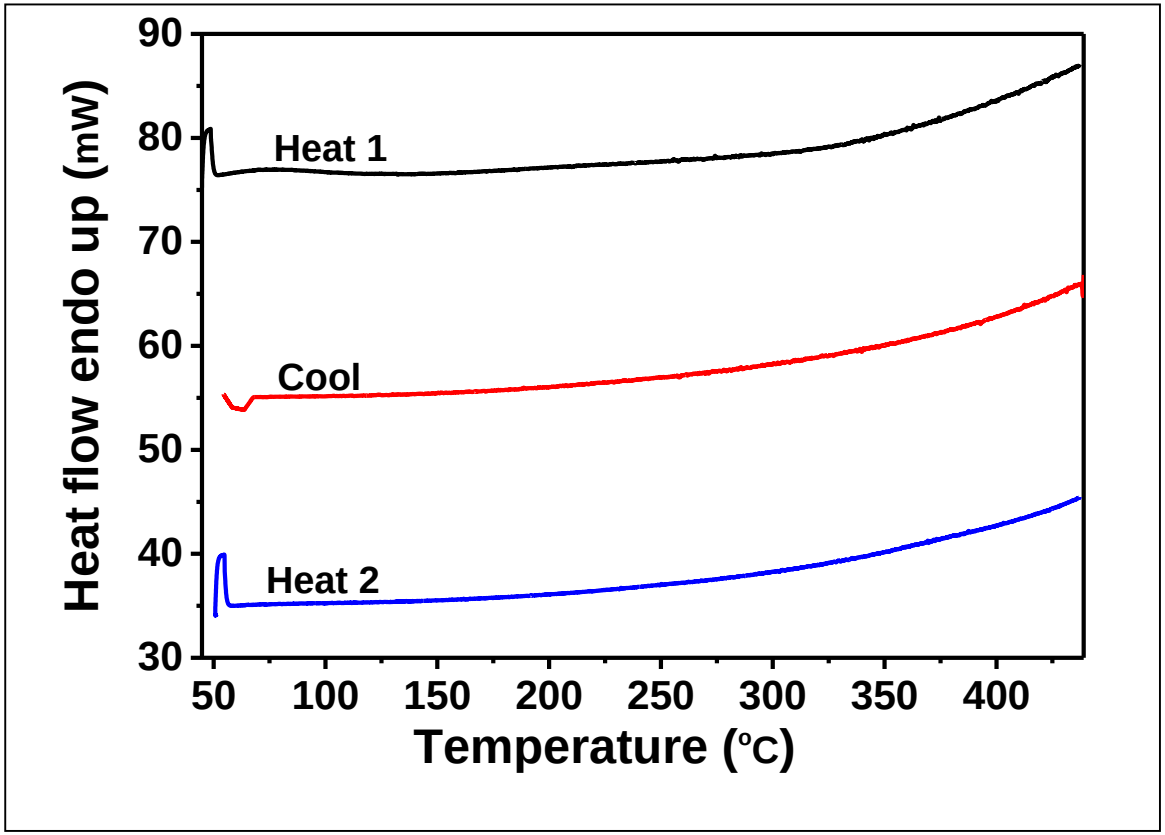

Figure 4.55: DSC-Diagram of BPDA-PDA

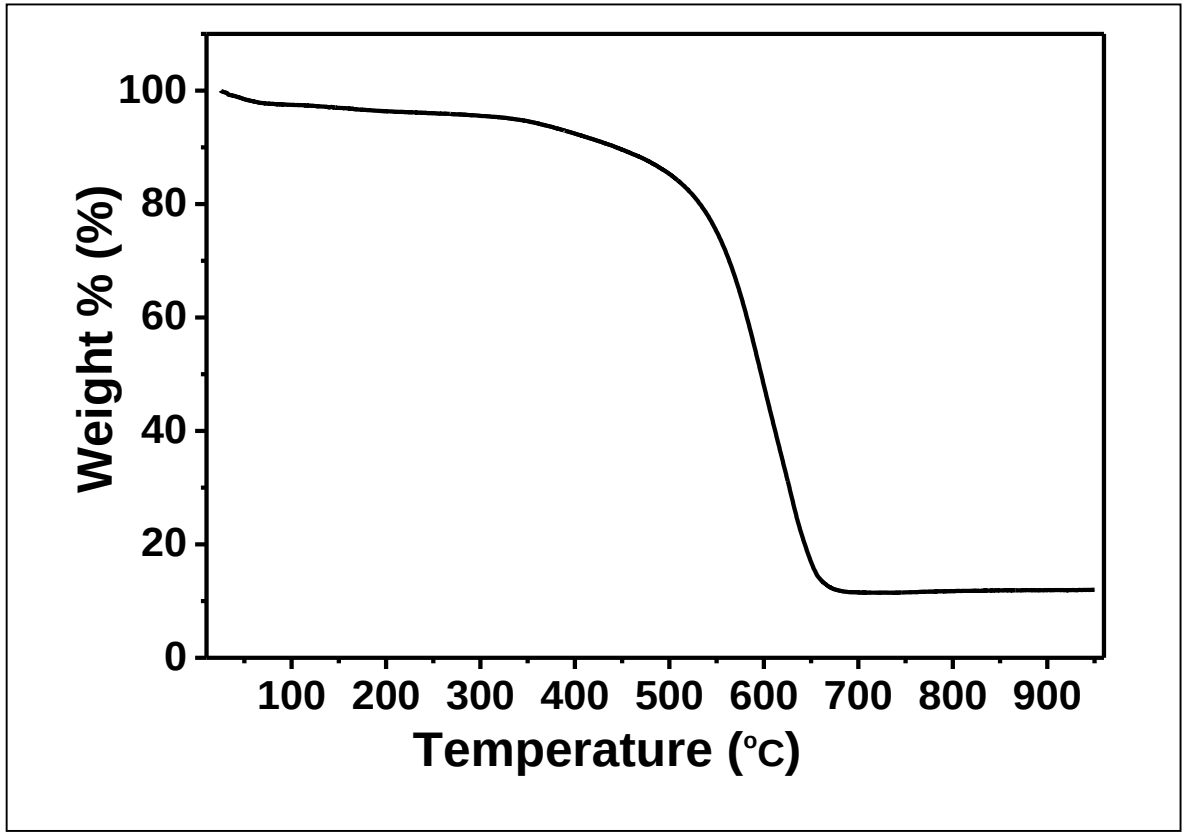

Figure 4.56: TGA-Thermograms of BPDAI-PDI

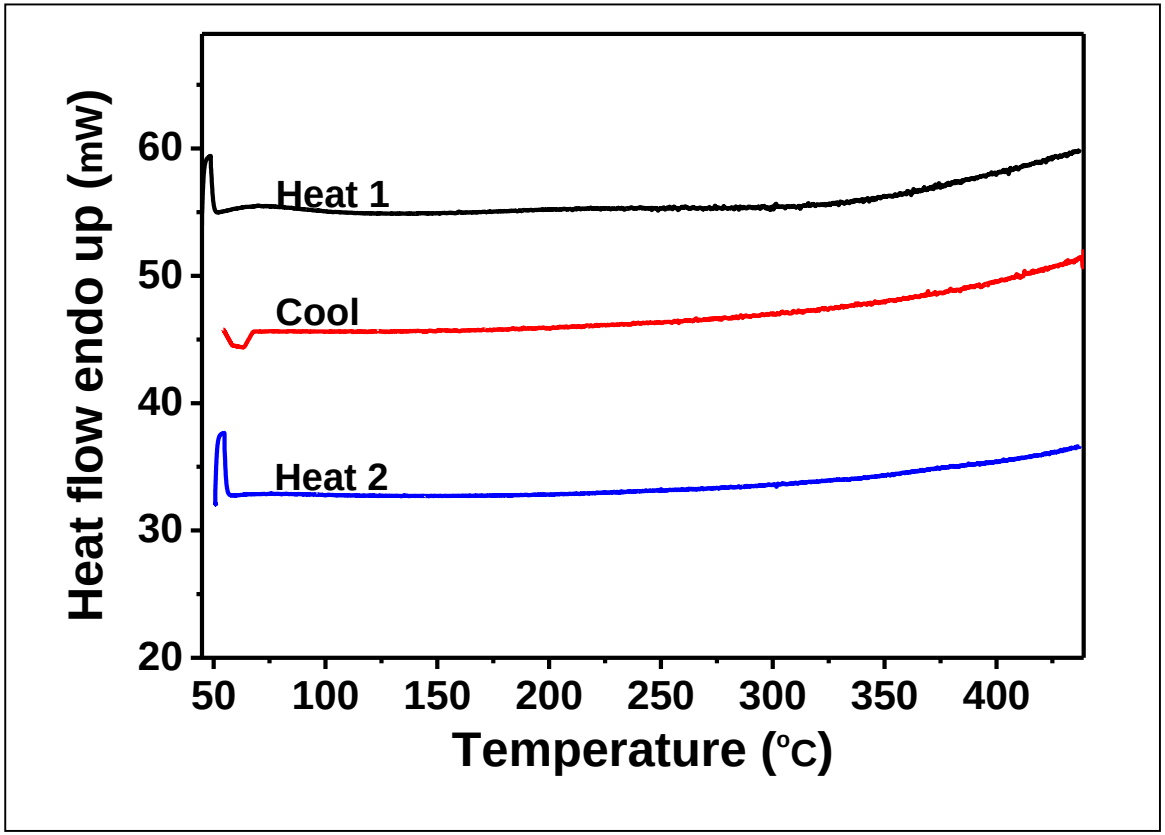

Figure 4.57: DSC-Diagram of BPDI-PDI

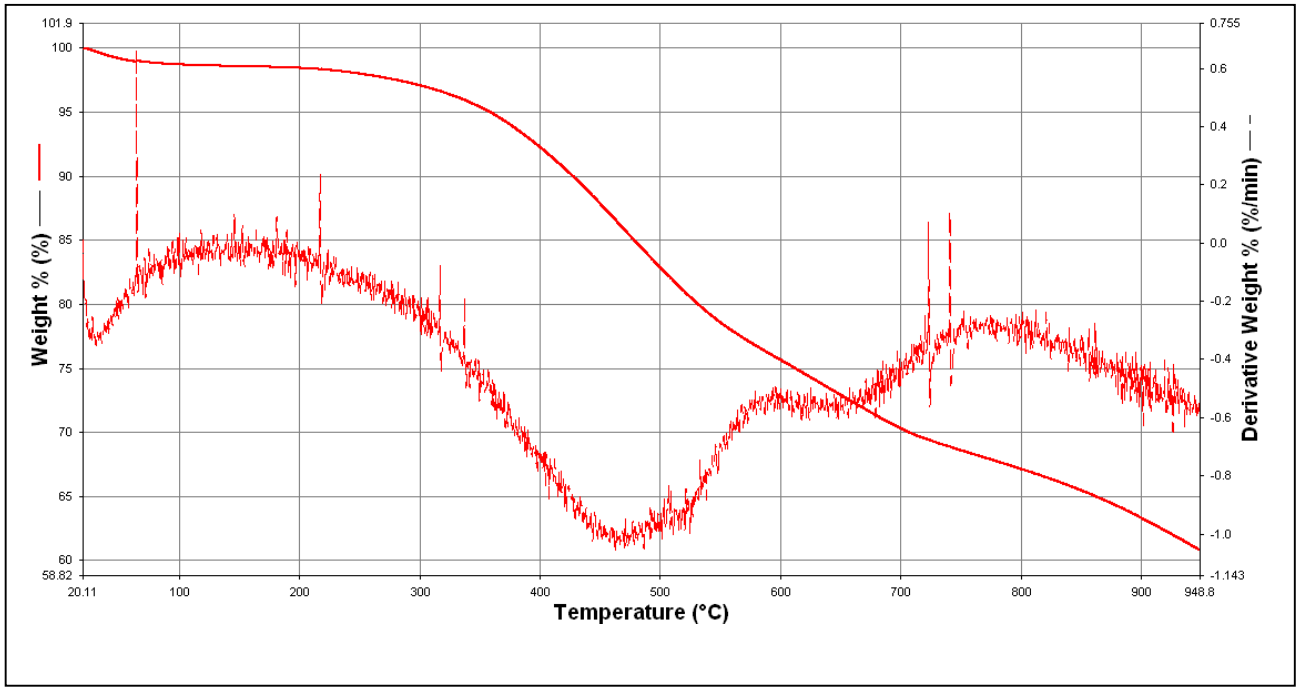

Figure 4.58: TGA-Thermograms of BP-PDSi

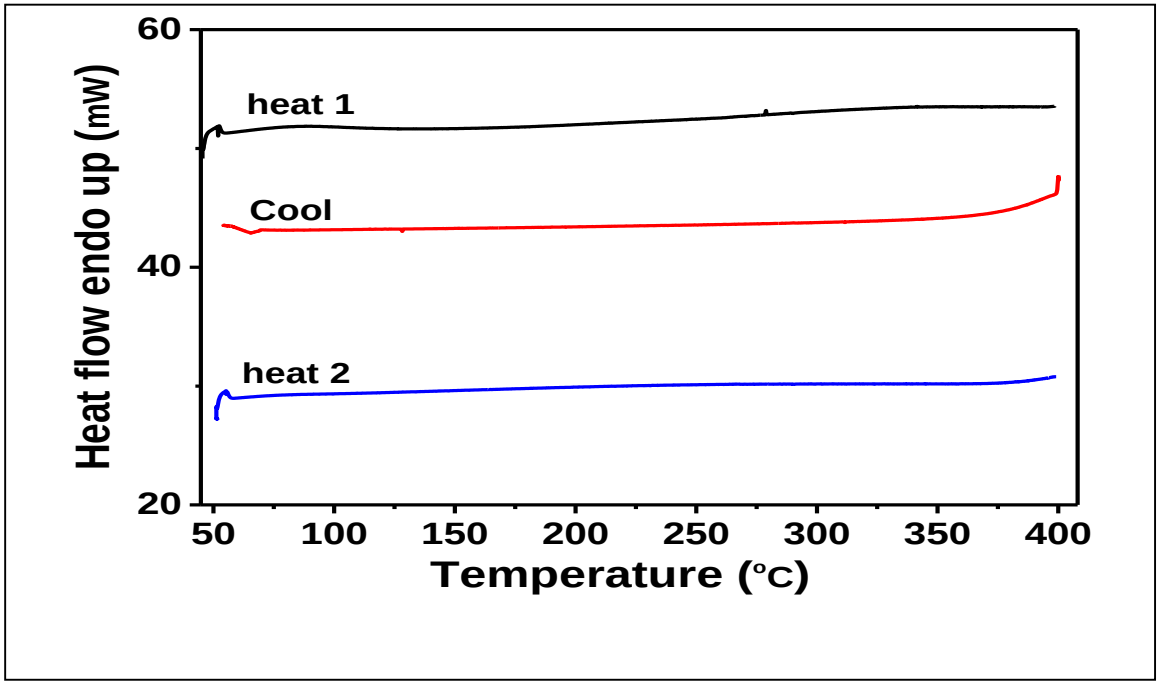

Figure 4.59: DSC-diagram of BP-PDSi

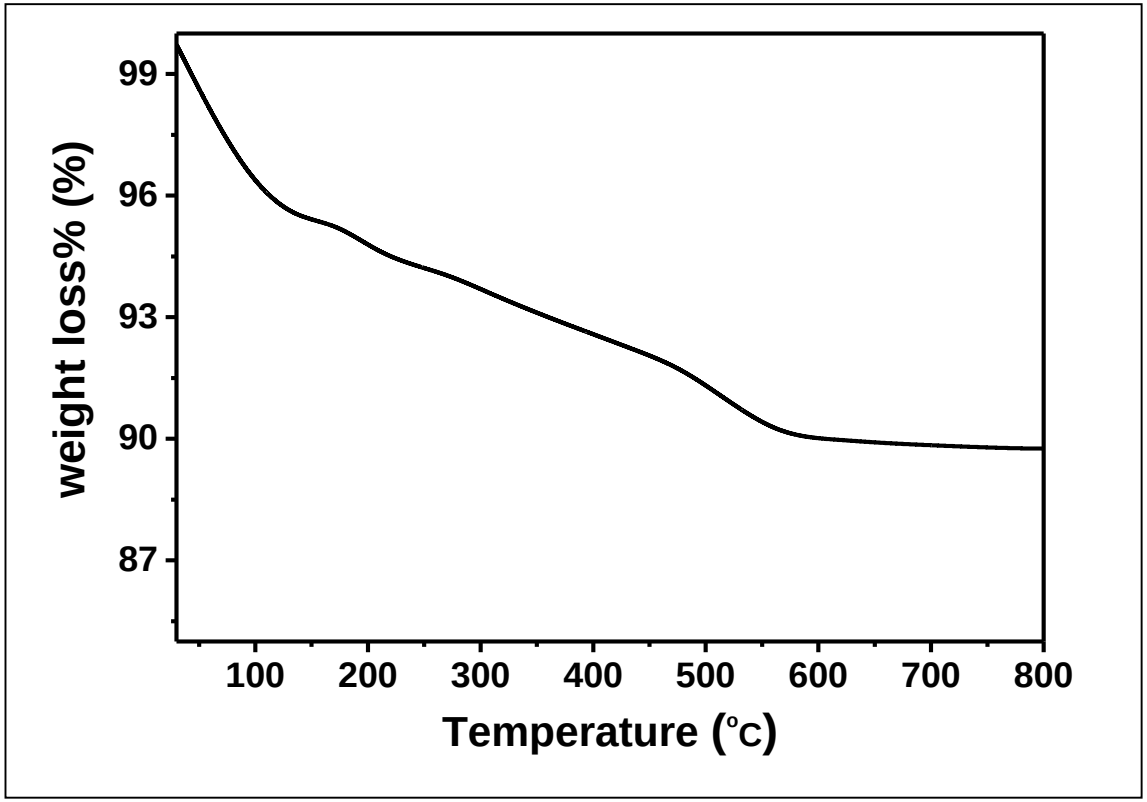

Figure 4.60: TGA-Thermograms of Nanosilica

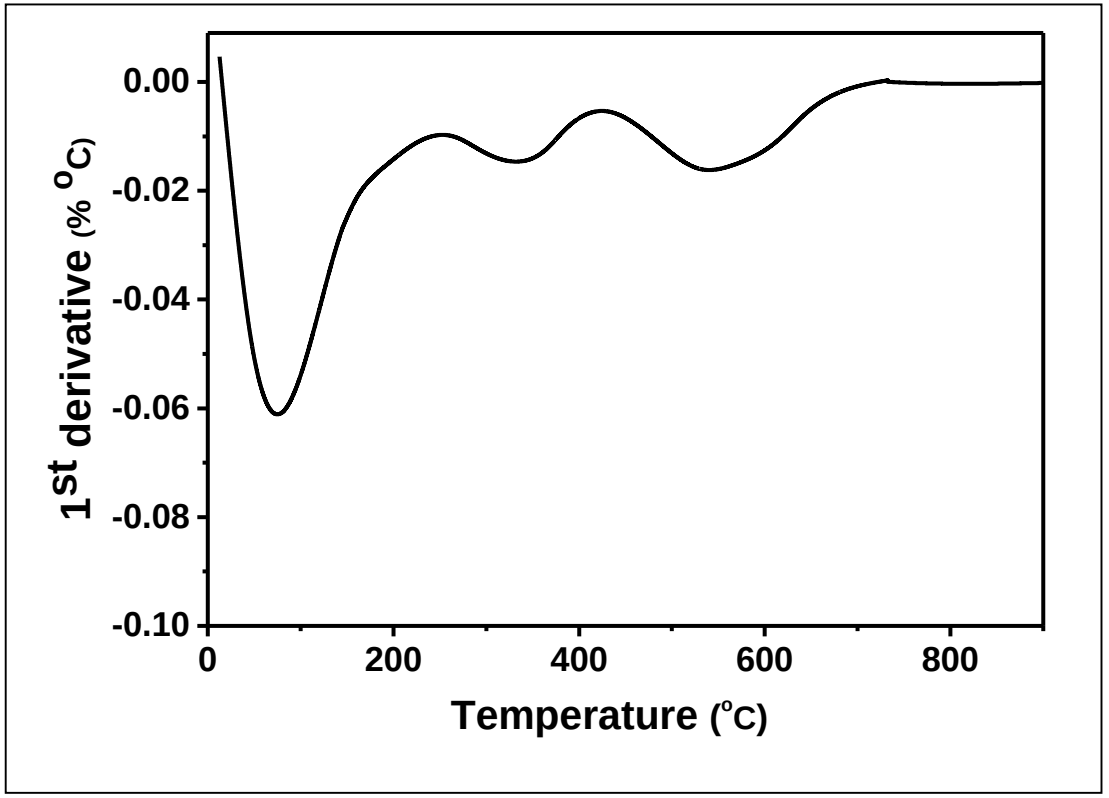

Figure 4.61: DSC Diagram of Nanosilica

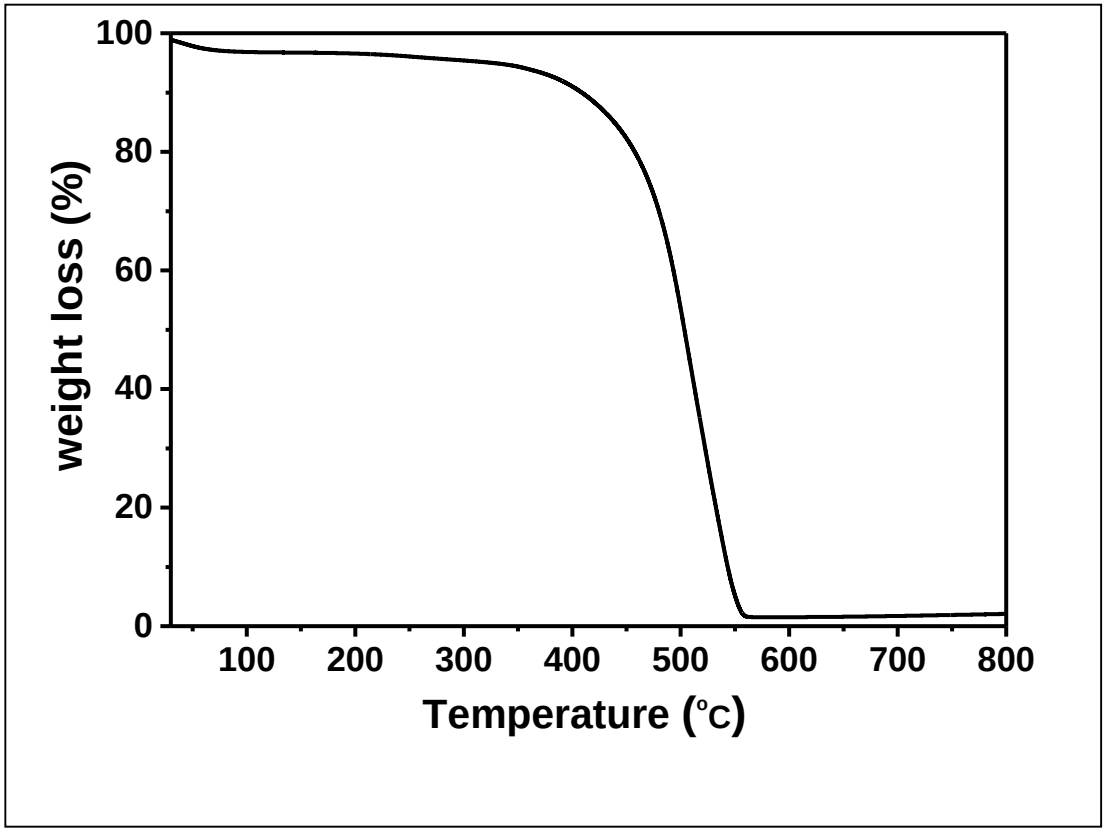

Figure 4.62: TGA-thermograms of NSPDI

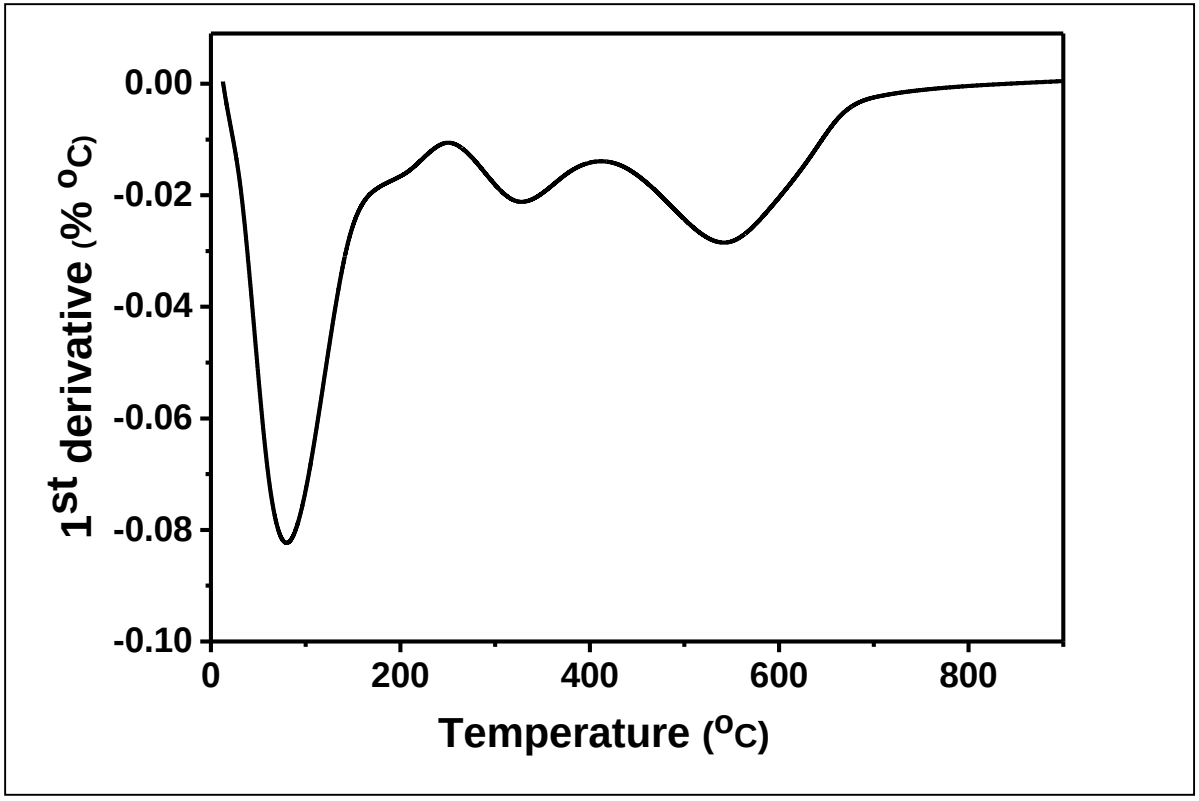

Figure 4.63: DSC-Diagram of NSPDI

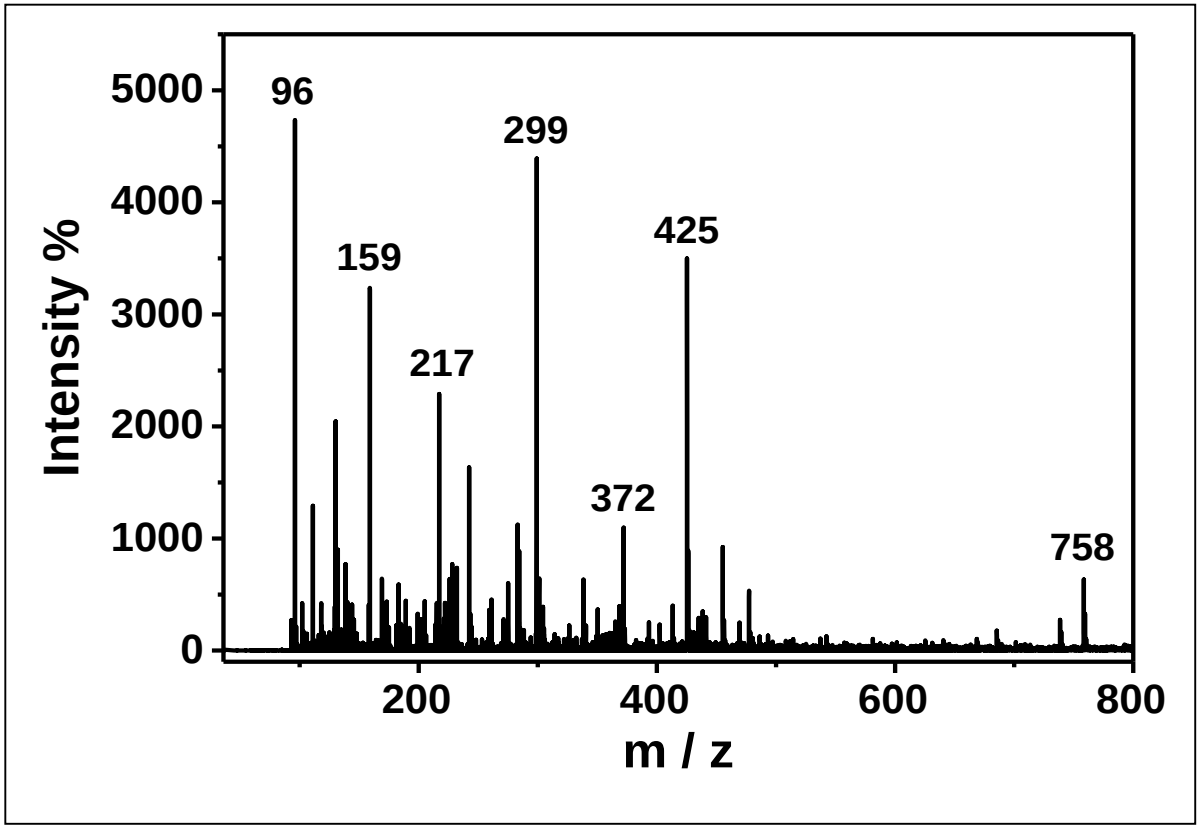

Figure 4.64: Mass Spectrum of BP-PPI

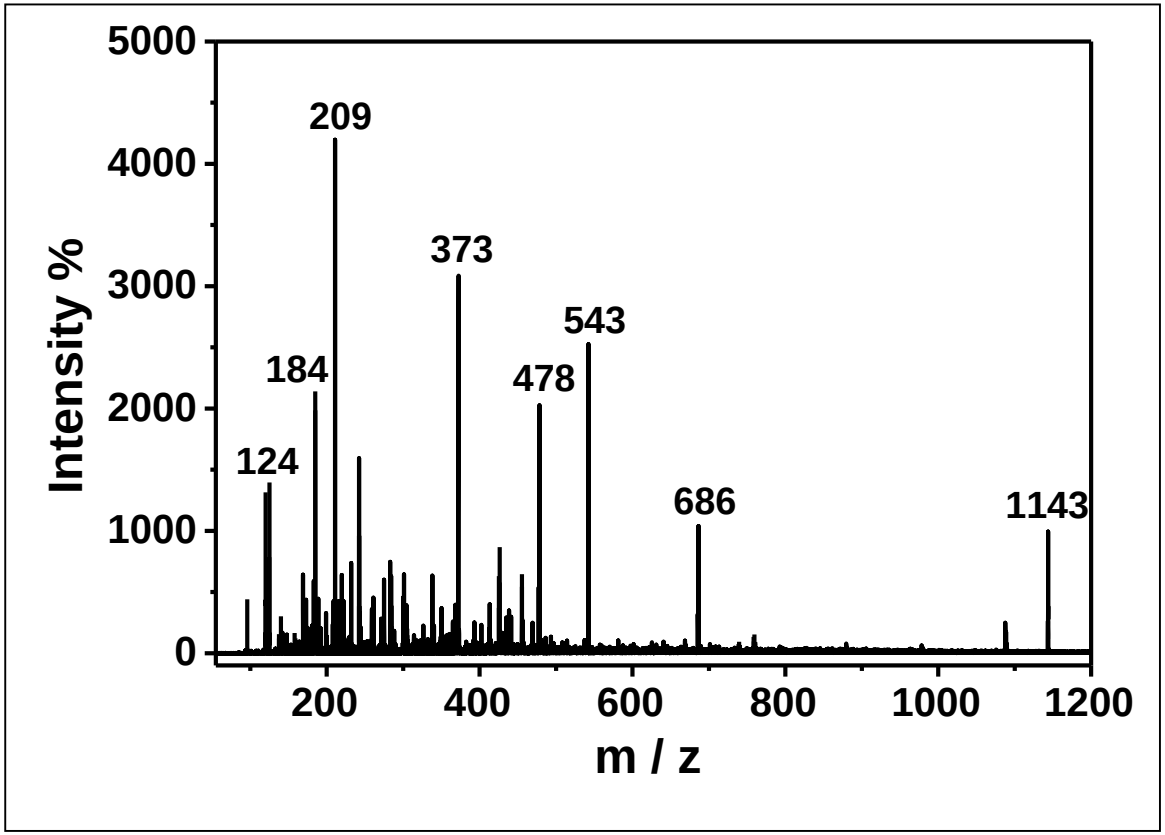

Figure 4.65: Mass Spectrum of BC-PDD

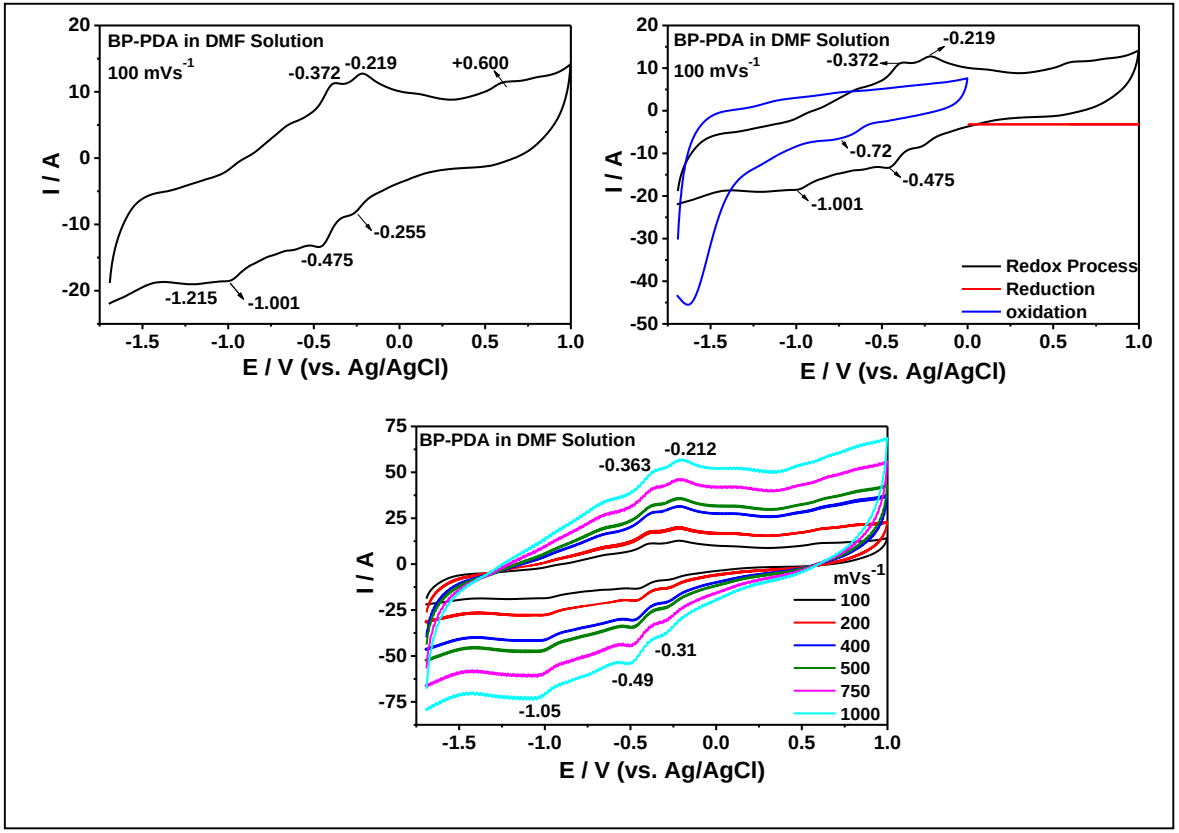

Figure 4.66: Cyclic-Voltammogram of BP-PDA, on the Left Only at 100 mVs^{-1}, on the Right at Different Scan-Rate (100-1000 mVs^{-1}) in DMF

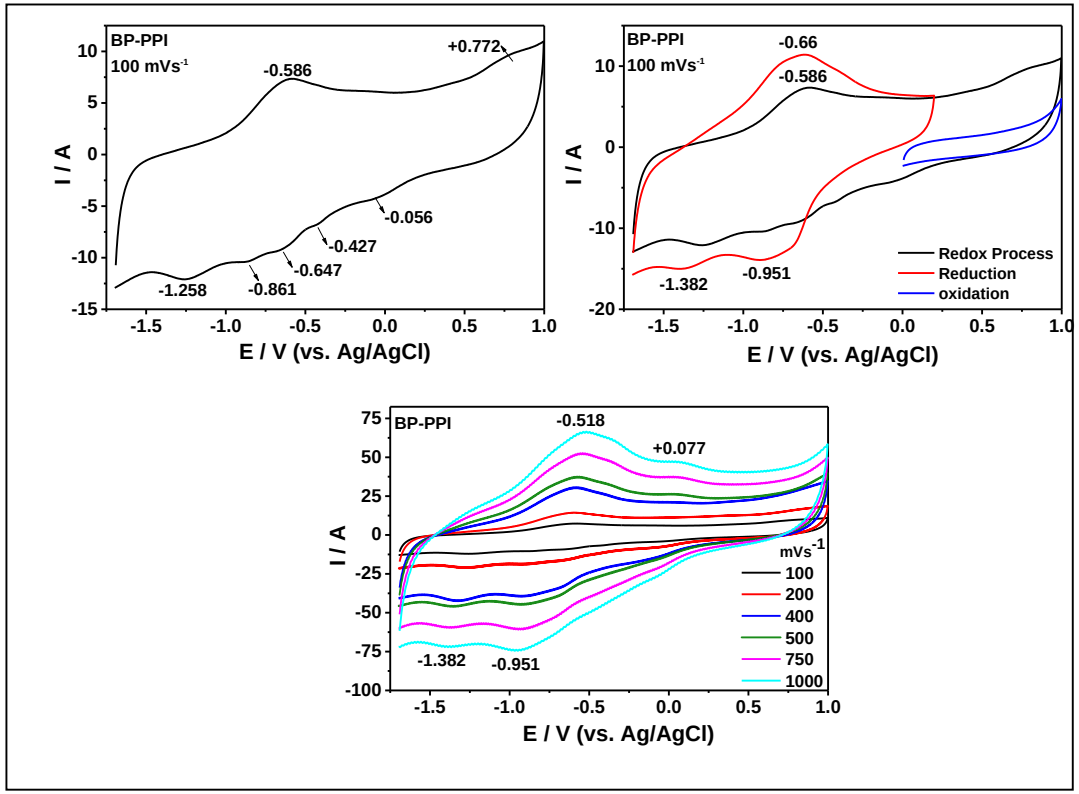

Figure 4.67: Cyclic-Voltammogram of BP-PPI, on the Left Only at 100 mVs^{-1}, on the Right at Different Scan-Rate (100-1000 mVs^{-1}) in DMF

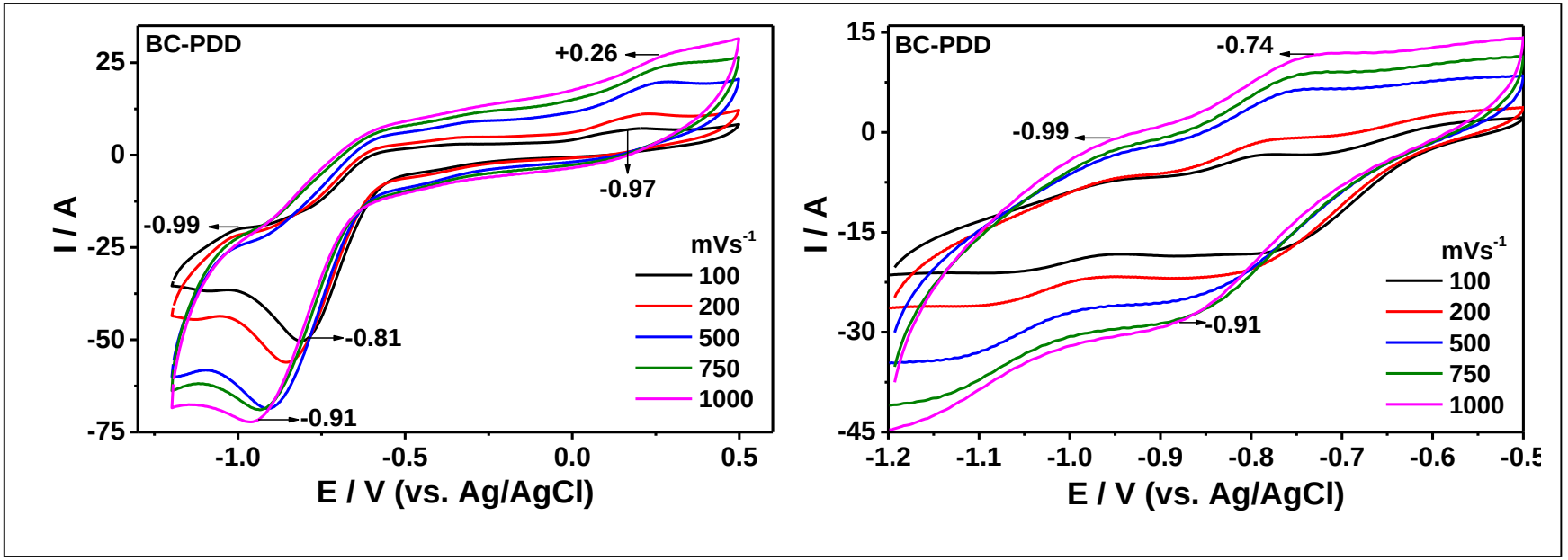

Figure 4.68: Cyclic-Voltammogram of BC-PDD, Different Scan-Rate (100-1000 mVs^{-1}) in DMF Solution

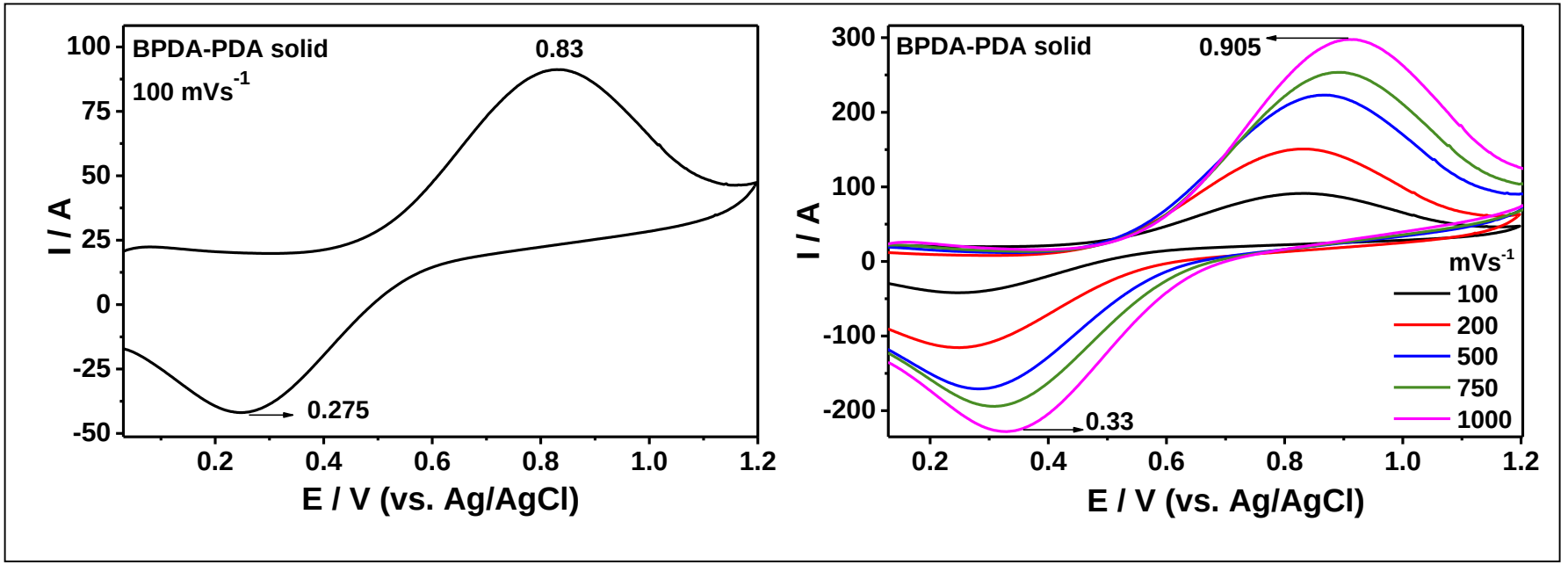

Figure 4.69: Cyclic-Voltammogram of BPDA-PDA, Scan Rate (100 mVs^{-1}) in Solid-State

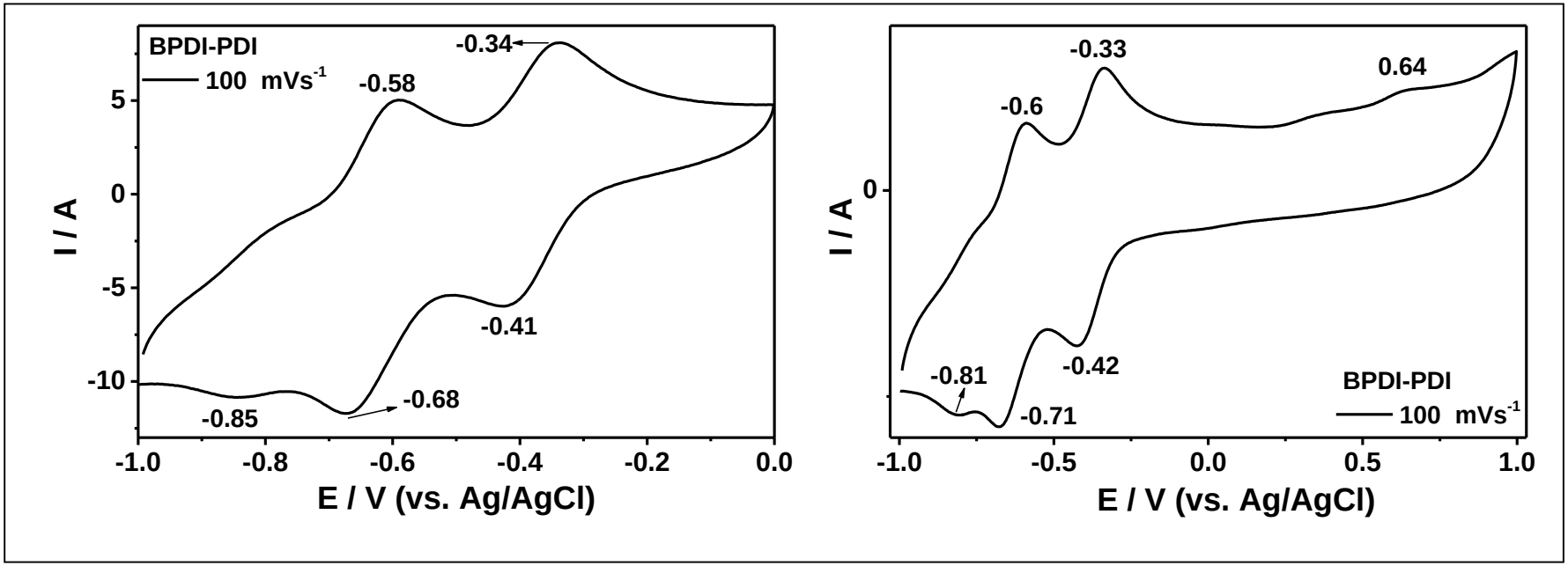

Figure 4.70: Cyclic-Voltammogram of BPDI-PDI, Scan-Rate (100 mVs^{-1}) in DMF Solution

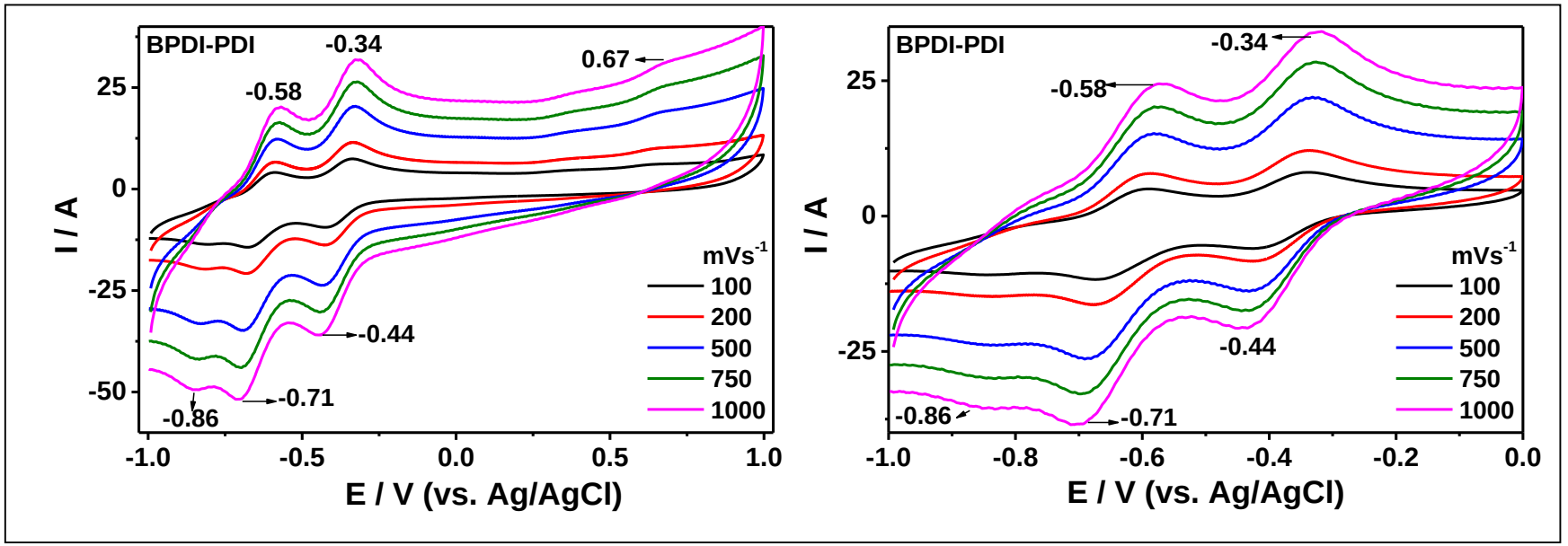

Figure 4.71: Cyclic-Voltammogram of BPDI-PDI, at Different Scan-Rate (100-1000 mVs^{-1}) in DMF Solution

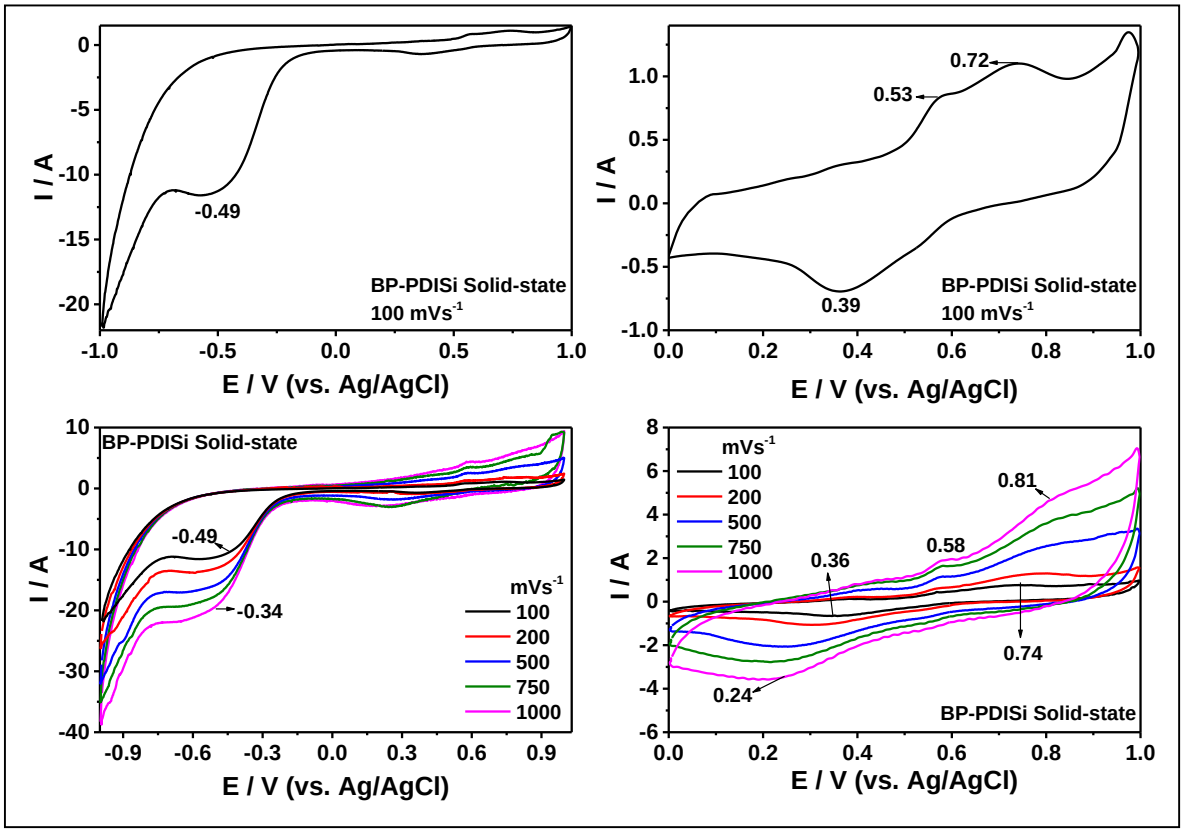

Figure 4.72: Cyclic-Voltammogram of BP-PDISi, at Different Scan-Rate (100-1000 mVs^{-1}) in Solid-State

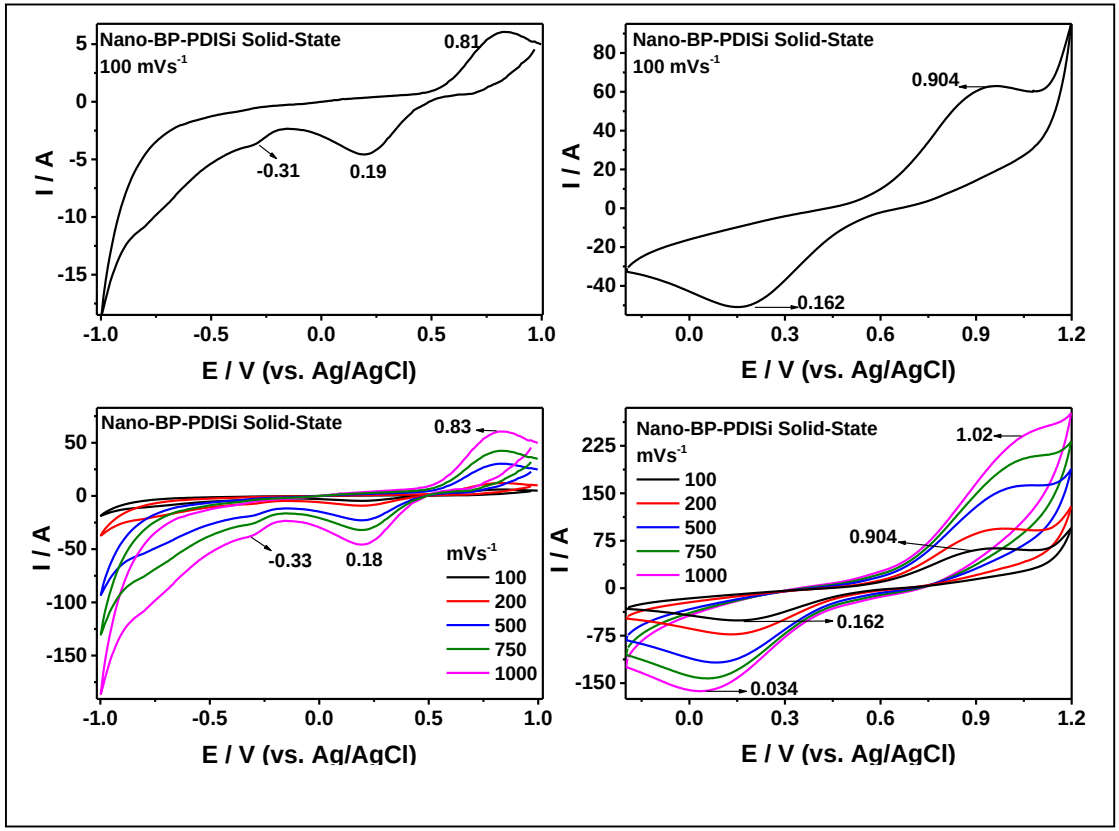

Figure 4.73: Cyclic-Voltammogram of Nano-BP-PDISi, at Different Scan-Rate (100-1000 mVs-1) in Solid-State

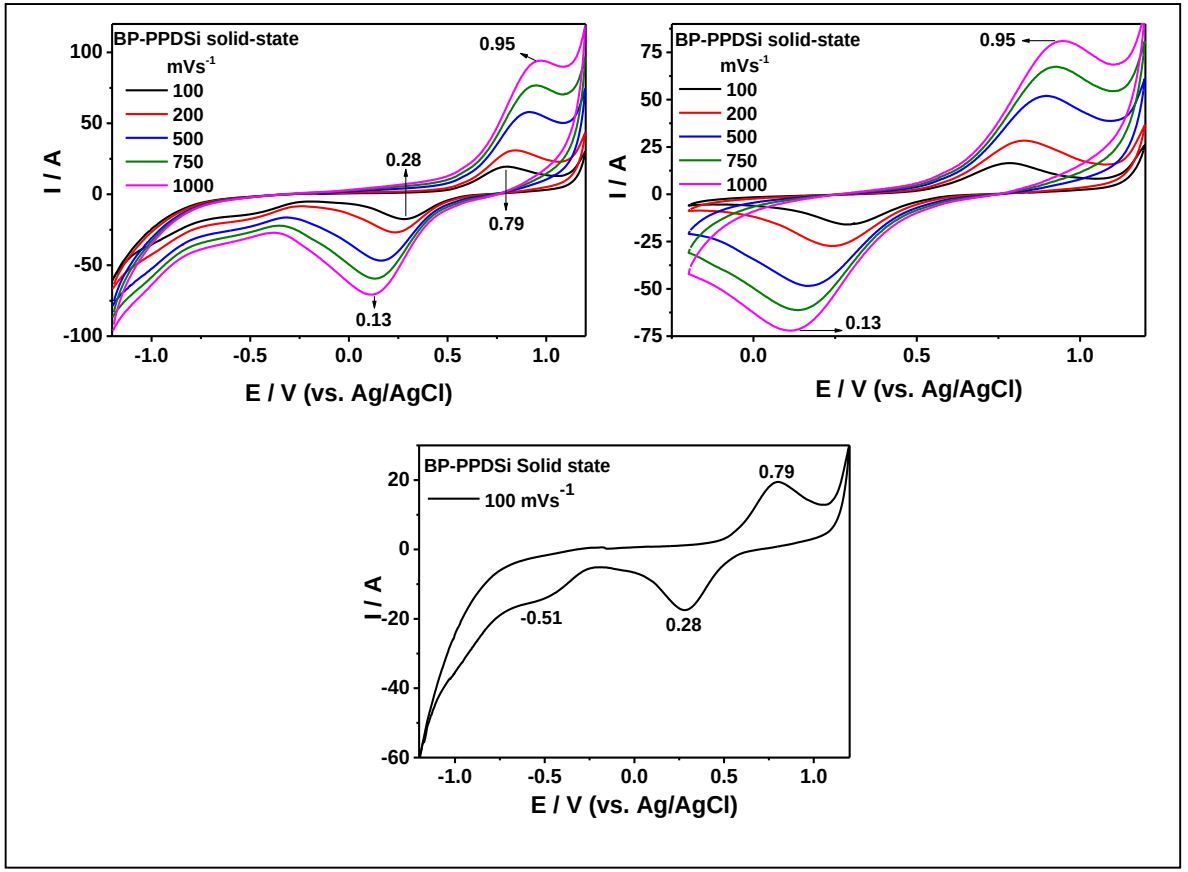

Figure 4.74: Cyclic-Voltammogram of BP-PPDSi, at Different Scan-Rate (100-1000 mVs^{-1}) in Solid-Stat

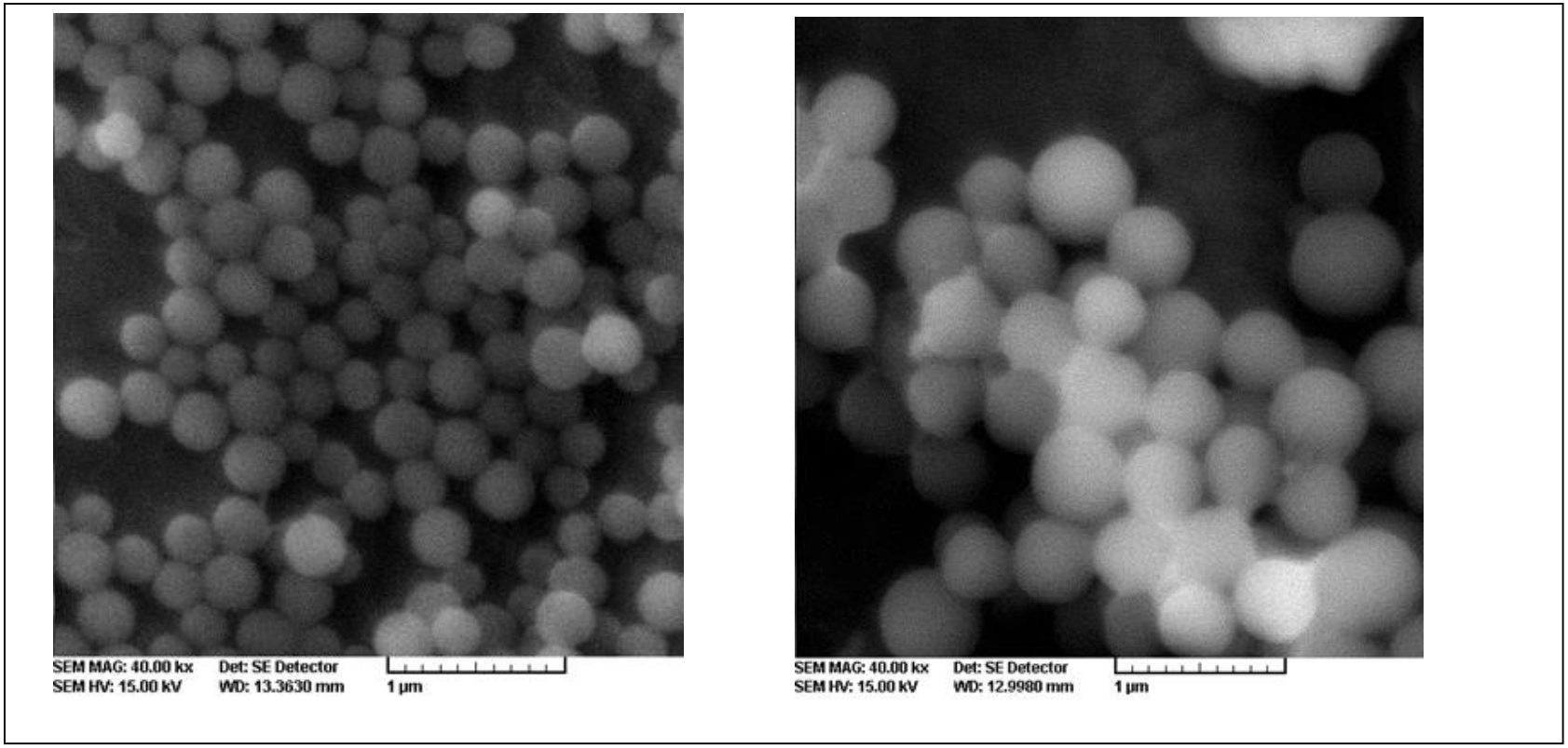

Figure 4.75: SEM image of Nano Silica

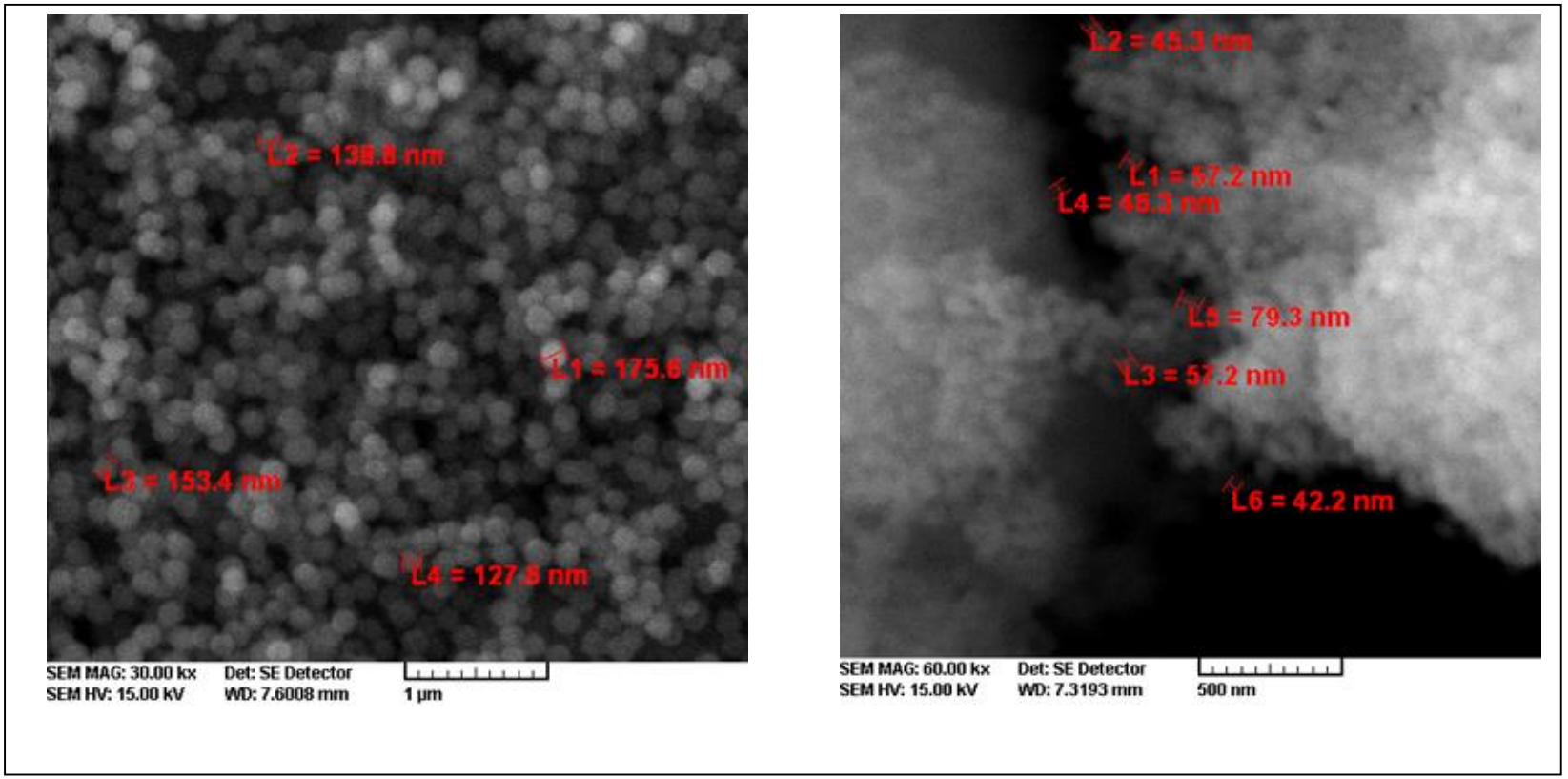

Figure 4.76: SEM Image of Nano Silica

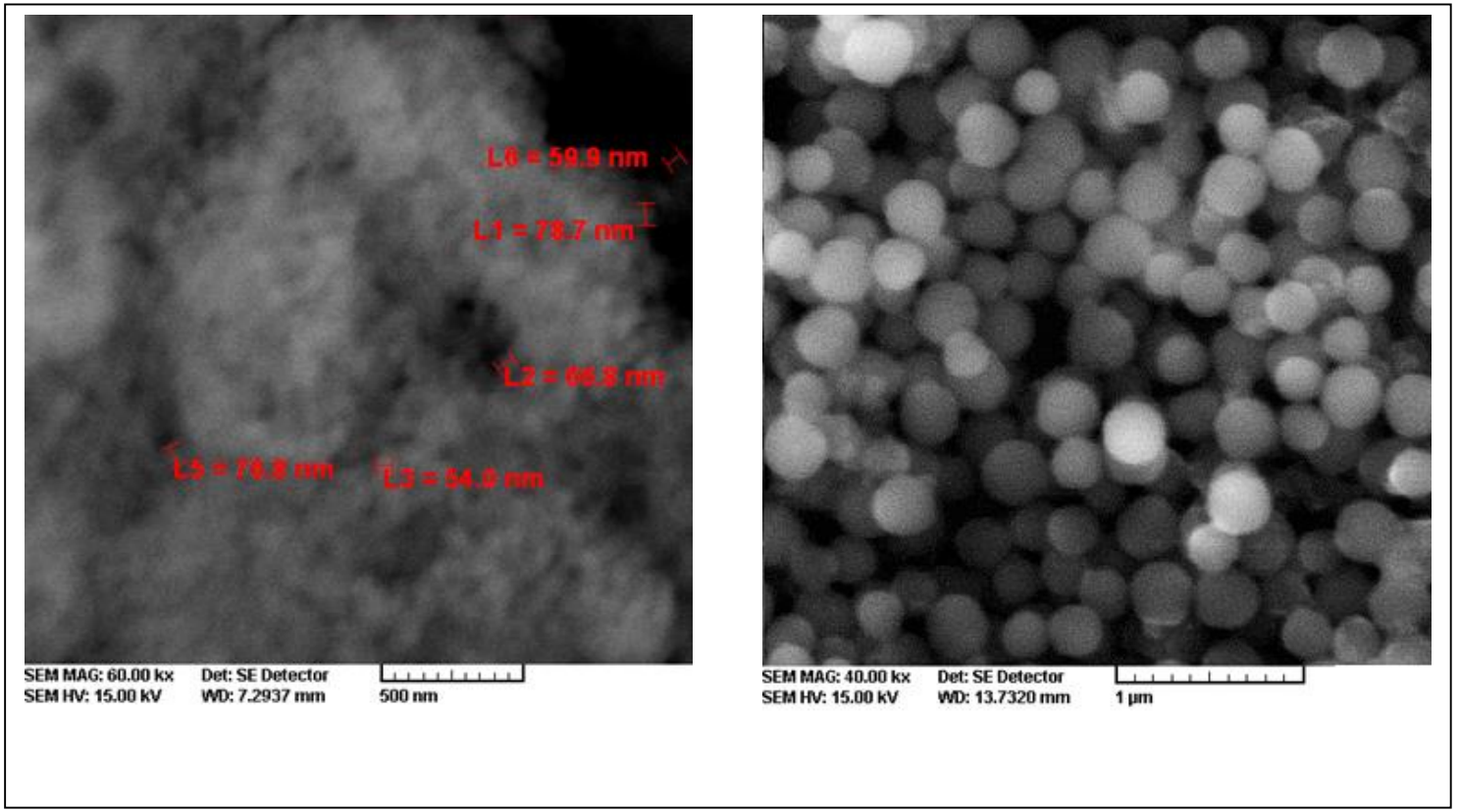

Figure 4.77: SEM Image of Nano Silica

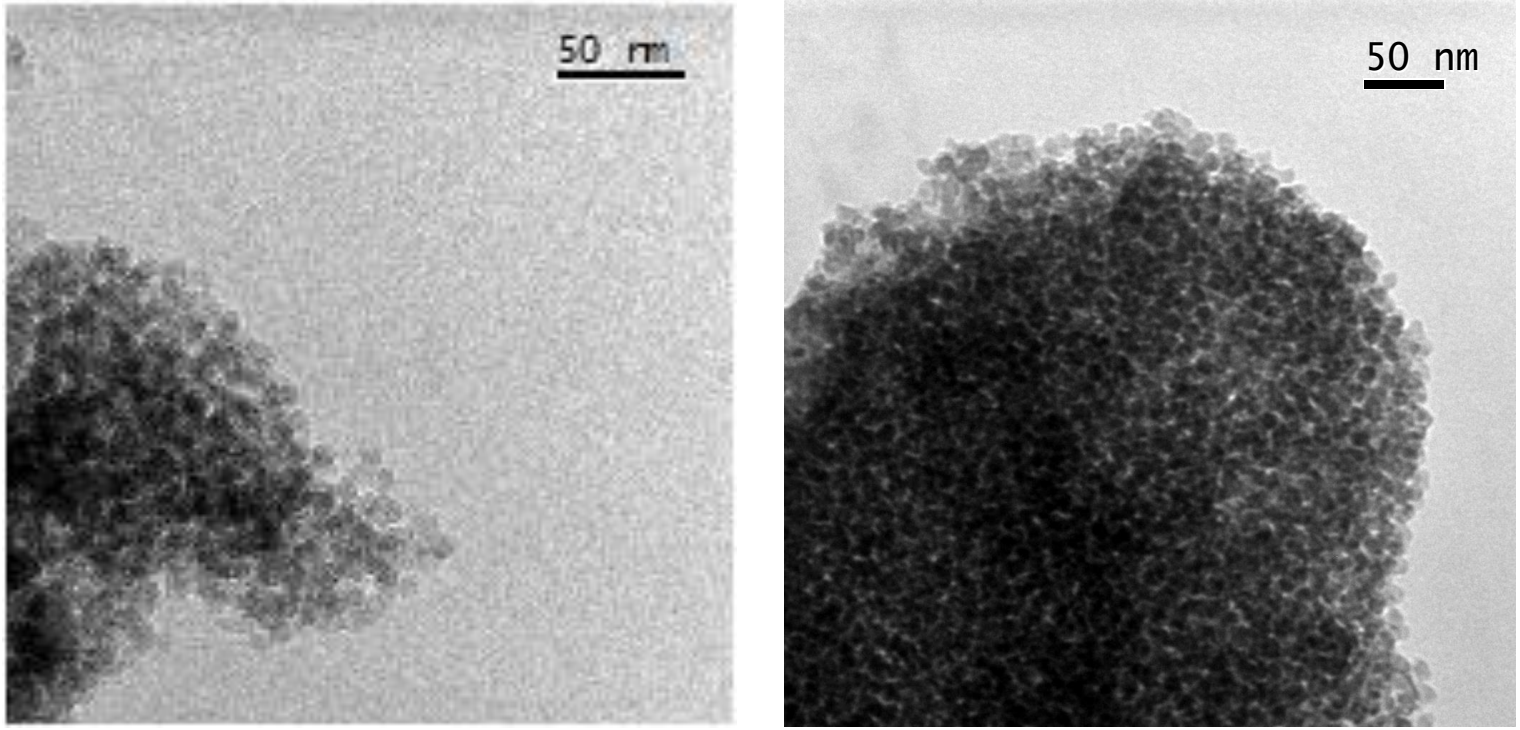

Figure 4.78: SEM Image of Nano Silica

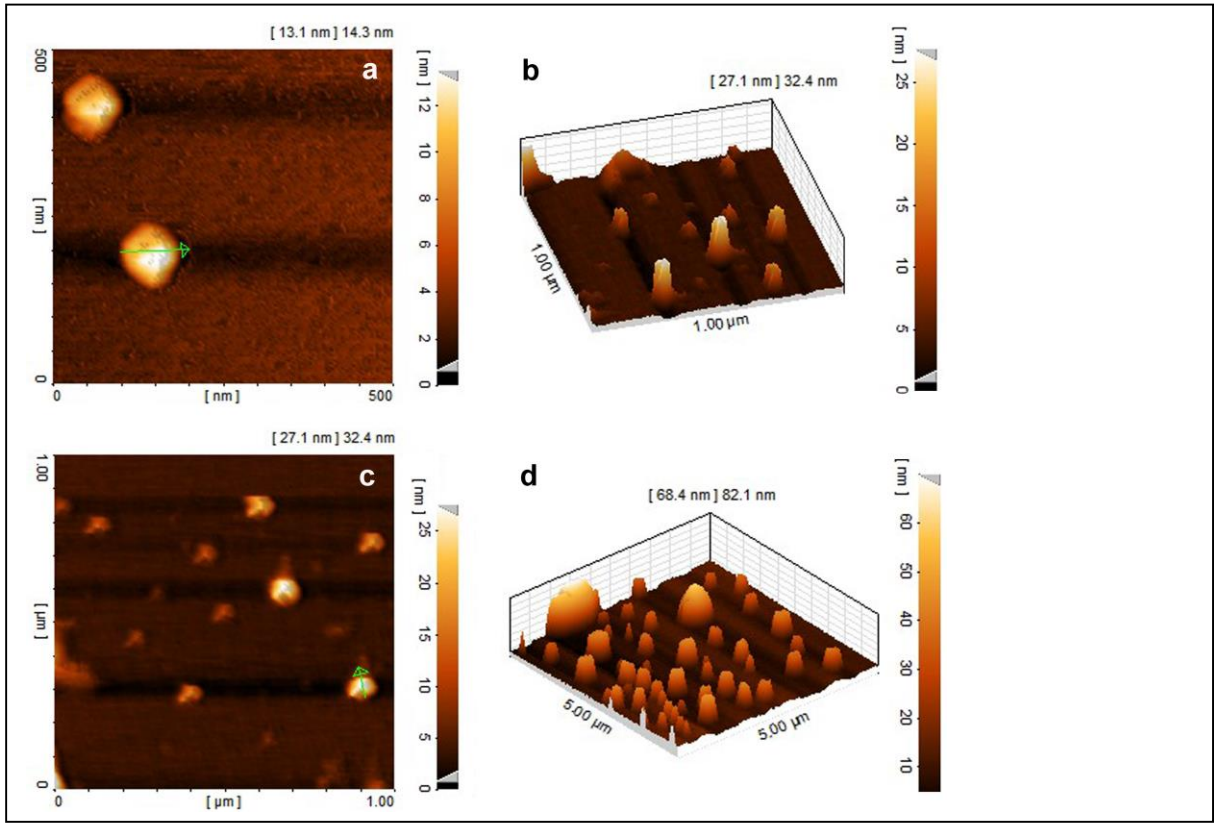

Figure 4.79: AFM Images of Nano Silica

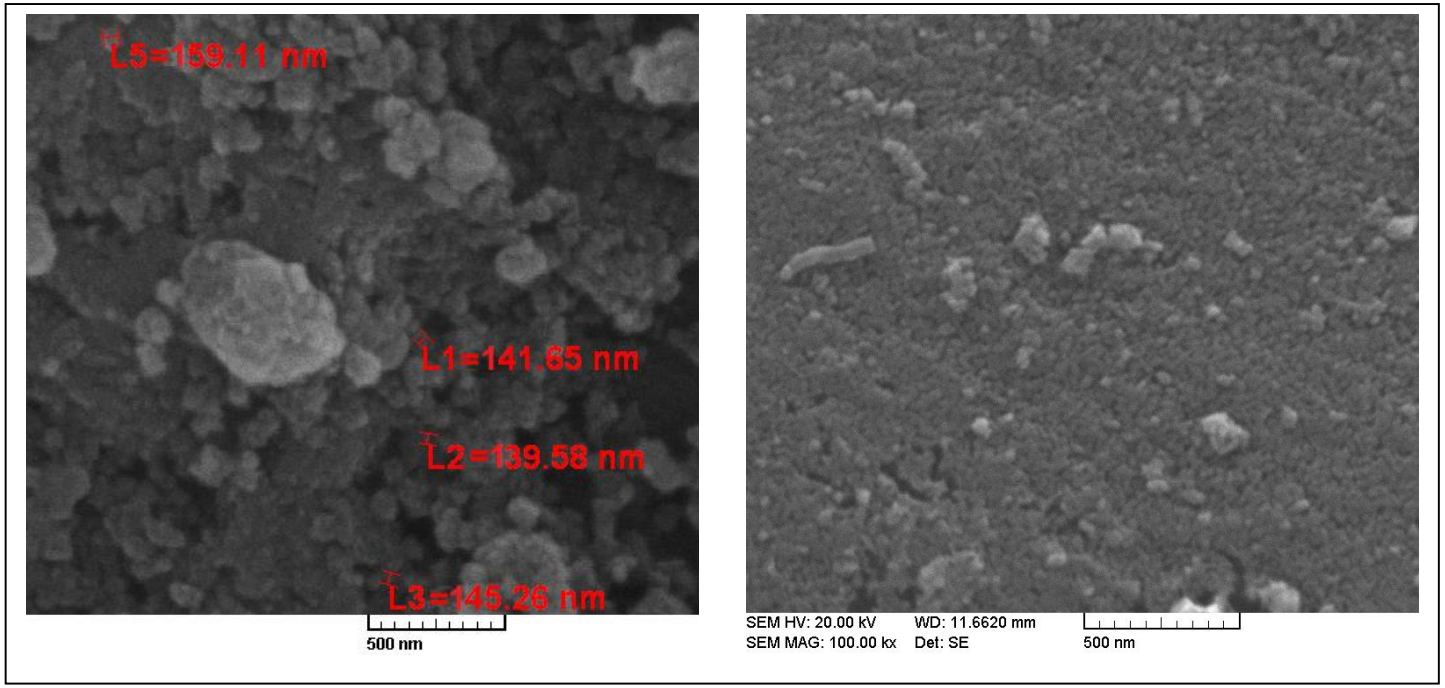

Figure 4.80: SEM of Nano-BP-PDISi

Chapter 5

RESULTS AND DISCUSSIONS

5.1 Synthesize of Bay-Substituted Compounds and Nano-Composites

The all of "bay-substituted" compounds were produced in this research, in the first step are started by bromination of 3,4,9,10-perylenetetracarboxylic dianhydride by iodine catalyzed in 98% concentrated H_2SO_4 and in the second step, the brominated perylene followed by replacement of brome with phenol then finally, imidization with imides.

The last part of research belongs to synthesized nano composites of perylene, which is started by hydrolysis of tetraethyl ortho-silicate to produce nano silica particles also the effects of different parameters of nanaoparticles size is studded. The synthesized nanosilica particles are attached to the perylene diimides to produced nanocomposites. The structur of synthesized compoundes were confirmed by FT-IR spectra of KBr pellets.

At the first step after bromination of perylene anhydride the phenol group is substituted to bromine to produced BP-PDA, which its IR spectrum is confirmed the substitution in characteristic peacks at 1199 (C-O-C ether) and 1014 cm^{-1} (C-O-C str) also, in BC-PDD substitution of bromine with 3-amino-9-ethylcarbazole is confirmed by characteristic bands at 1251(C-O-C ether) and 1163 (C-O-C str). In the second part,

by imidization of BP-PDA with, the characteristic bands of imides is appeared, in BP-PPI at 1700 and 1655 (imide C=C), 1357 (C-N str), similar in BC-PDD the charactrestic bands at 1698and 1660 (imide C=C), 1322 (C-N str) also, in BPI-PDI 1698 and 1656 (imide C=C), 1334 (C-N str) and finally in BP-PDISi, 1698 and 1656 (imide C=C), 1334 (C-N str).

5.2 Solubility of Compounds

The bay-substituted compounds have shown good solubility compare to their perylene dimides. The solubility of BP-PDA and BP-PPI and 4-amino phenol have been compared and summarized in table 5.1 and compared to BP-PDA, BP-PPI have exhibited good solubility.

Table 5.1: Solubility of 4-Aminophenol, BP-PDA and BP-PPI in Various Solvents

solvent	4-aminophenol	BP-PDA	BP-PPI
THF	(++++) Brown	(++−−) Pale red	(++++) Dark brown
m-Cresol	(++++) Brown	(++++) Pale red	(++++) Dark brown
Acetone	(++++) Brown	(−−−−) Colorless	(−−−−) Colorless
Ethanol	(++++) Brown	(−−−−) Colorless	(−−−−) Colorless
CH_3OH	(++++) Brown	(−−−−) Colorless	(−−−−) Colorless
NMP	(++++) Brown	(+++-) Red	(+++-) Dark brown
DMF	(++++) Brown	(++++) Red	(++++) Dark brown
DMAC	(++++) Brown	(−−−−) Colorless	(++−−) Brown
DMSO	(++++) Brown	(++++) Red	(++++) Dark brown

2 mg mL^{-1} in different solvents at 25 °C. (+): (++++): soluble at room -temperature; (+++−) good soluble at room-temperature (50-70 mg/ml), (++−−) partially soluble

BP-PDD compare with BP-PPI showed less solubility due to the more aromatic rings in bay positions, while in aprotic solvents it exhibited good solubility. Table (5.2)

Table.5.2: Solubility of N,N′-Didodecyl-1,7-Di (3-Amide-9-Ethylcarbazole) Perylene-3,4,9,10 -Etracarboxylic Acid Diimide (BC-PDD)

Solvents	Solubility[a]/or[a]
H_2O	(−−−−) Colorless
DMSO	(++−−) Brown
DMF	(++++) Brown
CH_3OH	(−−−−) Colorless
C_2H_5OH	(−−−−) Colorless
$C_2H_2Cl_2$	(+−−−) Light Brown
NMP	(+++−) Brown
Acetone	(−−−−) Colorless
H_2SO_4	(+++−) Light Black
$CHCl_3$	(++++) Dark Brown
m-Cresol	(+++−) Dark Brown
Dioxane	(++−−) Brown

1 mg/ml at 25 oC (++++): soluble at room temperature; (−−−−): insoluble at room temperature (50-70 mg/ml)

In table 5.3 the solubility of BPDA-PDA is compared with BPDI-PDI, in BPDA-PDA aromatic rings without aliphatic chains exhibited poor solubility in all organic solvents, while BPDI-PDI showed good solubility by existence of aliphatic groups in imide position.

Table 5.3: Solubility of (+)-Dehydroabietylamin, BPDA-PDA and BPDI-PDI in Various Solvents

solvent	Dehydroabiethyl amine	BPDA-PDA	BPDI-PDI
THF	(++++) Brown	(−−−−)	(++−−) Dark red
CH_3OH	(++++) Brown	(−−−−)	(++++) Red
NMP	(++++) Brown	(−−−−)	(+++-) Red
DMF	(++++) Brown	(−−−−)	(+++−) Red
DMAC	(++++) Brown	(−−−−)	(+−−−) Pale red
DMSO	(++++) Brown	(−−−−)	(+++−) Red

2 mg mL^{-1} in different solvents at 25 °C. (+): (++++): soluble at room-temperature; (+++−) good soluble at room-temperature (50-70 mg/ml), (++−−) partially soluble at room-temperature.

In table 5.4 the solubility of BP-PDSi, Nano-BP-PDSi and BP-PPDSi is compared. BP-PDSi, Nano-BP-PDSi and BP-PPDSi exhibited poor solubility in organic solvent. Compare with BP-PDSi, nano-BP-PDSi the solubility doesn't changed by decreasing of particle size, likewise with polymerization in BP-PPDSi the solubility is decreased. (Table 5.4)

Table 5.4: Solubility of (3-Aminopropyl) Triethoxysilane, BP-PDSi, Nano-BP-PDSi and BP-PPDSi in Various Solvents

solvent	(3-Aminopropyl) triethoxysilane	BP-PDSi	Nano-BP-PDSi	BP-PPDSi
THF	(+++)Colorless	(+−−)Pale red	(+−−) Pale red	(−−−)Colorless
m-Cresol	(+++)Colorless	(+−−)Pale red	(+−−) Pale red	(−−−)Colorless
Acetone	(+++)Colorless	(−−−)Colorless	(−−−) Colorless	(−−−)Colorless
Ethanol	(+++)Colorless	(−−−)Colorless	(−−−) Colorless	(−−−)Colorless
CH_3OH	(+++)Colorless	(−−−)Colorless	(−−−) Colorless	(−−−)Colorless
NMP	(+++)Colorless	(+−−)Pale red	(+−−)Pale red	(−−−)Colorless
DMF	(+++)Colorless	(+−−)Pale red	(+−−)Pale red	(+−−)Pale red
DMAC	(+++)Colorless	(−−−)Colorless	(−−−) Colorless	(−−−)Colorless
DMSO	(+++)Colorless	(+−−)Pale red	(+−−) Pale red	(+−−) Pale red

2 mg mL^{-1} in different solvents at 25 °C. (+): (+++): soluble at room-temperature; (++−) good soluble at room-temperature (50-70 mg/ml), (+−−) partially soluble at room temperature

5.3 NMR Spectra Analysis

5.3.1 The Structure of BP-PPI for NMR Analysis:

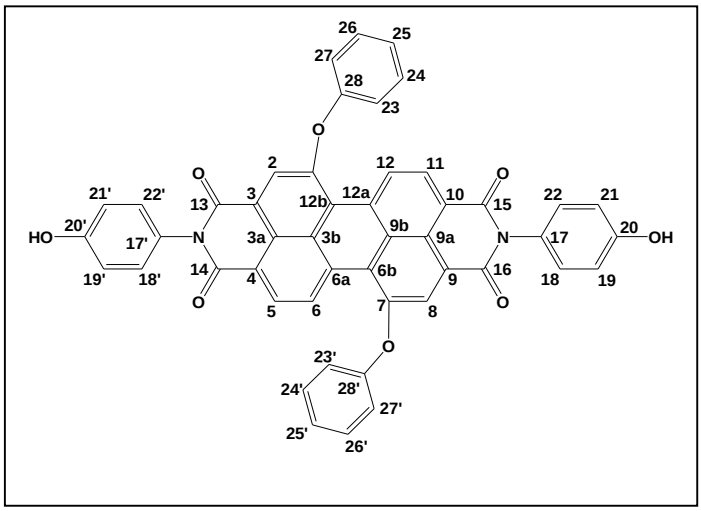

Figure 5.1: Structure of BP-PPI for NMR Analysis

^{1}H NMR (400 MHz, DMF): δ = 9.23(d, *J*=8 Hz, H-C (6), H-C (12)), 8.65 (d, *J*=8 Hz, H-C (11), H-C (5)), 8.56 (d, *J*=8 Hz, H-C (8), H-C (2)), 6.99 (t, *J*=8 Hz, H-C (26), H-C (24), H-C (26'), H-C (24')), 6.85 (t, *J*=8 Hz, H-C (23), H-C (27), H-C (23'), H-C (27')), 6.40 (d, *J*=8 Hz, H-C (18), H-C (22), H-C (18'), H-C (22')), 6. 27 (d, *J*=8 Hz, H-C (19), H-C (21), H-C (19'), H-C (21')).

^{13}C NMR (100 MHz, DMF, ppm): δ = 162.67-161.36 (4C=O, 8C, C (13-16), C (20), C (20'), C (28), C (28')), 122.10-120.72 (8C, 18C, C (5, 6, 11, 12, 18, 19, 21, 22, 24, 25, 26, 18',19', 21', 22', 24', 25', 26'), C (20), C (20'), C (28), C (28')), 118.45-109.95 (20C, C (1-12), C (3a), C (3b), C (6a), C (6b), C (12a), C (12b)).

5.3.2 The Structure of BC-PDD for NMR Analysis:

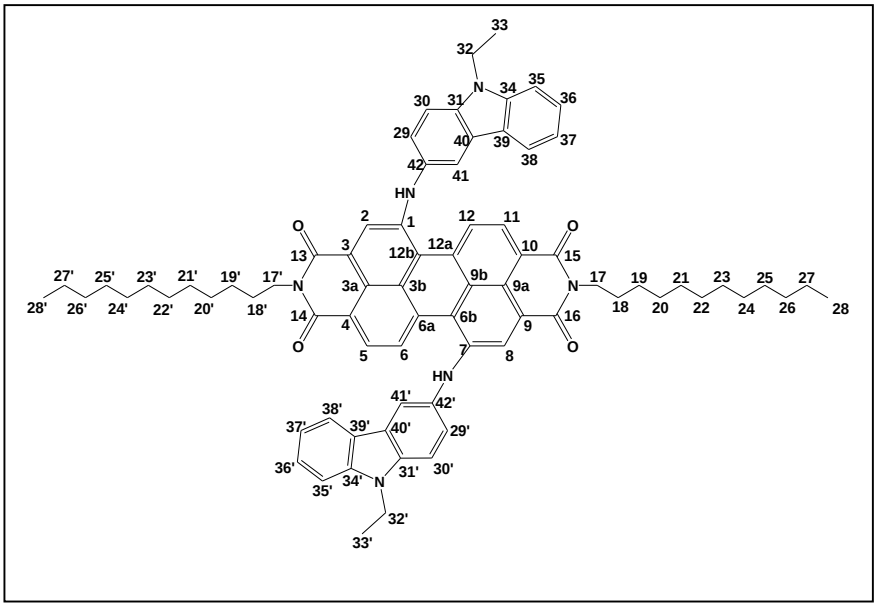

Figure 5.2: Structure of BC-PDD for NMR Analysis

^{1}H NMR (400 MHz, $CHCl_3$): δ = 9.02 (d, *J*=8 Hz, H-C (6), H-C (12)), 8.59 (d, *J*=8 Hz, H-C (11), H-C (5)), 7.68 (s, 2H) (d, *J*=8 Hz, H-C (8), H-C (2)), 7.02 (d, $2CH_2$, C-H(30), C-H(30')), 6.34 (d, *J*=8 Hz, $4CH_2$, C-H(29, 41, 29',41')), 6.31 (d, *J*=8 Hz, $4CH_2$, C-H(35-38), C-H(35'-38')), 4.02 (d, 2H of NH), 3.29 (b, $2CH_2$, C-H(17), C-H(17')), 1.59 (s, 2 OH), 1.28 (d, 4H, *J*=13.5 Hz, CH_2, H-C (18-27, 18'-27')), 0.96 (s, $2CH_3$, H-C (28), H-C (28')).

5.3.3 The Structure of BPDI-PDI for NMR Analysis:

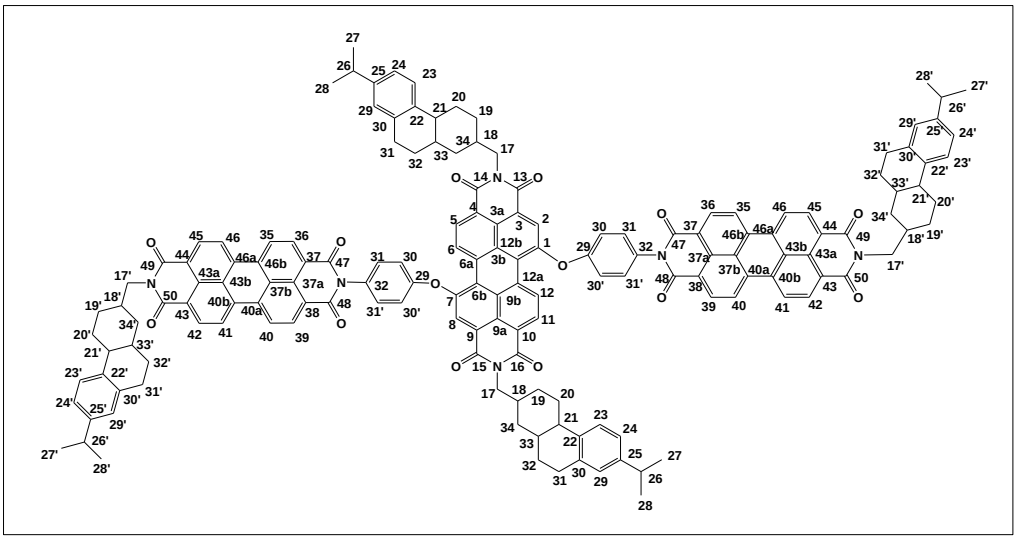

Figure 5.3: Structure of BPDI-PDI for NMR Analysis

^{1}H NMR (400 MHz, $CHCl_3$): δ = 8.96 (d, *J*=8 Hz, H-C (6), H-C (12), H-C (35), H-C (40), H-C (41), H-C (46)), 8.26 (d, *J*=8 Hz, H-C (5), H-C (11), H-C (36), H-C (39), H-C (42), H-C (45)), 8.12 (d, *J*=8 Hz, H-C (8), H-C (2)), 7.68 (t, 4H, *J*=8 Hz, H-C (31), H-C (31')), 7.14 (t, 4H, *J*=8 Hz, H-C (30), H-C (30')), 6.97 (d, 4H, *J*=8 Hz, H-C (24), H-C (24'), H-C (29), H-C (29')), 3.52 (d, *J*=8 Hz, H-C (17), H-C (17')), 3.03 (d, 4H, *J*=8 Hz, H-C (26), H-C (26')), 2.26 (s, H-C (21), H-C (21')), 1.54 (d, 4H, *J*=8 Hz, H-C (33), H-C (33')), 1.26 (d, 4H, *J*=8 Hz, H-C (19), H-C (19')), 1.07 (d, 4H, *J*=8 Hz, H-C (34), H-C (34')), 0.92 (s, 8CH_3, H-C (27), H-C (28), H-C (27'), H-C (28')). **^{13}C NMR (100 MHz, DMF, ppm):** δ = 164.1 (12 C=O, C (13-16), C (47-50)), 147.6 (C, C (29), C (29')), 145.5-135.1 (24C, C (23-30), C (23'-30'), C (25), C (25')), 130.0 (8C, C (30), C (31), C (30'), C (31')), 127.2-109.9 (60C, C (1-12), C (3a), C (3b), C (6a), C (6b), C (12a), C (12b), C(35-46), C(37a), C(37b), C(40a), C(43a), C(43b),

C(46a), C(46b)), 46.4-30.5 (20C, C (17-21), C (17’-21’), C (31-34), C (31’-34’), 26.2 (8C, C (27-28), C (27’-28’)).

5.3.4 The Structure of BP-PDSi for NMR Analysis:

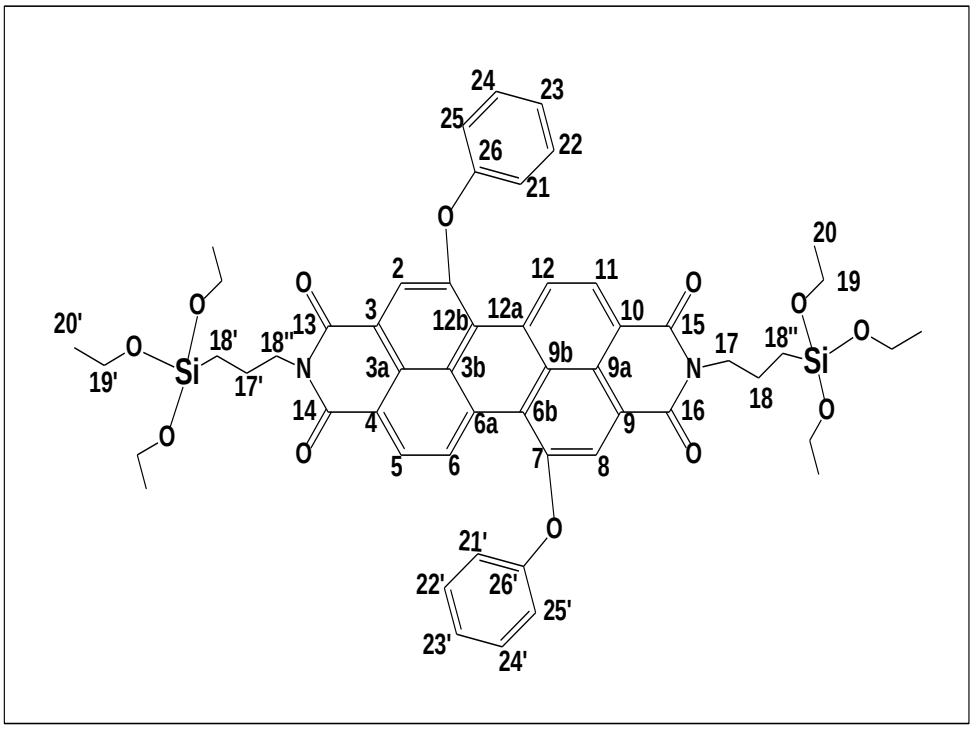

Figure 5.4: Structure of BP-PDSi for NMR Analysis

^{13}CNMR (300 MHz, solid-state, ppm): δ = 162.1 (13 C=O, 14 C=O, 15 C=O, 16 C=O, C (26), C (26’)), 127.7 (C (1-12), C (21-25), C (21’-25’)), 58.3-40.96 (C (17), C (19), C (17’), C (19’)), 19.8 (C (18), C (18’), C (20), C (20)), 8.87 (18’’)).

5.4 Electrochemistry of Synthesized Compounds

5.4.1 Electrochemical of BP-PDA

The cyclic-voltammetry results of BP-PDA in DMF at different scan rates are tabled (table 5.5). Its redox potential, LUMO, Eg and HOMO valued are calculated in table 5.6.

Table 5.5: Cyclic-Voltammetry Data of BP-PDA in DMF Solution[a] at Different Scan-Rate

Scan-rate (mVs^{-1})	i_{pa} / μA	i_{pc} / μA	E_{pa} / V	E_{pc} / V	ΔE_p / mV	$E_{1/2}$(V)vs. (Ag/AgCl)	E_{Fc} (V) vs. (Ag/AgCl)
100	8.91	-5.44	-0.38	-0.47	90	-0.425	0.592
	8.9	-2.33	-0.219	-0.29	71	-0.2545	0.592
200	7.16	-7.88	-0.38	-0.47	90	-0.425	0.592
	6.65	-4.59	-0.223	-0.27	47	-0.2465	0.592
500	7.78	-10.0	-0.35	-0.48	130	-0.415	0.592
	9.51	-5.22	-0.224	-0.26	36	-0.242	0.592
750	8.09	-11.6	-0.35	-0.49	140	-0.42	0.592
	9.63	-5.40	-0.226	-0.25	24	-0.238	0.592
1000	9.55	-11.45	-0.34	-0.51	170	-0.425	0.592
	2.01	-5.73	-0.227	-0.24	13	-0.2335	0.592

BP-PDA at all scan rates is shown two reversible one-electron reduction (table 5.6), at 100 mVs^{-1} scan rate, first reduction is absorbed at -1.017 and second one at -0.84 V. The scan rates square root from drown plot in DMF was a straight line with R^2= -0.282 (Figure 5.5)

Table 5.6: Redox Potential, LUMO, Eg and HOMO Values of BP-PDA in DMF Solution

Scan rate (mVs^{-1})	E_{pc} / V	E_{pa} / V	$E_{1/2}$ vs. Fc / V	E_{LUMO} / eV	E_g / eV	E_{HOMO} / eV
100	-0.47	-0.38	-1.017	-3.783	2.08	-5.863
	-0.29	-0.219	-0.8465	-3.9535	2.08	-6.035
200	-0.47	-0.38	-1.017	-3.783	2.08	-5.863
	-0.27	-0.223	-0.8385	-3.9615	2.08	-6.042
500	-0.48	-0.35	-1.007	-3.793	2.08	-5.873
	-0.26	-0.224	-0.834	-3.966	2.08	-6.046
750	-0.49	-0.35	-1.012	-3.788	2.08	-5.868
	-0.25	-0.226	-0.83	-3.97	2.08	-6.050
1000	-0.51	-0.34	-1.017	-3.783	2.08	-5.863
	-0.24	-0.227	-0.8255	-3.9745	2.08	-6.055

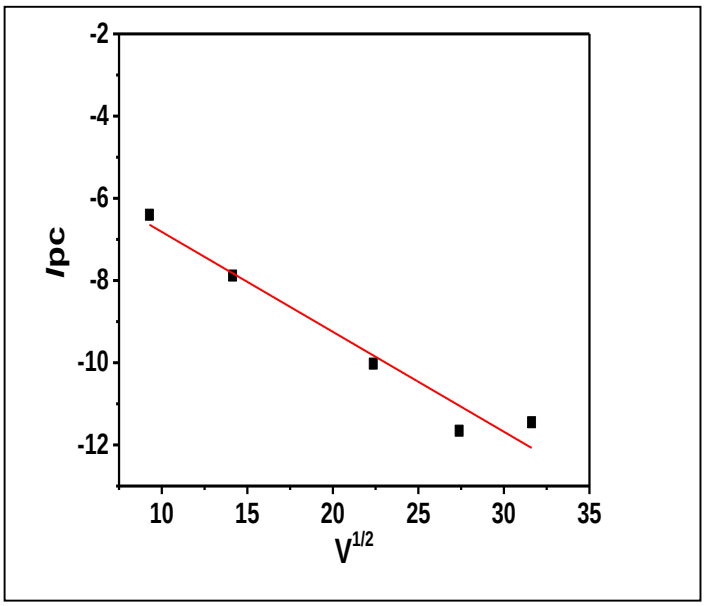

Figure 5.5: Plot of *i*pc vs $V^{1/2}$. Scan Rate of BP-PDA, the Slope of ipc vs. $V^{1/2} = 0.029\ (\mu A)\times(mV)^{-1/2}\times(s)^{1/2}$

$$D=\frac{\left(\frac{IPC}{\sqrt{V}}\right)^2}{\left[\left(2.69\times10^5\ As\ mol^{-1}V^{-1/2}\right)^2\times\left(n^{3/2}\right)^2\times(Ac)^2\right]}$$

$$D=$$

$$\frac{\left(-0.24311\left[(\mu A)\times(mV)^{-1/2}\times(s)^{1/2}\right]\right)^2}{\left[\left(2.69\times10^5\ As\ mol^{-1}V^{-1/2}\right)^2\times\left(4^{3/2}\right)^2\times\left(\left(3.14\times(0.1\ cm)\right)^2\times(1\times10^{-6}molcm^{-3})\right)^2\right]}$$

5.4.2 Electrochemical of BP-PPI

The cyclic-voltammetry results of BP-PPI in DMF at different scan-rates are tabled in table 5. 7 its redox potential, LUMO, Eg and HOMO valued are calculated (table 5.8.).

Table 5.7: Cyclic Voltammetry Results of BP-PPI in DMF Solution at Different Scan-Rate

Scan-rate (mVs^{-1})	i_{pa} / μA	i_{pc} / μA	E_{pa} / V	E_{pc} / V	ΔE_p / mV	$E_{1/2}$ (V) vs. (Ag/AgCl)	E_{Fc} (V) vs. (Ag/AgCl)
100	3.735	-8.03	-0.59	-0.67	78	-0.64	0.62
	2.731	-4.74	-0.34	-0.42	80	-0.38	0.62
200	5.12	-11.46	-0.59	-0.67	84	-0.63	0.62
	3.24	-6.478	-0.34	-0.42	78	-0.38	0.62
500	7.59	-16.521	-0.59	-0.69	100	-0.64	0.62
	5.47	-9.818	-0.33	-0.43	92	-0.38	0.62
750	9.28	-21.6	-0.58	-0.69	110	-0.64	0.62
	5.81	-13.65	-0.33	-0.43	98	-0.38	0.62
1000	10.07	-20.494	-0.57	-0.70	131	-0.64	0.62
	6.17	-13.328	-0.33	-0.44	112	-0.38	0.62

Two reversible one-electron reduction of BP-PPI at 100 mVs^{-1} scan rate is tableted in table 5. 8, first reduction is absorbed at -1.257 and second one at -1.003 V. The scan rates square root from drown plot in DMF was a straight line with R^2= -0.084 (Figure 5.6).

Table 5.8: Redox potential, LUMO, Eg and HOMO-Values of BP-PPI in DMF Solution

Scan-rate (mVs^{-1})	E_{pc} / V	E_{pa} / V	$E_{1/2}$ vs. Fc / V	E_{LUMO} / eV	E_g / eV	E_{HOMO} / eV
100	-0.67	-0.59	-1.257	-3.543	1.86	-5.403
	-0.42	-0.34	-1.003	-3.797	1.86	-5.657
200	-0.67	-0.59	-1.256	-3.544	1.86	-5.404
	-0.42	-0.34	-1.002	-3.798	1.86	-5.658
500	-0.69	-0.59	-1.259	-3.541	1.86	-5.401
	-0.43	-0.33	-1.003	-3.797	1.86	-5.657
750	-0.69	-0.58	-1.258	-3.542	1.86	-5.402
	-0.43	-0.33	-1.002	-3.798	1.86	-5.658
1000	-0.70	-0.57	-1.259	-3.541	1.86	-5.401
	-0.44	-0.33	-1.004	-3.796	1.86	-5.656

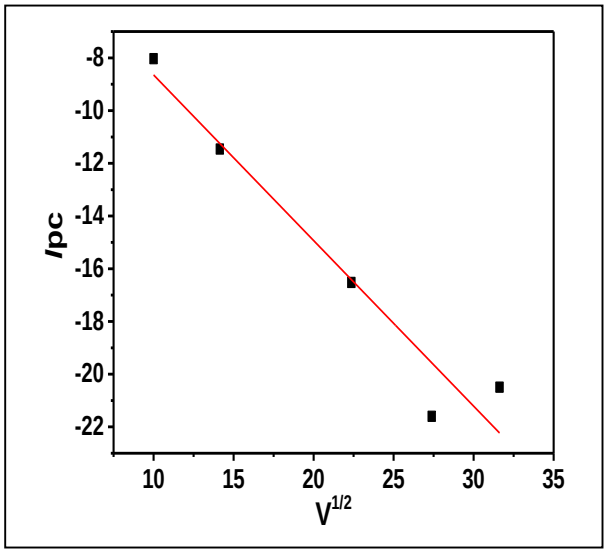

Figure 5.6: Plot of i_{pc} vs $V^{1/2}$.

5.4.3 Electrochemical of BC-PDD

The cyclic voltammetry data of BC-PDD in DMF solution at at 100 mVs^{-1} are tabled in table 5. 9, also its redox potential, LUMO, Eg and HOMO valued are calculated in table 5.10.

Table 5. 9: Cyclic-Voltammetry Results of BC-PDD in DMF Solution

Scan rate	i_{pa} μA	i_{pc} / μA	E_{pa} / V	E_{pc} / V	ΔE_p / mV	$E_{1/2}$ (V) vs. (Ag/AgCl)	E_{Fc} (V) vs. (Ag/AgCl)
100	-2.8	-6.33	0.814	0.581	-11	-1.298	0.601

Single reversible one-electron reduction of BP-PPI at different scan rate is tabled in table 5.10, at 100 mVs^{-1}, the reduction is absorbed at -1.38 V. The scan rates square root from drown plot in DMF was a straight line with R^2= -0.0083.

Table 5.10: Redox Potential, LUMO, Eg and HOMO Values of BC-PDD in DMF Solution

Scan rate	E_{pc} / V	E_{pa} / V	$E_{1/2}$ vs. Fc / V	$E_{1/2}$ vs. / V	E_{LUMO} / eV	E_g / eV	E_{HOMO} / eV
100	0.814	0.581	-1.298	-0.697	-3.501	1.550	-5.052
		0.201					

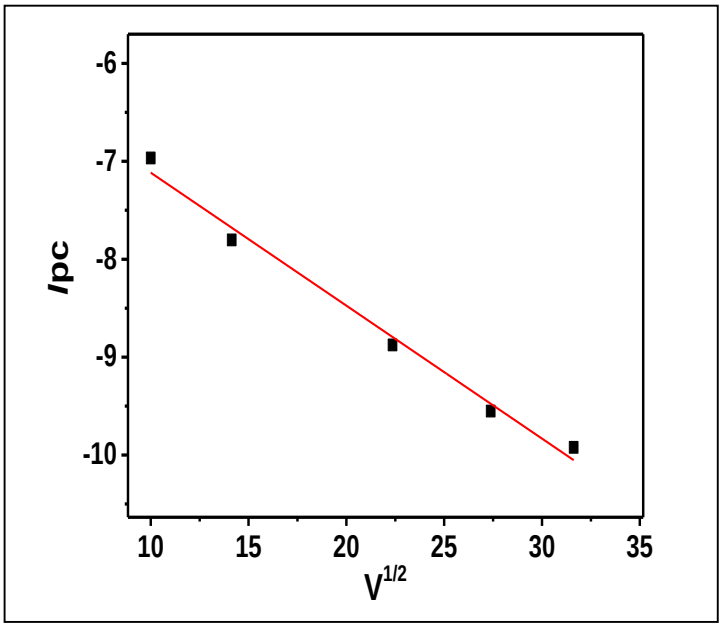

Figure 5.7: Plot of *i*pc vs. Scan Rate of BC-PDD, the Slope of ipc vs. $V^{1/2} = 0.0083$ (μA)×(mV)$^{-1/2}$×(s)$^{1/2}$

5.4.4 Electrochemical of BPDA-PDA

The cyclic voltammetry data of BPDA-PDA in solid state at 100 mVs^{-1} are tabled in table 5. 11, also its redox potential, LUMO, Eg and HOMO valued are calculated in table 5.12.

Table 5.11: Cyclic Voltammetry Data of BPDA-PDA in Solid State

Scan rate (mVs^{-1})	i_{pa} / μA	i_{pc} / μA	E_{pa} / V	E_{pc} / V	ΔE_p / mV	$E_{1/2}$ (V) (Ag/AgCl)	E_{Fc} /V
100	62.46	-29.535	0.275	0.830	565	-0.083	0.634

Single reversible one-electron reduction of BPDA-PDA at different scan rate is tableted in table 5. 12, at 100 mVs^{-1}, the reduction is absorbed at -0.098 V. The scan rates square root from drown plot in DMF was a straight line with R^2= 0.475 (Figure 5.8).

Table 5.12: Redox Potential, LUMO, Eg and HOMO of BPDA-PDA in Solid State

Scan rate	Epc / V	Epa / V	$E_{1/2}$ / V	$E_{1/2}$ Fc / V	E_{LUMO} / eV	Eg / eV	E_{HOMO} / eV
100	0.275	0.830	0.553	-0.083	-4.715	2.140	-6.859

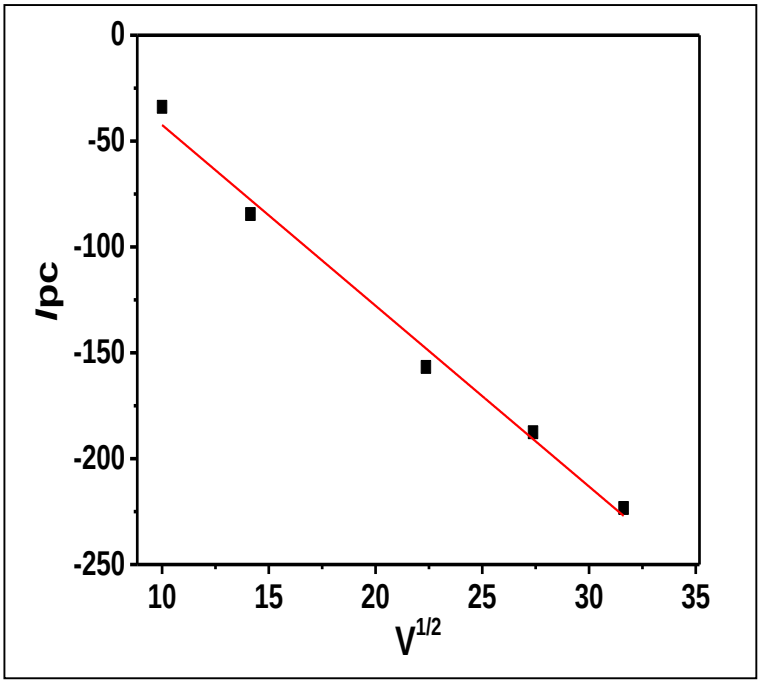

Figure 5.8: Plot of *i*pc vs. Scan Rate of BPDA-PDA, the Slope of ipc vs. $V^{1/2} = 0.475\ (\mu A)\times(mV)^{-1/2}\times(s)^{1/2}$

$$D_{BPDA-PDA} = 6.39 \times 10^{-5} cm^2 s^{-1}$$

5.4.5 Electrochemical of BPDI-PDI

The cyclic voltammetry data of BPDA-PDA in DMF solution at at 100 mVs^{-1} are tabled in table 5. 13, also its redox potential, LUMO, Eg and HOMO valued are calculated in table 5.14.

Table 5.13: Cyclic Voltammetry Data of BPDI-PDI in DMF

Scan rate (mVs^{-1})	ipa / μA	ipc / μA	Epa / V	Epc / V	ΔEp / mV	$E_{1/2}$ (V) vs . (Ag/AgCl)	E_{Fc} (V)vs.
100	4.95	-9.37	-0.682	-0.585	72	-0.6335	0.61
	6.2707	-5.19	-0.414	-0.342	67	-0.378	0.61

Two reversible one-electron reduction of BPDI-PDI at different scan rate is tabled in table 5. 8, at 100 mVs^{-1} first reduction is absorbed at -1.243 V and second one at -0.987 V. The scan rates square root from drown plot in DMF was a straight line with R^2= 0.319 (Figure 5.9)

Table 5.14: Redox Potential, LUMO, Eg and HOMO Values of BPDI-PDI in DMF

Scan rate	E_{pc} / V	E_{pa} / V	$E_{1/2}$ vs. / V	$E_{1/2}$ vs. Fc / V	E_{LUMO} / eV	E_{HOMO} / eV
100	-0.682	-0.585	-0.6335	-1.244	-3.556	-5.246
	-0.414	-0.342	-0.378	-0.988	-3.812	-5.501
		+0.648				

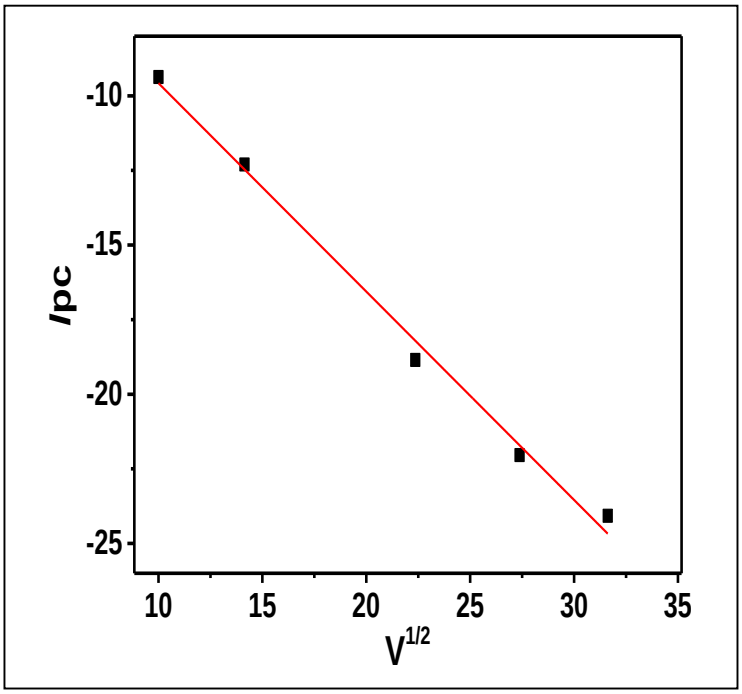

Figure 5.9: Plot of i_{pc} vs. Scan Rate of BPDI-PDI, the Slope of i_{pc} vs. $V^{1/2} = 0.0314\ (\mu A)\times(mV)^{-1/2}\times(s)^{1/2}$

$$D_{BPDI-PDI} = 1.07 \times 10^{-7} cm^2 s^{-1}$$

5.4.6 Electrochemical of BP-PDSi

The cyclic voltammetry data of BP-PDSi in solid state at at 100 mVs^{-1} is tabled in table 5. 15, also its redox potential, LUMO, Eg and HOMO valued are calculated in table 5.16.

Table 5. 15: Cyclic Voltammetry Data of BP-PDSi in Solid State

Scan rate (mVs^{-1})	i_{pa} / μA	i_{pc} / μA	E_{pa} / V	E_{pc} / V	ΔE_p / mV	$E_{1/2}$ (V) vs. (Ag/AgCl)	E_{Fc} (V) vs.
100	0.365	-7.017	0.743	0.364	1035	+0.554	0.352
	0.491	-0.406		0.571			

Two reversible one-electron reduction of BP-PDSi at solid state in at 100 mVs^{-1} is tabled in table 5. 16, at 600 mVs^{-1} first reduction is absorbed at 0.36 V and second one at 0.571 V. The scan rates square root from drown plot in solid state was a straight line with R^2= 0.024 (Figure 5.10)

Table 5.16: Redox Potential, LUMO, Eg and HOMO Values of BP-PDSi in Solid State

Scan rate	Epc / V	Epa / V	$E_{1/2}$ vs. / V	$E_{1/2}$ vs. Fc / V	ELUMO / eV	EHOMO / eV
600	0.364	0.743	+0.554	+0.202	-5.002	-6.442
	0.571					

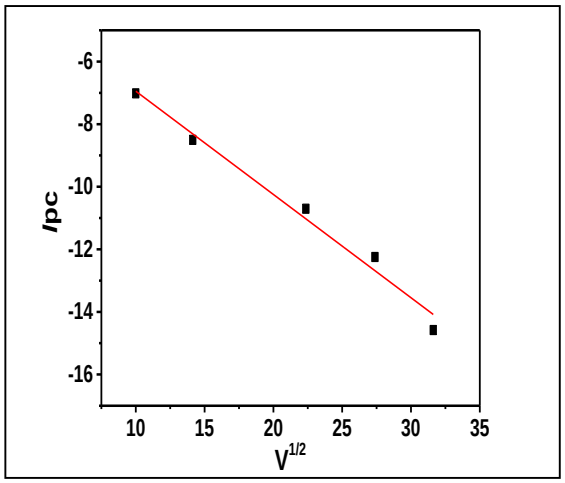

Figure 5.10: Plot of i_{pc} vs. Scan Rate of BP-PDSi, the Slope of ipc vs.

5.4.7 Electrochemical of Nano-BP-PDSi

The cyclic voltammetry data of Nano-BP-PDSi in solid state at at 100 mVs^{-1} are tabled in table 5. 17, also its redox potential, LUMO, Eg and HOMO valued are calculated in table 5.18.

Table 5. 17: Cyclic Voltammetry Data of Nano-BP-PDSi in Solid State

Scan rate (mVs^{-1})	i_{pa} / µA	i_{pc} / µA	E_{pa} / V	E_{pc} / V	ΔE_p / mV	$E_{1/2}$ (V) vs. (Ag/AgCl)	E_{Fc} (V) vs.
100	4.454	-1.675	0.904	0.162	1129	+0.533	0.354

The one-electron reduction of Nano-BP-PDSi at solid state at 100 mVs^{-1} is tableted in table 5. 16, at 100 mVs^{-1} the reduction is absorbed at -0.099 V. The scan rates square root from drown plot in solid state was a straight line with R^2= 0.038 (Figure 5. 11)

Table 5.18: Redox Potential, LUMO, Eg and HOMO Values of Nano BP-PDSi in Solid State

Scan rate	E_{pc} / V	E_{pa} / V	$E_{1/2}$ vs. / V	$E_{1/2}$ vs. Fc / V	E_{LUMO} / eV	E_{HOMO} / eV
100	0.162	0.904	+0.533	+0.179	-4.979	-6.839

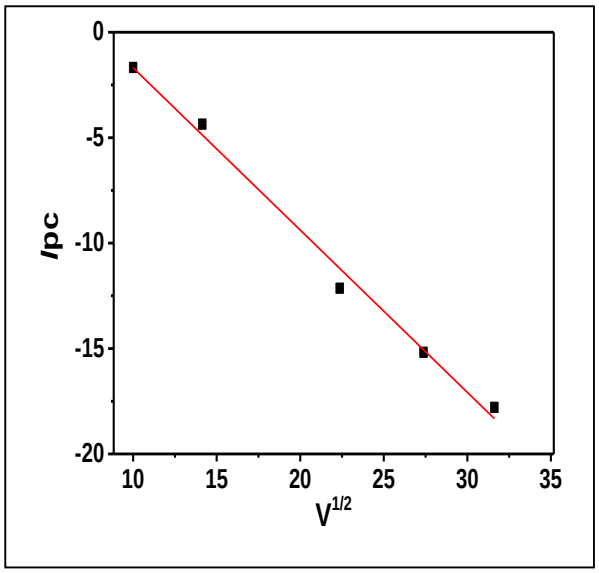

Figure 5.11: Plot of *i*pc vs Scan Rate of Nano-BP-PDSi,

$$D_{\text{nano BP-PDSi}} = 0.519 \times 10^{-6} \text{cm}^2\text{s}^{-1}$$

5.4.8 Electrochemical of BP-PPDSi

The cyclic voltammetry data of BP-PPDSi in solid state at 100 mVs^{-1} are tabled in table 5.19, also its redox potential, LUMO, Eg and HOMO valued are calculated in table 5.20.

Table 5. 19: Cyclic Voltammetry Data of BP-PPDSi in Solid State

Scan rate (mVs-1)	ipa / μA	ipc / μA	Epa / V	Epc / V	ΔEp / mV	$E_{1/2}$(V) vs. (Ag/AgCl)	EFc /V
100	16.95	-6.32	0.793	-0.486	1279	0.1535	0.373
	-	-16.91	-	0.285	-	-	-

Two reversible one-electron reduction of BP-PPDSi at solid state at 100 mVs^{-1} is tabled in table 5. 20, at 100 mVs^{-1} just first reduction is absorbed at -0.219 V. The scan rates square root from drown plot in solid state was a straight line with R^2= 0.096 (Figure 5.12)

Table 5.20: Redox Potential, LUMO, Eg and HOMO Values of BP-PPDSi in Solid State

Scan rate	E_{pc} / V	E_{pa} / V	$E_{1/2}$ vs. Fc / V	E_{LUMO} / eV	E_g / eV	E_{HOMO} / eV
100	-0.486	0.793	-0.219	-4.580	1.860	-6.440
	0.285	-	-	-		-

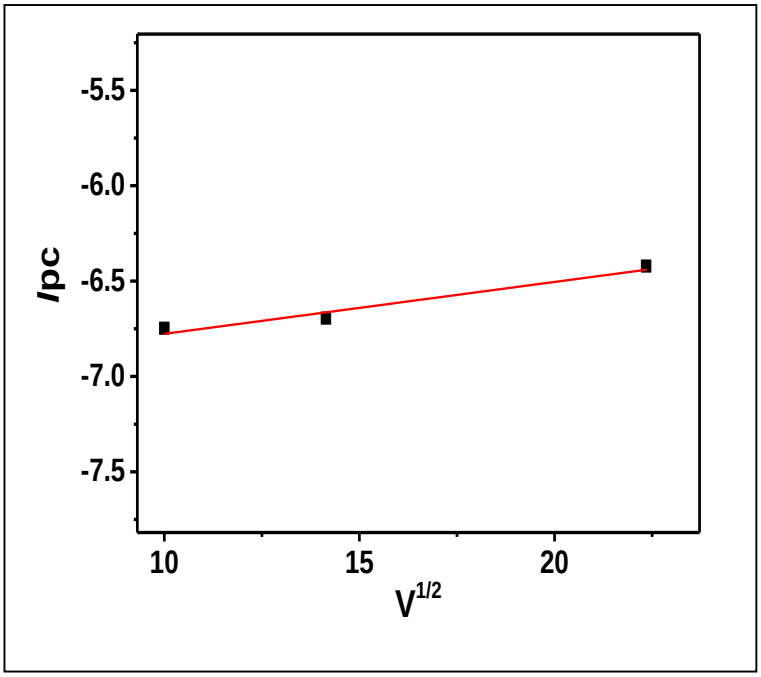

Figure 5.12: Plot of *i*pc vs. Scan rate of Nano-BP-PDSi, the Slope of ipc vs. $V^{1/2} = 0.038\ (\mu A)\times(mV)^{-1/2}\times(s)^{1/2}$

$$D_{BP-PPDSi} = 6.46 \times 10^{-10} cm^2 s^{-1}$$

Chapter 6

CONCLUSION

In this research novel bay-substituted Perylene macromolecules and Nano-Perylene diimides were synthesized and characterized. To produce nano-Perylene deliveries as an Organic-inorganic branch of compounds, nano silica is produced and effects of different synthetic parameters on nano particles were analyzed.

Tetraethylorthosilicate (TEOS) was used for producing Nanosilica particles with sol-gel method by the hydrolysis of TEOS, for this purpose the function of different parameters such as compositions of TEOS/NH_3, H_2O/NH_3, also temperature and time of reactions in sonication on particle size have been studied and summarized in table 1.1, distribution, shape and size of particle were determined by Scanning Electron microscopy (SEM) and Transmission electron microscopy (TEM). As a result of this research, the ideal synthesis conditions gained by the experimental plan method were as follows, [H2O/TEOS=2/3, 70 °C as a reaction temperature and 30 min as a reaction duration in sonication. By above optimal conditions nano silica particles with minimum particle size (~10nm) were produced and used to synthesize Nano-Perylene diimides. In the next step Nanosilica sulfunic acid (NSSA) were successfully prepared by sulfunating SiO_2 nanoparticles under argon atmosphere with the objective of improving the water retention ability and conductivity and hydrolysis stability.

3-Aminopropyltriethoxysilane (APTES) is used to directly imidization of bay substituted Perylene dianhydride, to produced N,N′-Didehyphenol-1,7-di(propyltriethoxylsiline) perylene-3,4,9,10-tetracarboxylic acid diimide (BP-PDSi), Perylene diimides and nano composites of perylene was directly attached to polymeric structure of Nanosilica.

Recently the fabrication of Perylene dyes with improved mechanical and electrical properties and good absorption property are extensively studied. The aim of this research were focused to synthesize the substitution of perylene diimides in bay position that causes a remarkable increase in optical, electronic properties, solubility, the more red shifted absorption band, good molar absorptivity and thermal stability. Therefore the substituents in the bay-position of perylene diimides with functional groups in the bay-region of PDI aromatic cores were applied to produce highly soluble perylene diimides. To achieve this aim we start with selective bromination of perylene dianhydride to produce 1, 6-dibromo-PDA, then two phenoxy groups were incorporated onto the dibrominated-bay-substituted perylene dianhydride by replacing bromine atoms in the bay positions with phenoxy groups to produce 1,7-diphenoxyperylene-3,4,9,10-perylenetetracarboxy-anhydride (BP-PDA).

1, 7-(diphenoxyperylene perylene-3, 4:9, 10-tetracarboxylic acid dicarboximide)-3,4:9,10-tetracarboxylic anhydride (BPDA-PDA) is produced by replacing of Bromine substituted on Brominated-PDA with phenoxy group on imide position of N,N′-Di(phenoxy)3,4,9,10-perylenetetracarboxy-diimide (PPI).

N,N′-Didehydroabiethyl-1,7-di((N`-dehydroabiethyl,N-phenoxy) perylene-3,4,9,10-tetracarboxylic acid diimide) perylene-3,4,9,10-tetracarboxylic acid diimide (BPDI-PDI) were successfully synthesized by normal imidization of BP-PDA with 4-dehydroabiethylamine.

In synthesizing of BC-PDD, after imidization of Br-PDA with Dodecylamine, N,N´-Di(dodecyl)-3,4,9,10-perylene-tetracarboxy-diimide (Br-PDD) is produced. Then 1,7-di-3-amino-9-ethylcarbazol-perylene-3,4,9,10-perylenetetracarboxy-anhydride (BC-PDD) is produced, by replacing of bromine group on Br-PDD with amine group of 3amino-9ethylcarbazole in bay substitution position.

The chemical structure of the nanocomposites and bay-substituted perylene macromolecules were characterized by IR, H^1-NMR and C^{13}-NMR. The solid state C^{13}-NMR is applied for characterization of BP-PDSi because of its poor solubility is normal organic solvents. Also their different characteristic analysis like, UV-vis, DSC, TGA, CV, SEM and elemental analysis; confirmed the chemical structures and their properties.

All synthesized compounds except BP-PDSi, were dissolved in most of polar aprotic solvents such as DMSO, DMF, DMAc and NMP. All of composite and nanocomposite were insoluble in most polar parotic solvents such as methanol and ethanol.

The scanning electron microscopy (SEM) images of nanosilica and Nano-BP-PDSi, are shown the average diameter of nanosilica particles which used as seed was 20-50 nm, and the diameter of nano-BP-PDSi was 95-159 nm. According to the SEM and

AFM results, it can be found that the core-shell, perylene nanocompsite containing perylene in shell and silica as seed, the thickness and diameter of nanocomposite could be controlled by varying the amount of perylene monomers. The thermochemical properties of compounds were studied with TGA and DSC, in all of synthesized compounds decomposition temperature were above 250 ^{o}C, with no glass temperature in DSC up to 350 ^{o}C.

The electrochemical analysis of compounds were applied in solid state and DMF solutions. In DMF solution, BPDI-PDI and BP-PPI showed two-electron reduction but BC-PDD exhibited only one-electron reduction, also in solid state BP-PDSi and BP-PPDSi are exhibited two-electron reductions while, nano-BP-PDSi and BPDA-PDA are shown single electron reductions. In all of compounds the LUMO, HOMO energies and Eg values are characterized from reduction peaks.

REFERENCES

[1] Acemioglu, B. (2004). Adsorption of Congo red from aqueous solution onto calcium-rich fly ash. *Journal of Colloids Interface Science,* 274, 371- 379.

[2] Inan, D., Dubey, R. K., Westerveld, N., Bleeker, J., Jager, W. F., & Grozema, F. C. (2017). Substitution effects on the photoinduced charge-transfer properties of novel perylene-3,4,9,10-tetracarboxylic acid derivatives. *Journal of Physical Chemistry A*, 121, 4633–4644.

[3] Kaur, B., Quazi, N., Ivanov, I.., & Bhattacharya, S. N. (2012). Near-infrared reflective properties of perylene derivatives. *Dyes and Pigments,* 92, 1108-1113.

[4] Bodapati, J. B., & Icil, H. (2008). Highly soluble perylene diimide and oligomeric diimide dyes combining perylene and hexa (ethylene glycol) units: Synthesis, characterization, optical and electrochemical properties. *Dyes and Pigments*, 79, 224-235.

[5] Ahmad, M., & Tan, T. W. (2001). Sensing material prepared from doped sol-gel film for use in acid- base titration. *Asian Journal on Science and echnology for Development,* 18.

[6] Ishi-i, T., Murakami, K., Imai, Y., & Mataka, S. (2005). Light-harvesting and energy-transfer system based on self-assembling perylene diimide-appended hexaazatriphenylene. *Organic. Letters,* 7, 3175–3178.

[7] Ahrens, M. J., Fuller, M. J., & Wasielewski, M. R. (2003). Cyanated perylene-3-4-dicarboximides and perylene-3,4:9,10-bis (dicarboximide): facile Chromophoric oxidants for organic photonics and electronics. *Chemistry of Materials,* 15, 2684-2686.

[8] Dubey, R. K., Inan, D., Sengupta, S., Sudhölter, E. J. R., Grozema, F. C., & Jager, W. F. (2016). Tunable and highly efficient light-harvesting antenna systems based on 1,7-perylene-3,4,9,10-tetracarboxylic acid derivatives, *Chemistry Science,* 7, 3517-3532.

[9] Amiralaei, S., Uzun, D., & Icil, H. (2008). Chiral substituent containing perylene monoanhydride monoimide and its highly soluble symmetrical diimide: synthesis, photophysics and electrochemistry from dilute solution to solid state. *Photochemical and Photobiological Sciences,* 7, 936-947

[10] Aleshinloye, A. O., Bodapati, J. B., & Icil, H. *(2015).* Synthesis, characterization, optical and electrochemical properties of a new chiral multichromophoric system based on perylene and naphthalene diimides. *Photochemistry and Photobiology A: Chemistry,* 300, 27-37.

[11] Asir, S., Demir, A. S., & Icil, H. (2009). The Synthesis of novel, unsymmetrically substituted, chiral naphthalene and perylene diimides: photophysical, electrochemical, chiroptical and intermolecular charge transfer properties. *Dyes and pigments,* 84, 1- 14.

[12] Beauvilliers, E. E., Topka, M. R., & Dinolfo, P. H. (2014). Synthesis and characterization of perylene diimide based molecular multilayers using CuAAC: towards panchromatic assemblies. *RSC Advance,* 4, 32866-32875.

[13] Saeed, A., & Shabir, G. (2014). New fluorescent symmetrically substituted perylene-3,4,9,10-dianhydride-azohybrid dyes: Synthesis and spectroscopic studies, *Molecular and Biomolecular Spectroscopy,* 10, 7-12.

[14] Bhat, S., Otsuka, T., & Srinivasan, A. *(1994).* Benzopurpurin and related compounds inhibit the binding of gp120 to galactosyl ceramide/sulfatide and infection of human immunodeficiency virus. *DNA Cell Biology,* 13, 211-6.

[15] Würthner, F., Stepanenko, V., Chen, Z. C. R., Saha-Möller, N., & Kocher, D. *(2004).* Preparation and characterization of regioisomerically pure 1,7-disubstituted perylene bisimide dyes. *Journal of Organic Chemistry,* 69, 7933–7939.

[16] Bodapati, J. B. (2005). Ms Thesis, Eastern Mediterranean University.

[17] Chen, Y., Kong, Y., Wang, Y., Ma, P., Bao, M., & Li, X. (2009). Supramolecular self- assembly study of a flexible perylenetetracarboxylic diimide dimer in langmuir and langmuir–blodgett films. *Journal of Colloid and Interface Science*, 330, 421–427.

[18] Perrin, L., & Hudhomme, P. (2011). Synthesis, electrochemical and optical absorption properties of new perylene-3,4:9,10-bis(dicarboximide) and perylene-3,4:9,10-bis(benzimidazole) derivatives, *European Journal of Organic Chemistry*, 28, 5427–5440.

[19] Dinçalp, H., kizilok, S., & Icli, S. (2010). Fluorescent macromolecular perylene diimides containing pyrene or indole units in bay positions. *Dyes and pigments,* 86, 32- 41.

[20] Jimenez, A. J., Lin, M. J., Burschka, C., Becker, J., Settels, V., Engels, B., & Würthner, F. (2013). Structure–property relationships for 1,7-diphenoxy-perylene bisimides in solution and in the solid state, *Journal of Chemistry Science.*

[21] Icil, H., & Arslan, E. (2001). Synthesis and properties spectroscopic properties oF highly pure perylene fluorescent dyes. *Spectroscopy Letters,* 34(3), 355–363.

[22] Raj, M. R., Ramkumar, S., & Anandan, S. (2013). Structure–property relationships for 1,7-diphenoxy-perylene bisimides in solution and in the solid state, *RSC Advances,* 3, 14595.

[23] Icil, H., & Icil, S. (1997). Synthesis and properties of a new photostable polymer: perylene -3, 4, 9, 10-tetracarboxylic acid-bis-(N, N-dodecylpolyimide). *Journal of polymer science*, 35, 2137-2142.

[24] Sun, M., Müllen, K., & Yin, M. (2016). Water-soluble perylenediimides design concepts and biological applications. Chemical Society Review. 45, 1513-1528.

[25] Lakwicz, J. R. (2006). Principle of fluorescence spectroscopy.

[26] Langhals, H., & Pust, T. (2010). Axially extended perylene dyes. *European Journal of Organic Chemistry*, 3140–3145.

[27] Aydin, E., Nisanci, B., Acar, M., Dastan, A., & Bozdemir, Ö. A. (2015). Synthesis and properties of perylene diimide dyes bearing unsymmetrical and symmetrical phenoxy substituents at bay positions. *New Journal Chemistry*, 39, 548-554.

[28] Zhao, H., Zhang, Y., Xu, H., He, Z., Zhang, Z. L., & Zhang, H. (2015). Synthesis and properties of perylene diimide dyes bearing unsymmetrical and symmetrical phenoxy substituents at bay positions. *Tetrahedron*, 71, 775-775.

[29] Kozma, E., Kotowski, D., Catellani, M., Luzzati, S., Cavazzini, M., Bossi, A., Orlandi, S., & Bertini, F. (2015). Design of perylene diimides for organic solar cell: Effect of molecular steric hindrance and extended conjugation. *Materials Chemistry and Physics*, 163, 152-160.

[30] Choi, J., Sakong, C., Choi, J. H., Yoon, C., & Kim, J. P. (2011). Synthesis and characterization of some perylene dyes for dye-based LCD color filters. *Dyes and Pigments*, 90, 82-88.

[31] Kotowski, D., Luzzati, S., Scavia, G., Cavazzini, M., Bossib, A., Catellania, M., & Kozma, E. (2015). The effect of perylene diimides chemical structure on the photovoltaic performance of P_3HT/perylene diimides solar cells. *Dyes and Pigments*, 120, 57-64.

[32] Mckitterick, C. B., Erb-Satullo, N. L., LaRacuente, N. D. Dickinson, A. J., & Collings, P. J. *(2010*). Aggregation properties of the chromonic liquid crystal. *Journal of Physical. Chemistry*, 1888-1896.

[33] Dubey, R. K., Efimov, A., & Lemmetyinen, H. (2011). 1,7- and 1,6-regioisomers of diphenoxy and dipyrrolidinyl substituted perylene diimides: synthesis, separation, characterization, and comparison of electrochemical and optical properties. *Chemistry of Materials*, 23, 778–788.

[34] Pasaogullari, N., Icil, H., & Demuth, M. *(2006).* Symmetrical and unsymmetrical perylene diimides: their synthesis, photophysical and electrochemical properties. *Dyes and Pigments*, 69, 118-127.

[35] Liu, C., Li, Z., Schöneboom, J., Eickemeyer, F., Pschirer, N. G., Erk, P., Herrmann, A., & Müllen, K. (2009). Perylenes as sensitizers in hybrid solar cells: how molecular size influences performance. *Journal of Materials Chemistry*, 19, 5405-5415.

[36] Chen, K. Y., & Chang, C. W. (2014). 1,7-Bis-(N,N-dialkylamino) perylene bisimides: facile synthesis and characterization as near-infrared fluorescent dyes. *Materials (Basel)*, 7, 7548-7565.

[37] Rashwan, F. A., Mohran, H. S., & El-samahy, A. A. (2005). Electrochemical Characteristics of Some Purpurins in Aqueous and Nonaqueous Solutions. *American Journal of Applied Sciences*, 2 (7), 1174-1177.

[38] Scaiano, J. C. (1989). Handbook of Organic Photochemistry, CRC Press.

[39] Dhanapal, R. (2012). Nanotechnology Engineering a Review, *Journal of Science,* 2, 13-25.

[40] Younan, X. (2009). Shape-Controlled Synthesis of Metal Nanocrystals: Simple Chemistry Meets Complex Physics. *Angewandte Chemie International Edited*, 48, 60–103